Final Report

Federal Agency/ Organization Element:	DOE/EERE/ Office of Advanced Manufacturing Program (AMO)
Award Number:	DE-EE0005775
Project Title:	High Thermal Conductivity Polymer Composites for Low-Cost Heat Exchangers
Project Period:	12/15/2014 to 09/30/2016
Recipient Organization:	United Technologies Research Center 411 Silver Lane East Hartford, CT 06108-1127
Principal Investigator:	Catherine Thibaud-Erkey; thibauc@utrc.utc.com
Team Members:	Abbas Alahyari, Justin Alms, Bob Brown, Jim Cardinale, Scott Eastman, Doug Logan, Matt Pearson, Ken Smith, John Wesson, Ryan Witherell, Hailing Wu
Partners:	University of Massachusetts – Lowell Professor Sobkowicz, Professor Stephen Johnston, Afrin Roja Jahir Hussain University of Akron Professor Alamgir Karim, Professor Sadhan Jana, Arvind Modi, Sung Jun Kim)

Executive Summary

Most heat exchangers are currently constructed from heavy and costly metals that are subject to corrosion and pose manufacturing constraints. This report identifies candidate commercially available composite materials that can be used as a replacement for metal in specific heat exchanger applications.

The project highlighted the following conclusions pertinent to the choice of a composite material for heat exchange application.

1- In most applications, the thermal conductivity target is much lower than the thermal conductivity of metals since the overall heat transfer is rapidly dominated by the fluid-side heat transfer and not by conduction through the solid. Indeed, materials with thermal conductivity in the 5-10 W/mK range were found to provide a competitive alternative to metals.
2- The strength of the material was not a limiting factor, a fact that will become even more widespread with the adoption of new low greenhouse gas potential (GWP) refrigerants that operate at lower pressure. Weak manufacturing points such as weld lines and joints are likely to drive the part design. Special care should be taken in assessing the effect of temperature, fluid compatibility and aging on the polymer strength as heat exchangers are expected to have a service life of at least 5 years.
3- Permeation of the heat exchange fluid across the pressure boundary was highlighted as a concern, driven by the strict requirement for containment of refrigerants. The use of a composite material can create defect within the end product that lead to fluid permeation. This containment requirement makes a heat exchanger application significantly more challenging than heat dissipation devices.
4- Equipment currently used for injection molding of plastics should be improved to accommodate the processing of high thermal conductivity filled material, both with respect to thermal management as well as filler orientation.
5- Redesign of heat exchanger components will be required to take full advantage of the use of thermoplastic materials, including geometry changes to accommodate material properties strength and manufacturing, and potential surface optimization.
6- Novel manufacturing techniques such as 3D printing should be explored as a way to increase the design space.
7- The full size demonstration of a heat exchanger made of commercially available polyphenylene sulfide (PPS) composite is recommended as a next step.

Table of content

Table of Figures

Table of Tables

1. Background and Project Goal

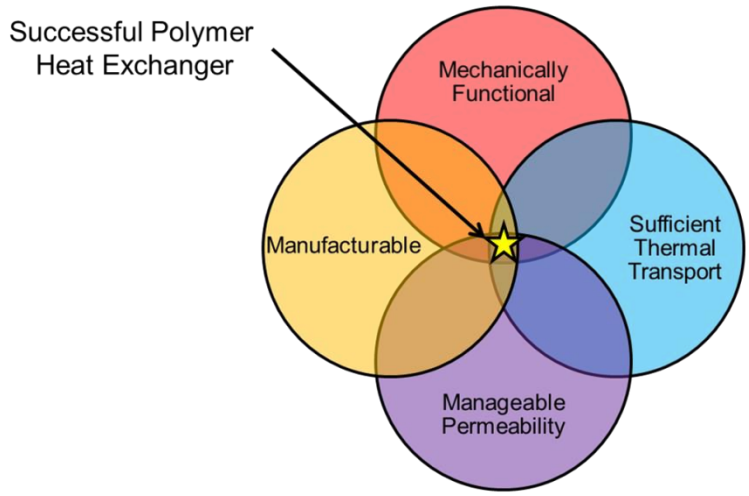

Figure 1. Attributes required for a successful polymer based heat exchanger

Heat exchangers (HXs) are critical components in a wide range of heat transfer applications, from HVAC (Heating Ventilation and Cooling) to automobiles to manufacturing plants. They require materials capable of transferring heat at high rates while also minimizing thermal expansion over the usage temperature range. Conventionally, metals are used for applications where effective and efficient heat exchange is required, since many metals exhibit thermal conductivity over 100 W/m K.
While metal HXs are constantly being improved, they still have some inherent drawbacks due to their metal construction, in particular corrosion. Polymeric material can offer solution to such durability issues and allow designs that cannot be afforded by metal construction either due to complexity or cost. A major drawback of polymeric material is their low thermal conductivity (0.1-0.5? W/mK) that would lead to large system size.

Recent improvements in the area of filled polymers have highlighted the possibility to greatly improve the thermal conductivity of polymeric materials while retaining their inherent manufacturing advantage, and have been applied to heat sink applications.

Therefore, the objective of this project was to develop a robust review of materials for the manufacturing of industrial and commercial non-metallic heat exchangers. This review consisted of material identification, literature evaluation, as well as empirical and model characterization, resulting in a database of relevant material properties and characteristics to provide guidance for future heat exchanger development.

2. Applications and Requirements

2.1 Application downselection

Based on a thorough review of the heat exchangers application space for commercial HVAC and aerospace obtained from open sources and internal UTC sources (operating conditions such as pressure, temperature and fluid) and market size data [1] the three main constructs below were downselected.

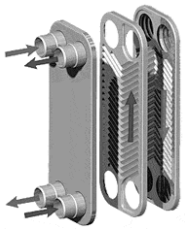

1- Plate and Frame Heat Exchanger (PFHE)
Fluids: Liquid/Liquid or Liquid/2-phase
Impact: Reduced weight and cost (currently made of stainless steel)
Applications: commercial HVAC chillers, aerospace, process industry

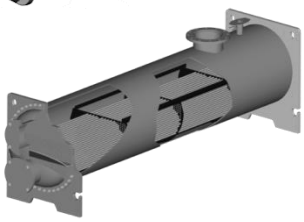

2- Shell and Tube
Fluids: Liquid/Liquid or Liquid/2-phase
Impact: reduced weight and cost (generally larger size HX using large amount of metal), potential for reduced fouling and erosion
Applications: chiller, industrial, food and beverage, marine

3- Enabling application:
Fluid: Air/2-phase condensers
Impact: increased cycle efficiency with evaporative cooling
Currently limited by corrosion resistance
Applications: HVAC, refrigeration

A common challenge for all applications is to avoid new designs that are impractical or too costly to manufacture out of metal.

A useful resource for this task was the work of Professor Jacobi at the University of Illinois [2].

2.2 Technical and cost requirements

We established a list of required material properties with their required range for use in the fabrication of non-metallic heat exchangers. Material properties included thermal conductivity, permeability, fluid compatibility, material chemical stability, mechanical stability and strength, flammability, manufacturability, and durability.

Early on into the project, the team evaluated the debit in performance for a composite material based heat exchanger compared to a metal heat exchanger for a given thermal conductivity. A typical heat exchanger design and a realistic thickness for the composite layer were assumed. A maximum performance debit of 10% was chosen. Such a debit was deemed reasonable as it may be recoverable through design changes that cannot be afforded by a metal construction. An example of the analysis output is shown in Figure 2.

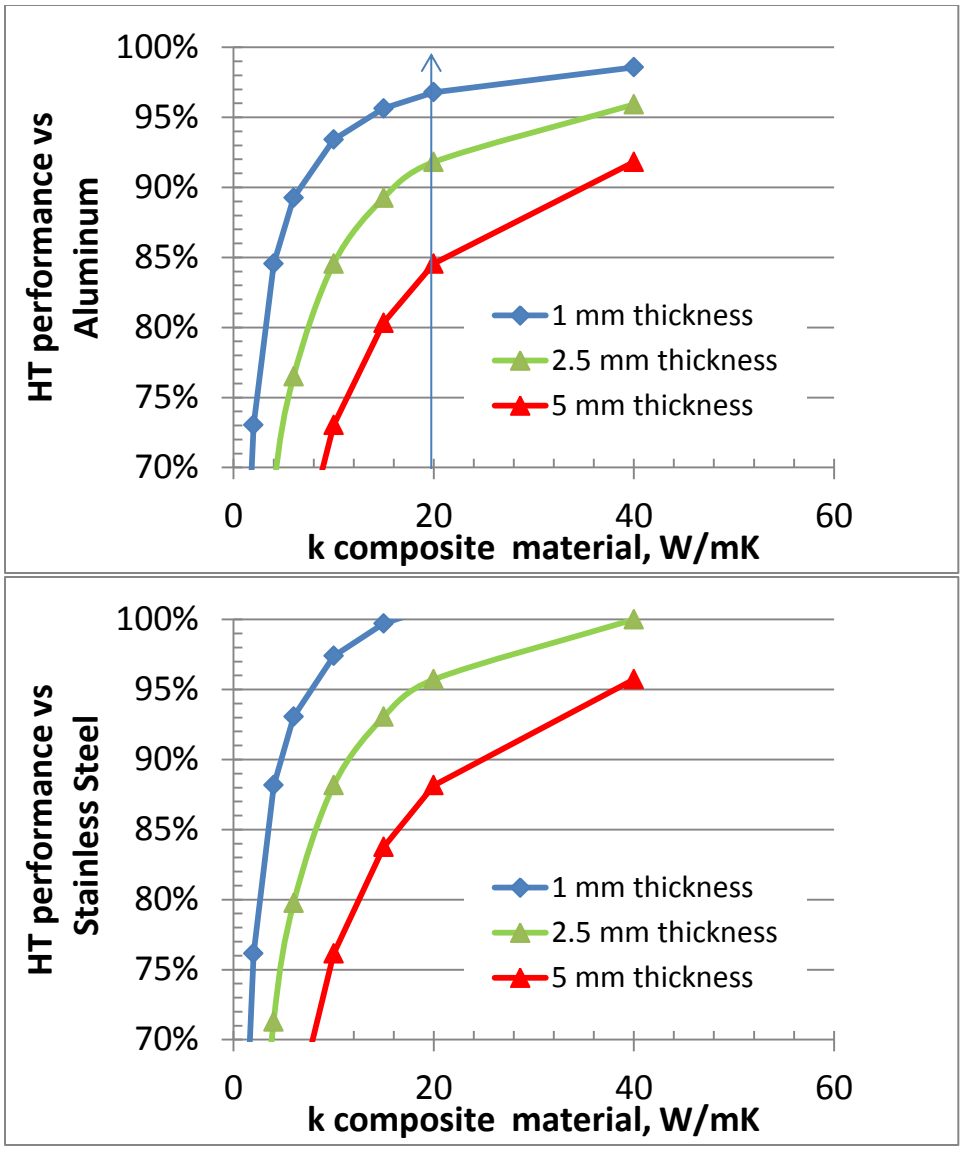

Figure 2. Performance debit versus aluminum (k=180 W/mK) and stainless steel (k=16 W/mK) shell and tube heat exchanger as a function of composite thermal conductivity (1 cm diameter tube – 1 mm metal tube thickness, h (liquid)= 1000 W/m W/(m^2K), h (2 phase)= 3000 W/(m^2K)

The maximum allowable pressure was calculated using Barlow's formula which relates the internal pressure (P) to the tube diameter (D) and thickness (t) and strength of the material (S):

$$P = \frac{2St}{D}$$

Results from the analysis are shown in Figure 3 and other selected targets are shown in Table 1.

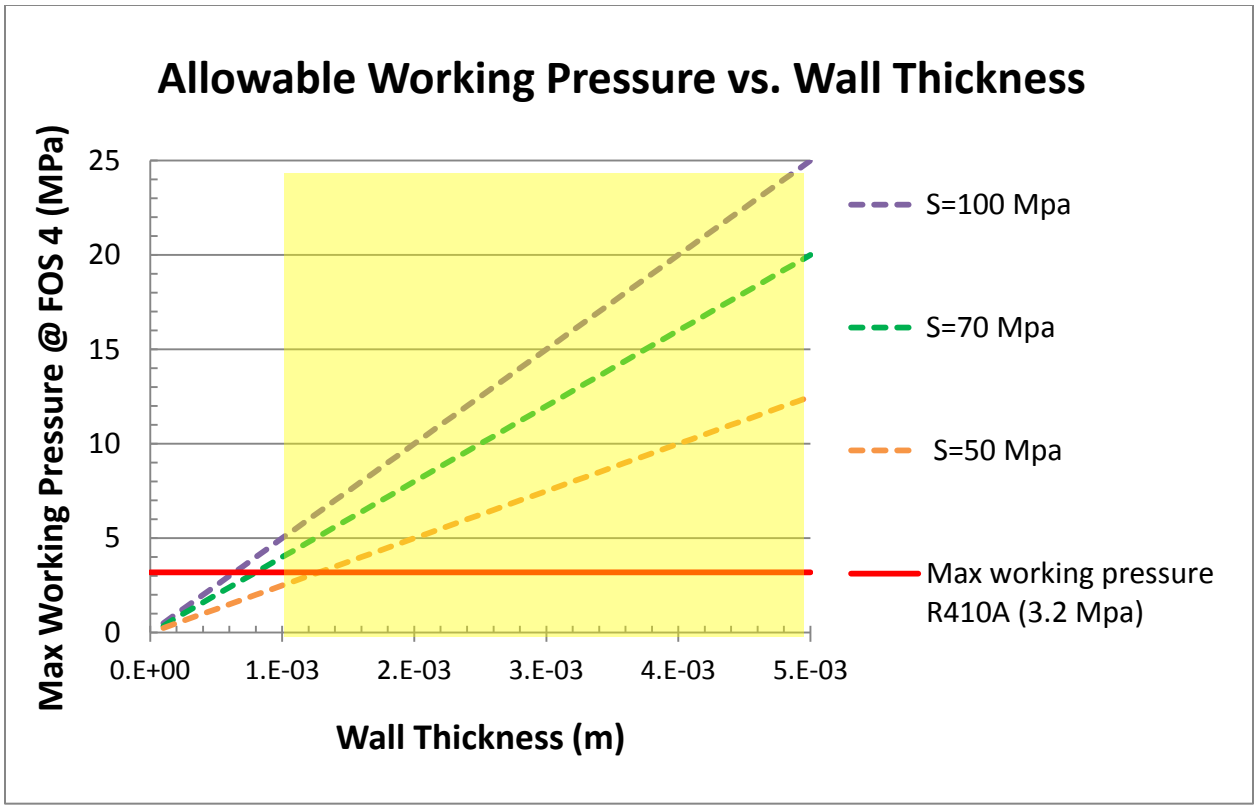

Figure 3. Maximum pressure calculated using Barlow's formula.

Table 1. Technical and cost requirements for the three downselected applications as well as the information for baseline materials.

Application	Thermal Conductivity W/mK	Strength . MPa	Fluid Compatibility	Permeability	Flammability	Manufacturability	Cost ($/lb)
Baseline Materials							
Baseline: aluminum 3003	180	130				Forming, welding	0.8-0.9
Baseline : 316 Stainless Steel	16	860				Forming, welding	1.5
Baseline: Copper	400	220				Forming, welding	3.0
Poly Phenylene Sulphide (PPS)	0.3	86.7					
Downselected applications							
BPHE Baseline: Stainless Steel	>20	>70	Compatible with current and next gen refrigerants/water/ ethylene glycol	1 oz./ yr./ unit	UL 94- V0	Injection molding	7-20
SNT Baseline: Copper, Aluminum	>20	>70	Compatible with current and next gen refrigerants/coolants	1 oz./ yr./ unit	UL 94- V0	Injection molding, Extrusion, Surface enhancement	7-20
Evaporative cooling HX Baseline: Aluminum	>20	>70	Compatible with current and next gen refrigerants/ humid air	1 oz./ yr./ unit	UL 94- V0	Injection Molding, Fin forming	7-20

3. Commercially Available and State-of-The-Art (SOTA) Composite Materials

From a thorough review of literature, web searches and discussions with suppliers and experts in the field, a compilation of the relevant Commercial-Off-The-Shelf (COTS) and SOTA materials was assembled. Materials with varying types of fillers, filler volume fractions, and polymer structures were identified which resulted in a wide range of composite performance.

3.1 Commercial Off The Shelf (COTS) materials

A summary of the COTS materials from MatWeb and a survey of suppliers are shown in Table 2. Some materials with very high thermal conductivity are shown in the table, many of which are very highly filled polymers. In addition, the team surveyed the materials listed within the MoldFlow software (Table 3). The most promising commercially available materials were acquired and some tested as detailed in Section 5 (Table 4).

Table 2. Review of current COTS materials from MatWeb (As of March 2015).

Vendor	Material	Thermal Conductivity (W/m-K)	Tensile Modulus (GPa)
Master Bond	Epoxy, Electrically Conductive	0.100 - 5.76	0.0179 - 17.9
Unknown	Epoxy/Carbon Fiber Composite	0.220 - 400	5.30 - 520
Victrex® PEEK polymer	Polyetheretherketone, Carbon Fiber Filled	0.240 - 22.0	1.00 - 138
Ultem® PEI	Polyetherimide (PEI)	0.0360 - 11.0	0.0370 - 42.0
Celanese	Polyphenylene Sulfide (PPS), Unreinforced, Extruded	0.288 - 22.0	3.20 - 14.0
Celanese	Liquid crystalline polymer with mineral filler	1	9.8
DuPont Performance Polymers	Polyphthalamide (PPA)	0.260 - 20.0	0.500 - 48.3
SBHPP	Silicone, Molded, Glass Fiber Filled	0.0600 - 32.0	0.00159 - 14.0
Bulk Molding Compounds, Inc.	BMC 940 Vinyl Ester Bipolar Plate Material	13.4	9.5
Cool Polymers	Polyphenylene Sulfide	10	12
Cool Polymers	Polypropylene	1.1	8.65
Cool Polymers	D5110 PPS with unknown fillers	2	14.6
Cool Polymers	D5112 PPS with unknown fillers	6	26.2
Cool Polymers	D5107 PPS with unknown fillers	1.4	12.6
Cool Polymers	D5109 PPS with unknown fillers	6	17.5
Cool Polymers	D5108 PPS with unknown fillers	10	23.6
Cool Polymers	E1201 PP with unknown fillers	10	5.62
Cool Polymers	E2 Liquid crystalline polymer	20	24.3
Cool Polymers	D5506 Thermally Conductive Liquid Crystalline Polymer	10	10.9
Cool Polymers	E3607 Thermally Conductive Polyamide (PA6)	14	10.6
Cool Polymers	E4301 Thermally Conductive Polybutylene Terephthalate	14	3.4
Cool Polymers	E5101 Thermally Conductive Polyphenylene Sulfide	20	13
Cytec Thornel	P-55 Carbon Fiber/Epoxy Advanced Composite System	74	220
Cytec Thornel	P-75 Carbon Fiber/Epoxy Advanced Composite System	110	320
Cytec Thornel	P-100 Carbon Fiber/Epoxy Advanced Composite System	321	470
Cytec Thornel	P-120 Carbon Fiber/Epoxy Advanced Composite System	400	520
PolyOne	SF-4500 TC Polyphenylene Sulfide (PPS)	11	31
PolyOne	LC-6000 TC Liquid Crystal Polymer (LCP)	19	20.7
PolyOne	NJ-6000 TC Polyamide 12 (Nylon 12)	11	20.7
PolyOne	NJC-7500 Nylon 12	25	14.5
PolyOne	SF-6000 TC Polyphenylene Sulfide (PPS)	10.0 - 11.0	26.2
PolyOne	Thermatech TT9200-8708-0 EC	18 (in plane) 4 (thru plane)	27.6
Lati Industria Termoplastici S.P.A.	52/11 GR/70 PP Homopolymer	15	8.2
Lati Industria Termoplastici S.P.A.	62 GR/70 PA 6, 70% Graphite Reinforced	15	22
Lehmann & Voss LUVOCOM	1105-8165 PEEK, with carbon fiber, lubricant modified	22	22
Lehmann & Voss	1301-8153 PPS, linear, unreinforced, thermally	15	11

LUVOCOM	conductive modified		
Lehmann & Voss LUVOCOM	1301-8312-1 PPS, linear, unreinforced, thermally conductive modified	18	13
Lehmann & Voss LUVOCOM	1301-8312 PPS, linear, unreinforced, thermally conductive modified	22	14
Ovation Polymers Nemcon	H PC DP105/X3 BK Polycarbonate	6.1	6.9
Ovation Polymers Nemcon	H PC DP120/X3 BK Polycarbonate, Thermally Conductive, Black	3.25 - 10.1	6.7
SABIC Innovative Plastics	LNP KONDUIT PX08321 PA 6 (Asia Pacific)	1.10 - 10.0	13.8
SABIC Innovative Plastics	LNP KONDUIT OX11315 PPS (Asia Pacific)	3.50 - 15.0	16.4
SABIC	Polypropylene sulfide with glass and other fillers	1.05	16.25
RTP Company	1300 TC-I-20 FR Polyphenylene sulfide	1	1.6
RTP Company	1300 TC-C-30FR polyphenylene sulfide (PPS)	8 (in plane) 2.3 (thru plane)	
RTP Company	1399 X 128638 Polyphenylene sulfide (PPS)	10 (in plane) 2 (thru plane)	17.2
RTP Company	1399 X 128637 B Polyphenylene Sulfide (PPS)	3.00 - 22.0	12.1
RTP Company	4099 X 131005 B Polyphthalamide (PPA)	3.00 - 20.0	20
RTP Company	3499-3 X 90363 Liquid Crystal Polymer (LCP)	125	58.6
RTP Company	1399 X 97649D polyphenylene sulfide	2.22	19.4
RTP Company	300 TC-C-20 polycarbonate	5 (in plane) 1.3 (thru plane)	6.9
RTP Company	199 X 104849 A polypropylene	1.7	6.2

Table 3. High thermal conductivity materials from the MoldFlow database.

Manufacturer	Trade name	Family	Thermal Conductivity (W/mC)	Filler data: Description	Filler Content (wt%)	Description
Zschimmer & Schwartz	FS0400G	PA	16	Ceramic Powder	87	FS0400G : Zschimmer & Schwartz
Bayer MaterialScience	Makrolon TC8030	PC	5.3			Makrolon TC8030 : Bayer MaterialScience
Tosoh Corporation	Susteel TCX-200	PPS	5	Carbon Fiber High Modulus	35	Susteel TCX-200 : Tosoh Corporation
Toray Industries Incorporated	H501B	PPS	2.287	Glass Fiber	25	H501B : Toray Industries Incorporated
EPIC Polymers Ltd	STAR THERM® W A-2 HT	PA66	2	Ceramic Powder	25	STAR THERM® W A-2 HT : EPIC Polymers Ltd
Solvay Specialty Polymers	AvaSpire PAEK AV-755 SL 45	PEEK	1.163	Carbon Fiber High Modulus	30	AvaSpire PAEK AV-755 SL 45 : Solvay Specialty Polymers
Evitron	Neotron N2A12 High Density	PA12	1.065	Neodymium-Iron-Boron	63	Neotron N2A12 High Density : Evitron
Evitron	Neotron N2A12	PA12	1.065	Neodymium-Iron-Boron	66	Neotron N2A12 : Evitron
DuPont Kabushiki Kaisha	Zenite ZE15801M3	LCP	1	Glass Fiber	65	Zenite ZE15801M3 : DuPont Kabushiki Kaisha

Table 4. Commercially samples acquired during the course of the project.

Material	Material Supplier	Base Polymer	Density-datasheet (g/cm^3)	In Plane Datasheet (25°C)	Through Plane Datasheet (25°C)	Ultimate Flex. Strength-datasheet (MPa), 25C	Flexural Modulus-Datasheet (MPa) 25C	Ultimate Tensile Strength-datasheet (MPa), 25C	Tensile Modulus-Datasheet (MPa) 25C
E5125	Cool Polymers	PPS	1.72	30	8.88			45	10500
E5501	Cool Polymers	LCP	1.72	35	10.4	48	8100	32	6100
D5506	Cool Polymers	LCP	1.8	10	N/A	84	12300	50	10900
E1201	Cool Polymers	PP	1.24	10	N/A	37	5410	22	5620
E5101	Cool Polymers	PPS	1.7	20	N/A	70	13000	45	13000
E5103	Cool Polymers	PPS	1.54	8	N/A	84	10100	49	11600
E5111	Cool Polymers	PPS	1.71	2.5	N/A	185	15400	110	18300
D5108	Cool Polymers	PPS	1.82	10	N/A	69	19400	37	23600
Pure PPS	McMaster Carr	PPS	1.36	0.3	0.3	N/A	N/A	N/A	N/A
Thermatech TT9200-8708-0 EC (PPS grey)	PolyOne	PPS	1.74	18	4	83	22100	55	27600
PP based on Thermatech TT11623-	PolyOne	PP	N/A	N/A	N/A	N/A	N/A	N/A	N/A
PPA based on Thermatech TT11623-002-01	PolyOne	PPA	N/A	N/A	N/A	N/A	N/A	N/A	N/A

3.2 State Of The Art (SOTA) materials

(A review article was written by the team and is pending publication in the Journal Applied Thermal Engineering [3]. Some of the information is included in this report but the interested reader is advised to consult the publication for further details).

A variety of composite polymers and fillers are detailed in the literature. Typical thermal conductivities are below 10 W/m.K although some have thermal conductivity >10 W/mK.

Strategies used in the synthesis of novel composite polymer materials include:

- Increase the filler amount
    - Thermal conductivity increases with filler loading
    - However, higher loading can cause mechanical instability and processing challenges by interfering with the shear rate-viscosity relationship
- Coating of the filler to improve mixing properties and dispersion; for example
    - Polymer coating: polyimide-coated h-BN particles for polyetherimide composites,
    - Silane coating: Polyhedral Oligosilsesquioxane-Modified BN Nanotube dispersed in epoxy,
    - Amine chemistry: Octadecylamine functionalized boron nitrile.
- Shape of the filler
    - Increase of aspect ratio of particles increased the thermal conductivity due to large effective thermal conductive networks
    - Fibers are better than flakes and flakes are better than spheres
    - Hybrid fillers: flakes, spheres, fibers
- Alignment of the fillers in the desired heat transfer direction.

a- <u>Filler composition</u>

The fillers fall into three categories: metal, carbon or ceramic.
Table **5** to Table 7 give the characteristics of each type of fillers.

<u>Metallic fillers</u>

Metallic fillers such as aluminum, silver, and copper, can impart both thermal and electrical conductivity to composites. Typically, metallic fillers are available in different dimensionalities: 3D isotropic (spherical or cubic), 2D platelets or flakes, and 1D rods or fibers. Shape and spatial distribution of the filler particles control the electrical and thermal properties of metal filled polymer systems [4]. Metallic fillers with smaller particle size impart higher thermal conductivity [5]. Mechanical properties such as modulus and stress at break typically increase when polymers are filled with metallic inclusions.

Boudenne et al. [5] incorporated copper particles in polypropylene (k = 0.24 W/m K) matrix and obtained a thermal conductivity of 2.45 W/m K at 45 vol% loading.

Table 5. Thermal conductivity of metallic fillers.

Material	K (W/m K)	CTE (10^{-6}/C)	Density (g/cm^3)
Aluminum	205	23	2.7
Copper	401	17	8.9
Nickel	91	13	8.9
Silver	429	18	10.49

Carbon based fillers

Carbon based fillers include carbon black, carbon fiber, graphite,graphene, single-wall and multiwall carbon nanotubes and nanosheets, all of which increase both thermal and electrical conductivity and mechanical properties of the composites [6,7]. Table 6 contains typical thermal conductivity ranges of carbonaceous fillers. The carbon fillers have relatively low bulk density in contrast to metallic fillers. They are found to be inert and compatible with thermoplastics. Conductivity depends on the regularity of the π-bonding structure and the freedom from defects. Graphene has the highest thermal conductivity, making it an excellent choice for heat transfer [8-36]. Single-walled and multi-walled carbon nanotubes have high inherent thermal conductivity; however, they are very expensive and difficult to disperse in a matrix. Carbon structures also have low coefficient of thermal expansion, and are resistant to corrosion and chemical decomposition [9]. Fibers show excellent properties along the long axis; however, properties are reported to be much lower along the transverse direction.

Carbon composites result in light weight thermoplastic composites possessing very high thermal conductivity. Chen and Ting [10] achieved 695 W/m K and density less than 1.5 g/cm3 by fabricating 56 vol% vapor grown carbon fiber-reinforced epoxy composites. Ha et al. [11] studied the thermal conductivity of graphite filled-liquid crystal thermoplastic composites; filler content was varied from 0 to 70 wt%. They found that addition of graphite significantly reduced thermal expansion. Thermal conductivity values were found to increase from 0.40 and 0.25 W/m K to 28.3 and 13.9 W/m K for in-plane and through-plane directions, respectively, which represents 71-fold and 56-fold increase.

Table 6. Thermal conductivity of carbon fillers.

Material	K (W/m K)
Carbon black	6–174
Carbon fiber (PAN)	8–70
Carbon fiber (Pitch)	530–1100 (axis)
Carbon nanotubes	2000–6000 (axis)
Graphite	100–400 (on plane)
Graphene	5000–6000

Ceramic based fillers

Ceramic fillers such as aluminum nitride, boron nitride, silicon carbide, and beryllium oxide are used when the final product needs to be thermally conductive but electrically resistive and possess low coefficient of thermal expansion. Boron nitride and aluminum nitride have

hexagonal planar structure similar to graphene which accounts for their high thermal conductivity. The atoms are connected via ionic and covalent bonds and this combination results in high thermal stability. Typical thermal conductivity ranges of ceramic fillers are shown in Table 7 [12].

Thermoplastic composites with ceramic fillers exhibit high thermal stability, lower shrinkage, and dimensional stability. They possess relatively lower density compared to metals and can endure very high service temperature ranges. Difficulties involved in preparation of ceramic fillers that are compatible with thermoplastics make them relatively more expensive than both metal and carbon fillers.

Leung et al. [13] achieved 800% improvement in thermal conductivity over neat polyphenylene sulfide by adding 33.3 vol% of hexagonal boron nitride spherical particles. Xu et al. [6] added aluminum nitride whiskers and particles to polyvinylidene fluoride, achieving 11.5 W/m K with 60 vol% and aluminum nitride whisker:particle ratio of 1:25.7. Ishida and Rimdusit [14] demonstrated 0.2 W/m K at 30 vol% of filler content to 32.5 W/m K at 78.5 vol% in boron nitride-polybenzoxazine composites, attributing the increase to the formation of conductive network.

Table 7. Thermal conductivity of ceramic based fillers.

Material	K (W/m K)	CTE (10^{-6}/C)	Density (g/cm^3)
Aluminum nitride	320	4.5	3.3
Beryllium oxide	260	6	3
Boron nitride	320	2.9	2.1
Silicon carbide	270	3.7	3.3

Hybrid composites

Hybrid systems involve a combination of fillers resulting in a synergistic effect and a balance in final properties. For instance, glass spheres or fibers are added along with carbon to provide mechanical stability to the resin at higher loading levels.

Yeol et al. [15] studied the synergistic improvement in thermal conductivity of polyphenylene sulfide composites with a combination of fillers and obtained highest thermal conductivity of about 1.74 W/m K with 1 wt% multiwalled carbon nanotubes and 50 wt% boron nitride. Wang et al. [16] embedded highly crystalline fibers such as Vectra, Kevlar, and Zylon in epoxy matrix and achieved 19 W/m K in case of Zylon AS and 23 W/m K for Zylon HM. However, when temperature was increased, they found a drop in thermal conductivity values of the composites, which could be attributed to expansion of aligned molecules and deterioration in conductive paths.

b- Filler modifications

Surface pretreatments, filler purification, and other modifications may be necessary to ensure proper mixing and dispersion of filler particles within the polymer. The amount of filler added and the filler aspect ratio are important parameters which determine the final thermal conductivity of the composite. Filler alignment can also affect thermal conductivity and depends on processing variables such as shear rate and temperature.

Thermoplastics are hydrophobic and, in some cases these materials may not bond well with the typically polar surfaces of metal, ceramic or carbon fillers. One strategy to mitigate effects of interfacial flaws and thermal contact resistance is to modify filler surfaces by purification, surface treatment or addition of functional groups. Improved wettability and dispersion of fillers reduces interfacial resistance, thereby increasing the thermal conductivity. Polymer chains can be grafted to filler particles, for example Kim et al. [17] grafted poly (L-lactide) to multi-walled carbon nanotubes, increasing thermal conductivity of the composite from 0.15 W/m K (neat PLLA) to 0.42 W/m K. Silane chemistry is a widely used and versatile modification scheme for hydroxyl-bearing surfaces. Some silane moieties can react with the polymer as well as the filler, creating siloxane bridges for strong and stable interfaces. Ahn et al. [18] surface treated boron nitride with polysilazane, fabricated a composite with nylon 6,6 matrix and observed increase in thermal conductivity from 0.37 to 0.42 W/m K through-plane and 4–4.9 W/m K in-plane after the surface treatment. The Muratov group [19] and demonstrated an increase from 0.256 to 0.369 W/m K in hexagonal boron nitride – polypropylene composites resulting from a silane surface treatment. Lee et al. used titanate couplers (KR 138S) to achieve an 86% increase in thermal conductivity, which was attributed to good wetting between aluminum nitride and high density polyethylene matrix [20]. Cao et al. achieved better dispersion of filler in the matrix when the filler particles were coated with polymers. Chiu et al. [21] modified aluminum nitride with polysilazane and amorphous silicon oxycarbide ceramic to obtain significant increase in thermal conductivity compared to untreated filler.

c- Filler volume fraction

While increasing filler loading enhances thermal conductivity, higher loading can also cause mechanical instability and processing challenges by interfering with the shear rate-viscosity relationship. Filler agglomerates may also form [22], increasing the effective filler size. The experimental data obtained during the course of the project corroborates theses finding as will be presented in Section 6.

d- Filler aspect ratio

High aspect ratio favors conductive network formation at lower volume fractions due to a lower percolation threshold [23, 24, 25]. As the aspect ratio increases, the probability that two adjacent particles are close enough for phonon transport increases, resulting in lower critical volume fraction [26]. It is desirable to incorporate the smallest volume fraction of filler possible, to keep the composite density low and reduce the number of “dead-ends” or areas for increased phonon scattering.

Ideally, using fillers with smaller sizes will result in a lower percolation threshold and formation of conductive pathways at lower loading [27-29]. Filler dimensionality also influences thermal conductivity; fibers are better than flakes and flakes are better than spheres [30,29]. Tekce et al. [31] studied the effect of particle shape on thermal conductivity in copper reinforced polyamide composites and found that the thermal conductivity after incorporating 30 vol% copper fibers was 8.71 W/m K and that by using 60 vol% spherical copper fillers was 3.66 W/m K, a more than 200% increase with only 50% of the filler content. Polydisperse fillers result in higher packing and better formation of conductive pathways, hence hybrid systems containing fillers of various shapes, size and type offer better thermal conductivity [32, 33]. Lee et al. [20] studied

incorporating aluminum nitride, silicon carbide and boron nitride in a hybrid system with high density polyethylene matrix. They found a rapid increase in thermal conductivity at filler volume fraction between 50 and 60 vol%. They obtained better results by using a treated, hybrid filler system with increased thermal conductivity and reduced thermal expansion.

It should be noted that all commercially available materials used micron size fillers, mostly carbon based. It is suspected that this is due to the difficulty in maintaining dispersion of nanofillers.

4. Material Characterization

UTRC developed characterization protocols for material properties and worked with external partners to evaluate properties (thermal conductivity, strength and permeability). Preferred material formulations were obtained from commercial suppliers both as plaques and pelleted material. The pelleted material was used by the University of Massachusetts team in fabrication trials.

Commercial plaques of promising COTS samples (Table 3) were obtained and tested for thermal conductivity and mechanical strength. A set of analysis routines for evaluating material requirements was developed and is summarized below with emphasis on describing the test methodologies, general observations, challenges experienced and overall process by which the materials were characterized.

4.1 Material characterization protocols

4.1.1 Scanning Electron Microscopy – Energy Dispersive Spectroscopy (SEM-EDS)

Equipment Used:
FEI Quanta FEG 650 environmental SEM equipped with an Oxford EDS system.

Test Method:
Plaques were received from suppliers with a typical geometry of 75x75x3 mm. These samples were made by injection molding using an edge-gated injection mold. The edge gate was noted to track the flow orientation, and samples were cut to reveal the face (plane) of interest. These samples were then mounted in epoxy with the face of interest exposed and polished smooth for SEM analysis. The analysis enabled the determination of the filler shape, orientation (Figure 4) and type, for example, glass or carbon (Figure 5). It also clearly indicated the anisotropic nature of most materials.

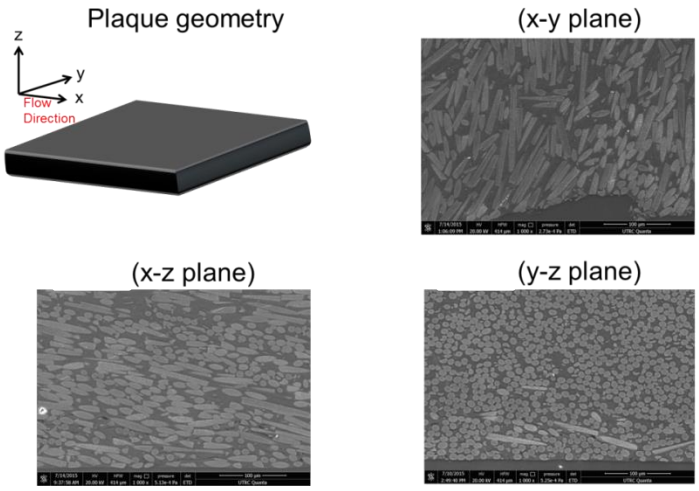

Figure 4. SEM micrograph of composite material showing the orientation of filler in the flow direction (x-axis)

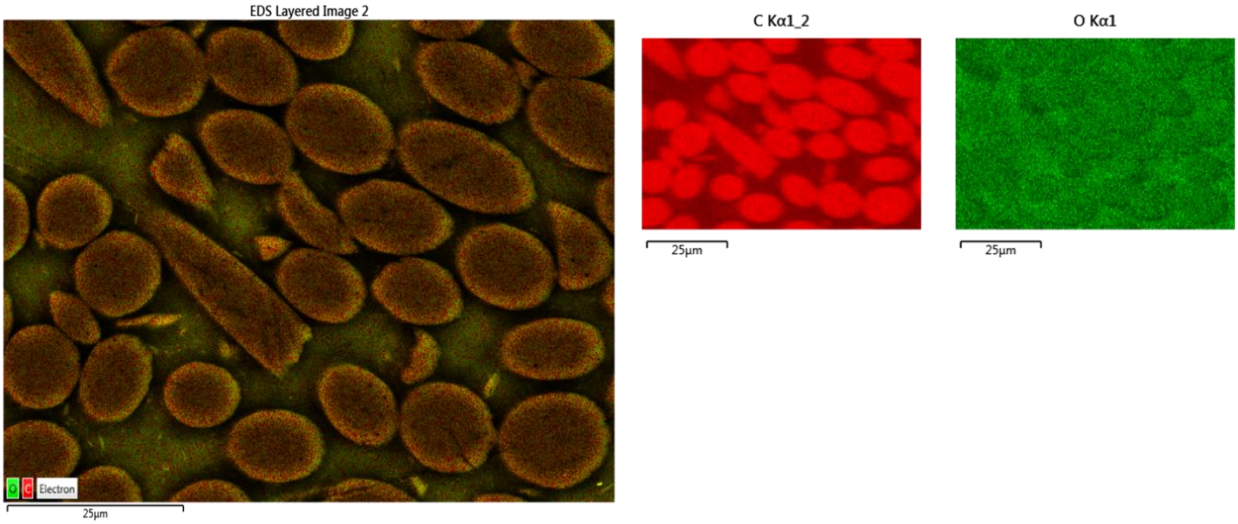

Figure 5. EDS elemental map of composite material with carbon filler in the through thickness dimension (y-z plane).

4.1.2 Thermogravimetric Analysis (TGA)

Equipment Used:

Netzsch Thermal Analyzer, Model STA 449 F3 Jupiter (Netzsch Instruments) equipped TG sample carrier system (part# HTP40000A58.010).

Test Method:

Samples were cut to approximately 60 mg, added to an alumina crucible and placed on to the TG sample carrier. The sample was heated from 30°C to 1400°C at a ramp rate of 10°C/min and then held at 1400°C for 30 minutes. Each material formulation was tested under an air and nitrogen atmosphere separately to characterize the weight loss profile of the material for filler weight percent determination. When conducting testing in a nitrogen atmosphere, an additional purging step was conducted to ensure there was no air in the system. A hermetically sealed furnace was subjected to a vacuum purge and subsequent nitrogen backfill to ensure all air was removed from the furnace prior to testing.

Results:

TGA was performed on all formulations mentioned above in both Nitrogen and Air. Based on the residual weight remaining after these runs, it was possible to estimate the amount of filler within each formulation. The easiest formulations to evaluate were the electrically insulating materials since the fillers are inorganic. A direct measure of the residual weight from the air trials allowed a fairly accurate calculation of filler weight percent. Determining the filler content of the electrically conductive materials was more difficult as the fillers are carbon based. The most accurate calculation of filler content from electrically conductive materials was obtained by comparing the residual weight from a thermally conductive material to that of its respective pure, unfilled resin. TGA results of the unfilled polymer resin (Figure 6, Figure 7 and Figure 8 and Table 8) provided the mass of the residue from the polymer component that could be subtracted from the mass of residue of the thermally conductive composite from the TGA analysis in nitrogen.

The equation below was used to calculate the filler content:

$$f_{fc} = (1 - f_{pc}) = \left(1 - \frac{f_{pr} * W_c}{W_r}\right)$$

Where f_{fc} is is the weight percent of filler in the composite material, f_{pc} is the weight percent of polymer in the filled composite material, f_{pr} is the weight percent of polymer in the pure polymer (100%), W_c is the weight loss percent remaining after the composite nitrogen TGA run, and W_r is the weight loss percent remaining after the pure polymer nitrogen TGA run. Table 8 is a summary of the estimated filler content for the thermally conductive materials analyzed. Filler contents varied from 40-65% by weight.

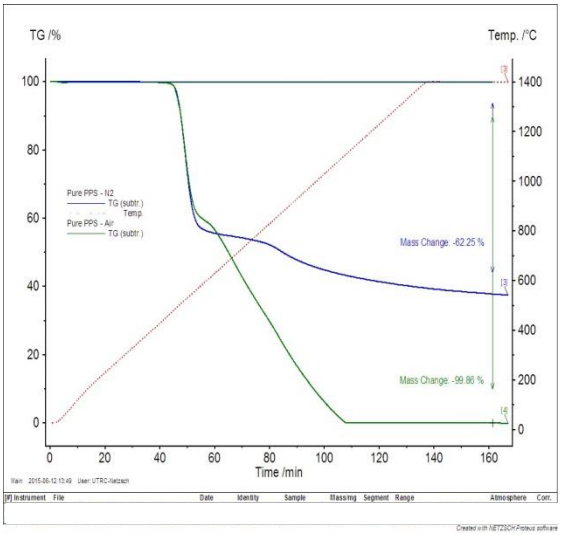

Figure 6. Representative thermal decomposition of unfilled polyphenylene sulfide resin under air and nitrogen environments.

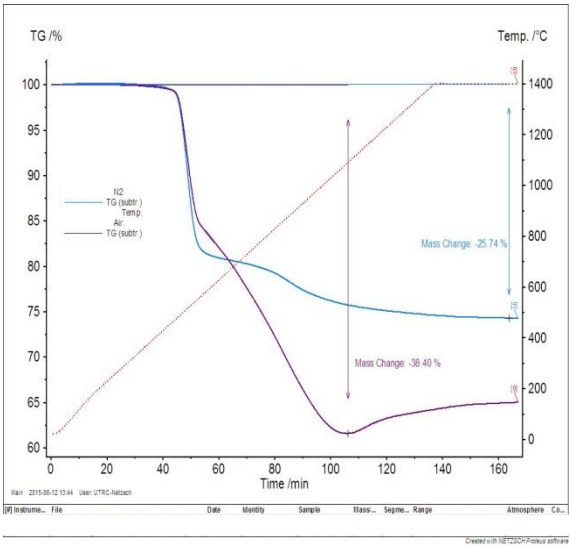

Figure 7: Representative thermal decomposition of inorganic-filler filled polyphenylene sulfide resin under air and nitrogen environments.

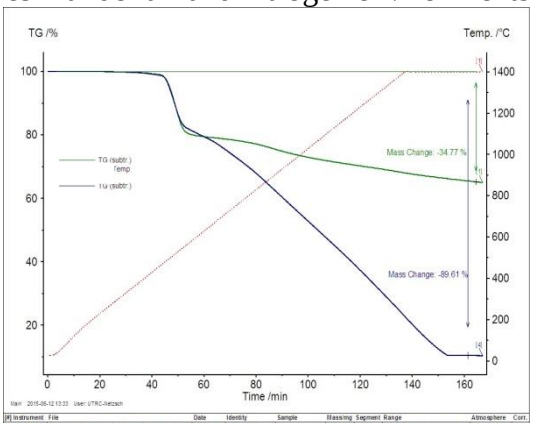

Figure 8: Representative thermal decomposition of carbon filled polyphenylene sulfide (PPS) resin under air and nitrogen environments

.

Table 8. Analysis of percent weight loss for relevant unfilled polymer resins in air and nitrogen atmospheres.

Pure Polymer	Weight Loss in Nitrogen (%)	Weight Loss in Air (%)
PP	100	100
PPS	62.75	100
LCP	50.8	100

4.1.3 Mechanical testing – 3-point bend

Equipment Used:

Tinius Olson mechanical test frame equipped with a 13MPa load cell and a three point bend fixture with a total fixture span length of 70mm.

Test Method:

Flexural testing loosely follows the ISO 178 standard. Samples were cut from plaques provided by the vendor. The typical sample geometry for flexural testing was 75x10x3mm. A

three point bend fixture with a total span of 70mm between contact points was used. The crosshead speed was set to 1.27 mm/min.

4.1.4 Mechanical testing – Tensile

Equipment:

Tinius Olson mechanical test frame equipped with an 827MPa load cell and hydraulic clamping grips.

Test Method:

Tensile testing loosely followed the ASTM D638 standard. Dogbone specimens were either supplied directly from the vendor or injection molded by UMass Lowell to an approximate dimension of 3.3mm thick, 165mm total length, 13mm gage width, and 60mm gage length. The cross head speed of the tensile test was 1.27 mm/min. Dogbone specimens from the material suppliers were tested at 25°C (minimum of three samples) and at 80°C (minimum of three samples) to evaluate the effects of temperature on mechanical stress and modulus. Temperature was regulated by enclosing the entire test fixture and sample in a clam shell furnace equilibrated to 80C. The sample was allowed to equilibrate for at least 5 minutes prior to testing.

Samples provided from UMass Lowell were processed via a single gate or dual gate injection molding process and tested at 25°C. Single gated samples provide test specimens that can be compared to test specimens provided by the material supplier. Dual gated samples provide an evaluation of weld (knit) line strength where both flow fronts meet in the center of the dogbone gage section (Figure 9).

Figure 9: Images of single gated (left) and dual gated (right) injection molded dog bone specimens made by the University of Massachusetts at Lowell.

4.1.5 Thermal conductivity by Flash Diffusivity

Equipment used
TA Instruments DLF 1200 Laser Flash equipped with an optional in-plane mask for measuring in-plane thermal conductivity

Test Method:
Samples were cut from plaques that were supplied by the vendor. Sample geometries were cut to 25.4 mm diameter disks and subsequently ground to a desired thickness of about 1mm. The samples were then sprayed on both sides with a graphite thermal spray to enhance energy absorption and by the laser flash uniformity of the testing surface. Any overspray on the sides of the sample was wiped clean and the samples were placed in the instrument. Thermal conductivity of each sample is typically measured at 4 different temperatures (25, 50, 75, and 100°C). To ensure consistent and accurate results, two thermal conductivity standards, Vespel which has a thermal conductivity around 0.5 W/mK and stainless steel which has a thermal conductivity around 16 W/mK are used.

<u>Discussion on Through Plane vs. In-Plane Thermal Conductivity Measurements</u>
For homogeneous materials, it is typically sufficient to measure thermal conductivity through the plane of a sample as homogeneous materials should have isotropic performance properties. For highly filled polymer composites, however, the filler incorporated into these polymer composites is highly aligned along the flow direction during processing and results in a highly anisotropic material in nearly all performance properties. Thermal conductivity of the polymer composites studied in this project have a significantly higher in-plane conductivity than through-plane as the fillers are aligned in the plane of the sample, thus it is important to measure both values to get a full understanding of how the material will transport heat. Figure 10 demonstrates the fundamentals of the flash diffusivity technique to calculate thermal conductivity in the through plane direction. In order to measure in-plane thermal conductivity, the sample specimen is sandwiched between a mask set (Figure 11) to drive thermal diffusion predominantly in the plane of the sample, however there is still a through plane component with this technique.

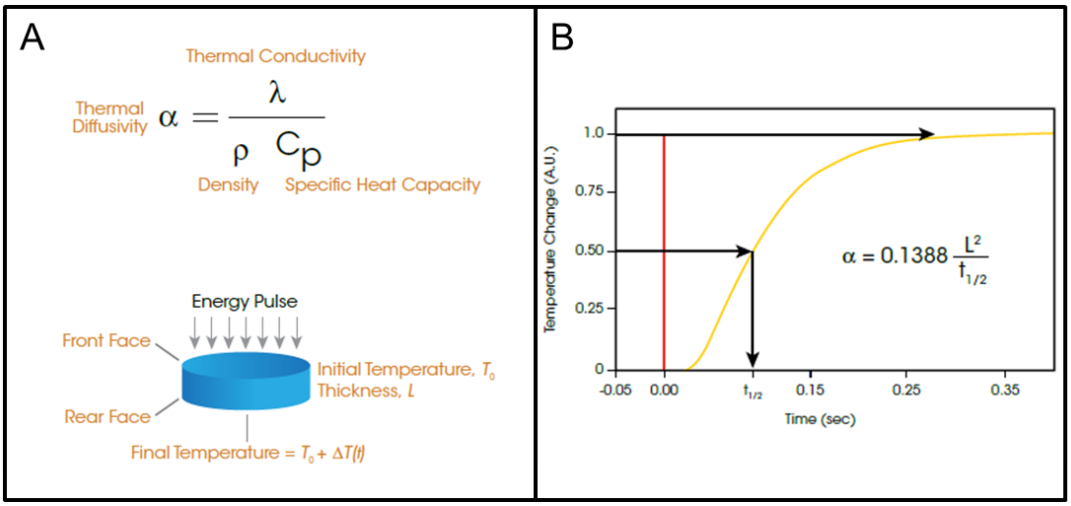

Figure 10: Fundamental representation of flash diffusivity theory (left) and typical output data (right). (http://thermophysical.tainstruments.com/PDF/brochure/BROCH-ThermalConductivityDiffusivity-2014-EN.pdf)

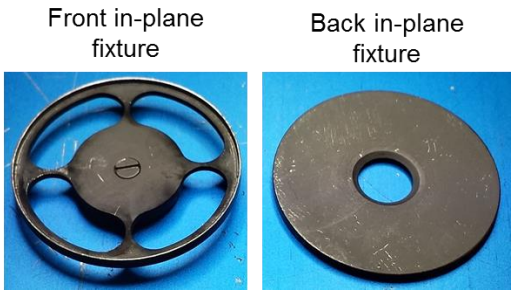

Figure 11: Images of front (left) and back (right) plates of the in-plane fixture for measuring in-plane thermal conductivity via flash diffusivity. Sample specimens are sandwiched in-between these plates during testing.

4.2 Composite testing

Laser Flash Diffusivity thermal conductivity testing

The through-plane thermal conductivity of composite materials obtained from two different suppliers was measured using LFD. As shown in Figure 12, there was a large variation in the magnitude of the through-plane thermal conductivities even with the same matrix. This can be due to the type and amount of filler as well as manufacturing techniques.

The through-plane thermal conductivity of three PPS composite materials obtained from one supplier was measured using LFD. The carbon filler loading was estimated based on thermogravimetric data. As expected, the thermal conductivity increases with the filler loading (Figure 13). When the data for LCP-based materials is added, the upward trend still holds (Figure 14).

Such trend experimentally confirms modeling results that suggest that materials with higher filler content have a higher thermal conductivity. However, this needs to be contrasted with the findings that highly filled materials are harder to process (see fabrication section).

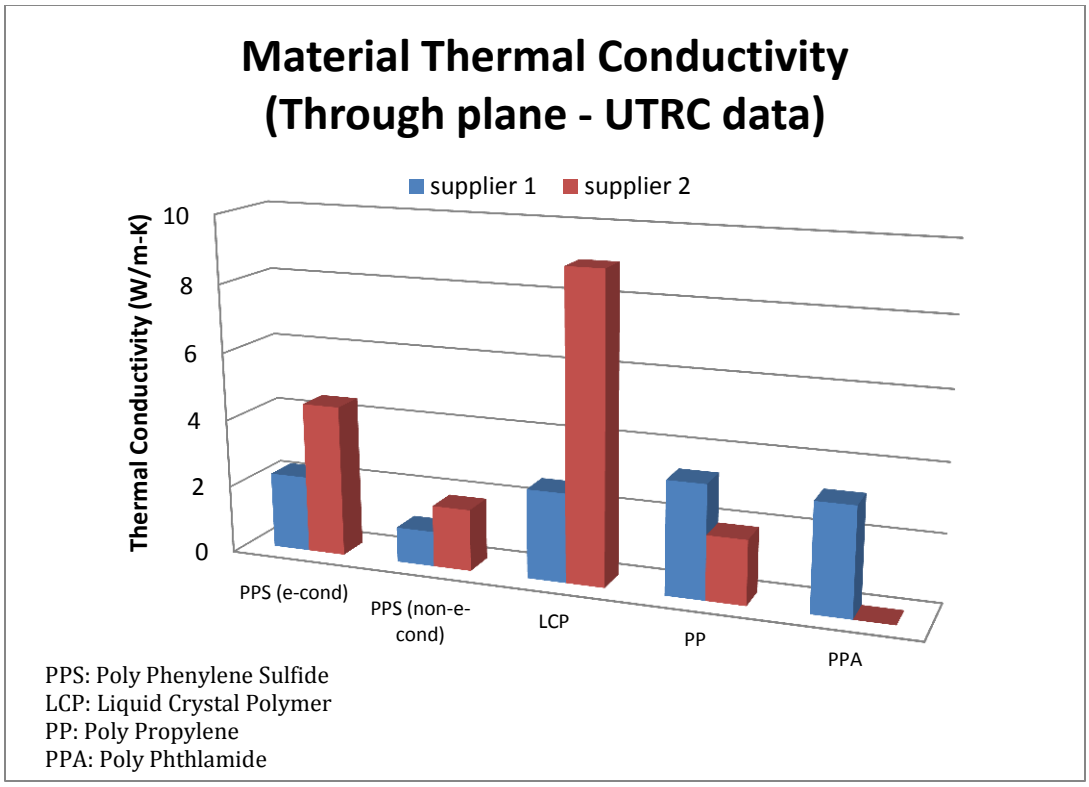

Figure 12. Through-plane thermal conductivity for commercially available materials from two different manufacturers (Laser Flash Diffusivity measurement).

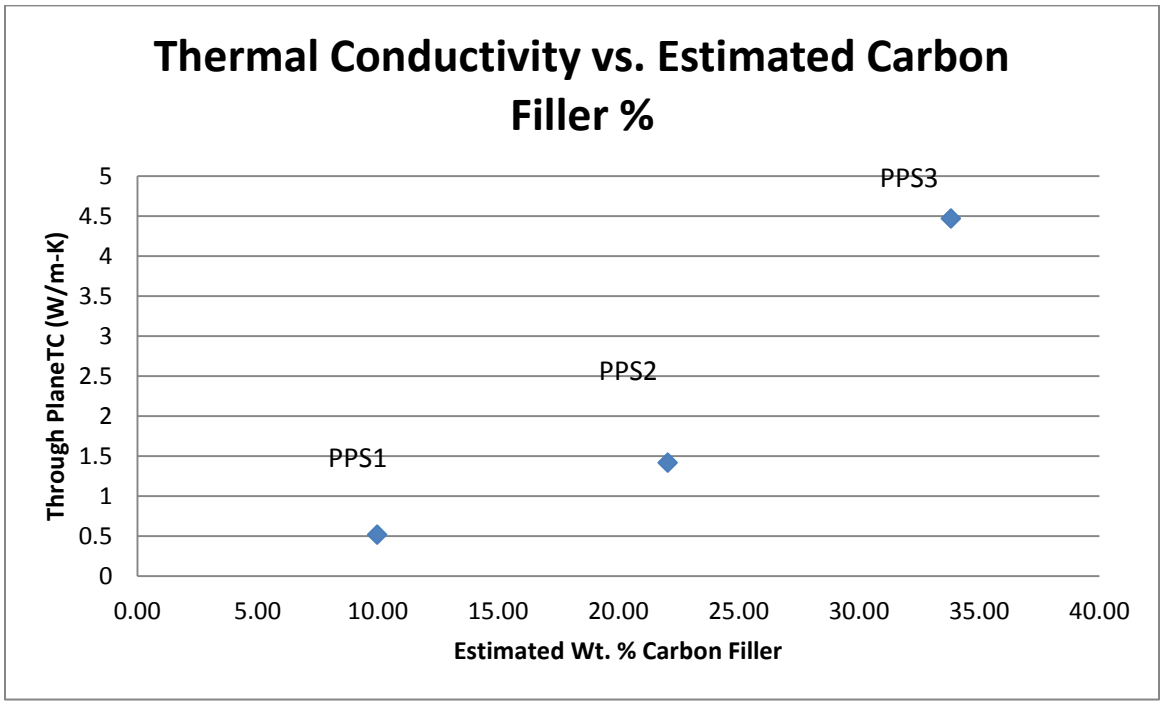

Figure 13. Through-plane thermal conductivity for three commercially available PPS materials with different carbon filler loading (UTRC Laser Flash Diffusivity measurement).

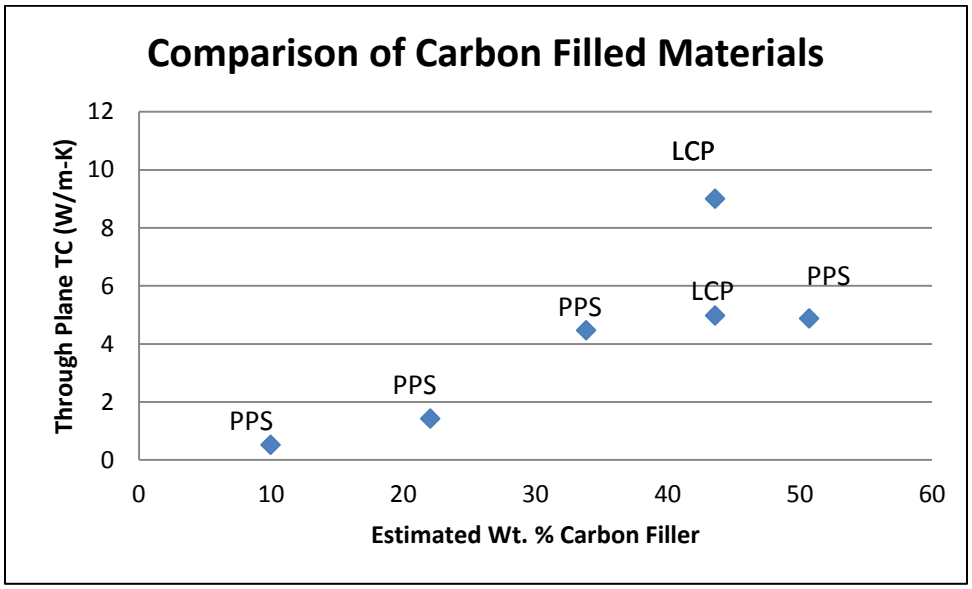

Figure 14. Through-plane thermal conductivity for PPS and LCP based composite materials with different carbon filler loading (UTRC Laser Flash Diffusivity measurement).

Evaluation of Material Strength vs Temperature

Tensile strength of various composite materials was measured at 25°C and 80°C. As expected, the tensile strength was highest at room temperature. All materials showed a substantial reduction in tensile strength and modulus (~20-60%) when tested at 80°C (Figure 15 and Figure 16). Preliminary results indicate that PPA may be least affected by temperature. Strength at temperature is a very important parameter for a polymer based HX assembly since the degradation of strength with temperature is very different for polymers and metals.

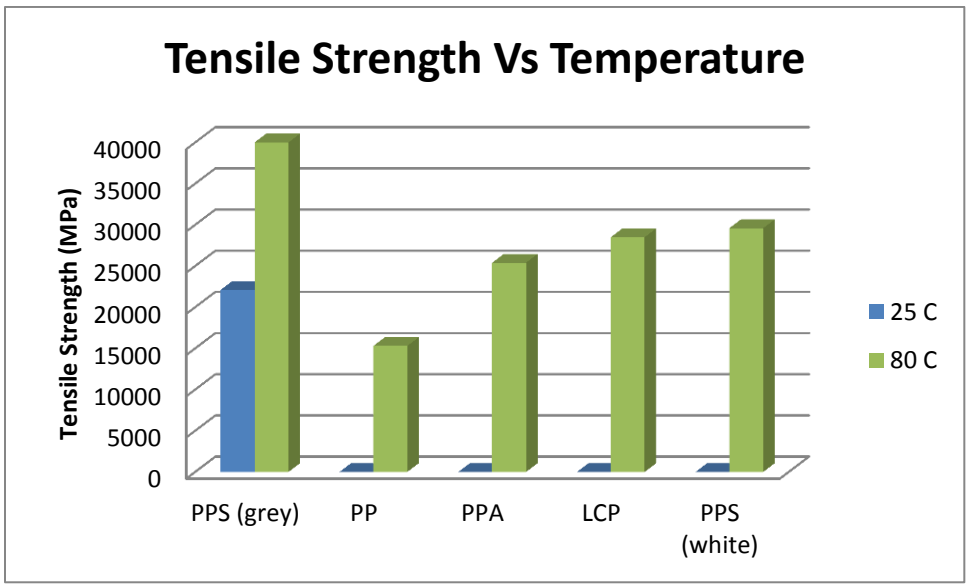

Figure 15. Tensile strength for polymer based composite materials with different polymer matrix at 25°C and 80°C (UTRC data)

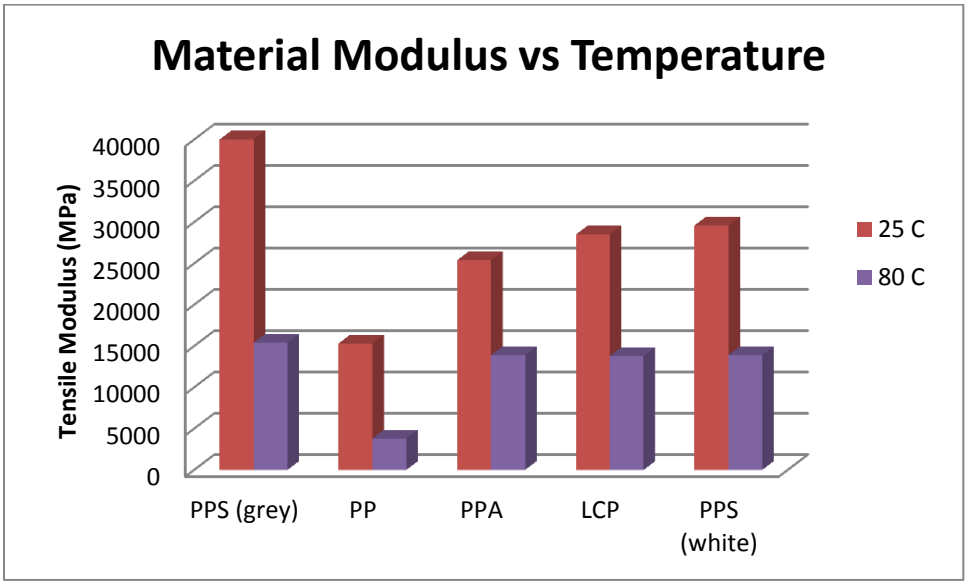

Figure 16. Tensile modulus for polymer based composite materials with different polymer matrix at 25°C and 80°C (UTRC data)

Evaluation of Strength vs Process Flow Direction

The flexural strength was measured parallel to the flow direction and perpendicular to the flow direction as defined by the manufacturing process (Figure 17). The flexural strength was noticeably lower when samples were tested perpendicular to the flow direction (Figure 18 and Figure 19) but the overall reduction was dependent on the material tested. This data can be used as an input for the ABAQUS strength modeling.

Strength differences are due to the anisotropy of the processed material and to fiber alignment within the composite material. From a strength view point, as one considers the symmetry of the final HX assembly, this data suggests that it may be more beneficial to seek an isotropic material.

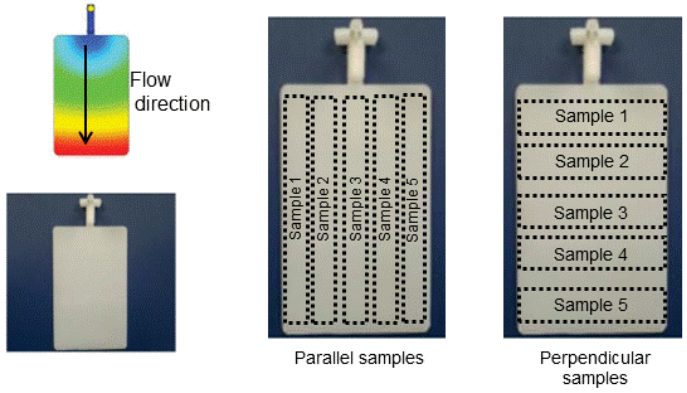

Figure 17. Representation of flow directionality and sample preparation for evaluation of strength versus direction

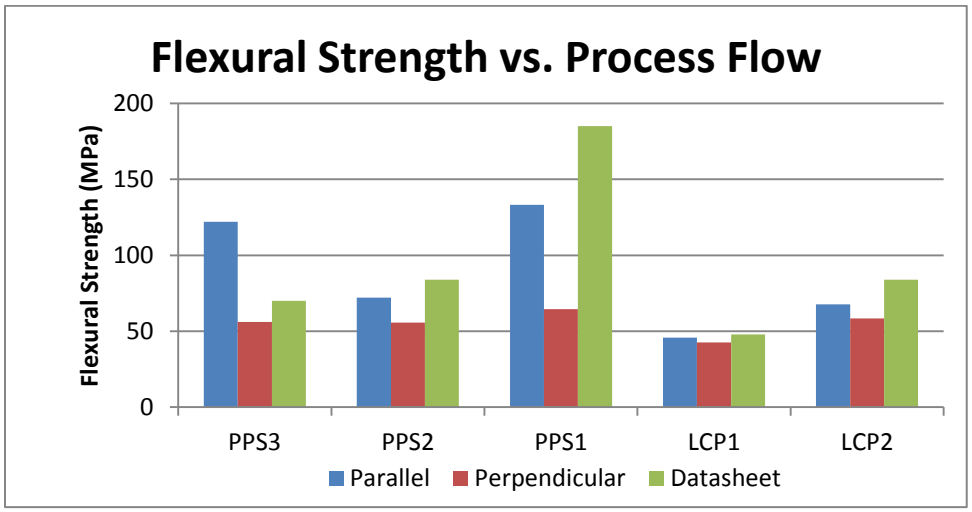

Figure 18. Flexural strength versus process flow direction for various polymer-based composite materials.

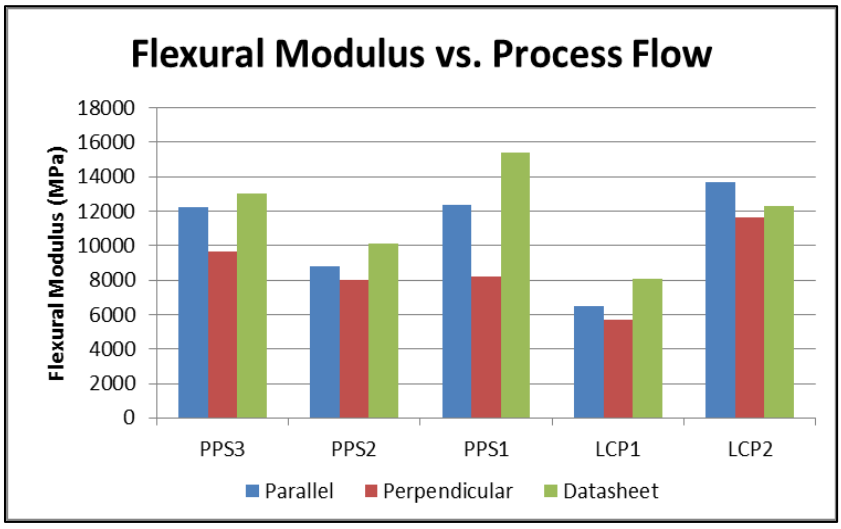

Figure 19. Flexural modulus versus process flow direction for various polymer-based composite materials.

Evaluation of Strength vs. Gating

The tensile strength was measured on single gated test specimens and dual gated test specimens fabricated by the University of Massachusetts – Lowell team (Figure 20). The single gated tensile strength and modulus were predominantly close to the values specified on the data sheet (Figure 21 and Figure 22). The tensile strength and modulus of dual gated test specimens were substantially lower than single gated specimens due to pronounced weld line that occur when melt fronts impinge. Such behavior is likely to limit the practical size of the HX element.

Figure 20. Picture of single gated and dual gated test specimens.

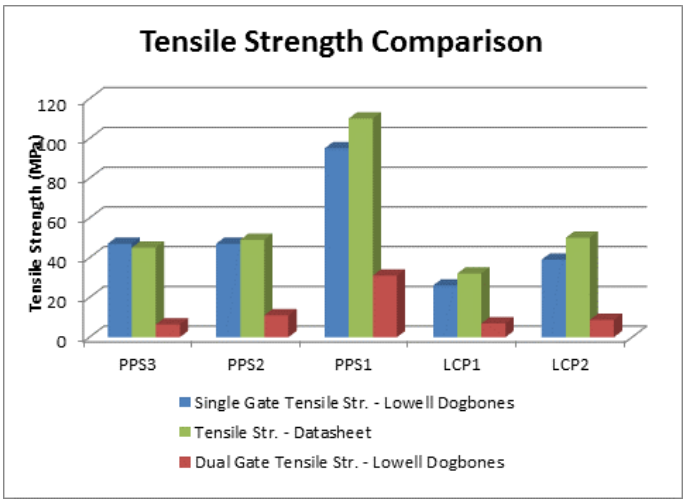

Figure 21. Tensile strength of single gated and dual gated test specimens fabricated at UMass Lowell (UTRC data).

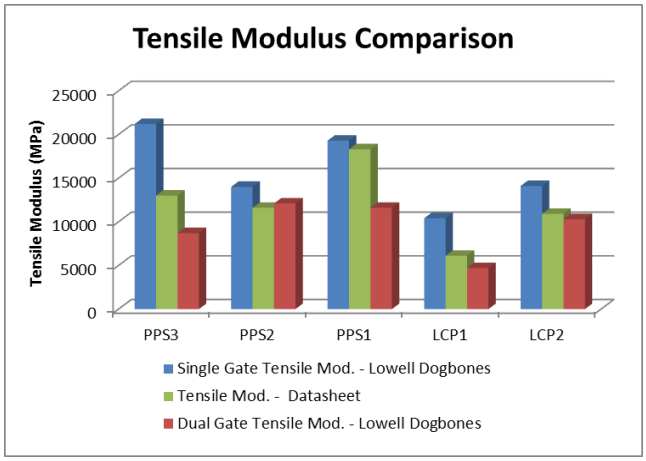

Figure 22. Tensile modulus of single gated and dual gated test specimens fabricated at UMass Lowell (UTRC data).

5.1.6 Permeability measurements:

Adding inorganic fillers to improve the thermal conductivity of a polymer heat exchanger *may result in either increase or decrease* of refrigerant permeance. It is therefore important that permeance measurements of the candidate composite structures are conducted as a part of the development. The most recent standard test for oxygen transmission rate of films and packages is ASTM D-3985.

Mocon Inc. of Minneapolis, MN, has developed commercially available instruments which comply with this standard and are widely employed by industry. The Mocon instruments employ a permeation cell (Figure 23) in which the sample material separates two chambers, as shown in the insert. An oxygen-rich gas, typically air or pure oxygen, passes on one side of the sample, while an oxygen-deficient carrier gas, such as nitrogen, passes on the opposite side. Oxygen permeates through the film from the side with high concentration and into the oxygen-deficient carrier gas stream. After leaving the sample chamber, the carrier gas passes through a highly sensitive coulometric oxygen sensor which measures the oxygen concentration in the carrier gas.

In order to establish whether the addition of fillers has changed the permeability of the polymer, samples of the composite structure were tested for oxygen transmission rates (OTR) vis-à-vis the unfilled polymer. Candidate composite samples were prepared by injection molding thicker plates which were subsequently ground to the maximum thickness required (0.04" or 1 mm).

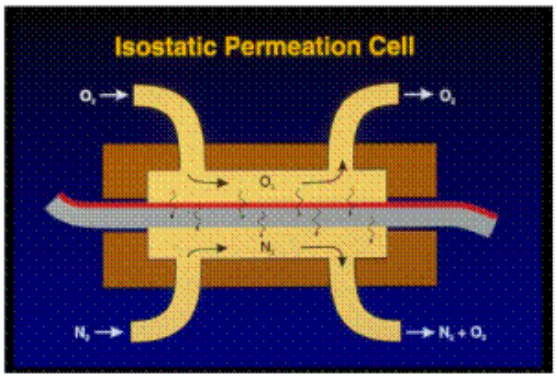

Figure 23. Isostatic Permeation Cell.

Table 9. MOCON Oxygen permeability results for PPS composite materials with other material parameters measured at UTRC.

	Oxygen Permeability (cc.mm /(m^2.day.bar)	Total Filler %	Estimated Inorganic Filler %	Estimated Carbon Filler %	Density-datasheet (g/cm^3)	Through Plane - UTRC (25°C)
PPS composite 1	TBD	44.22	10.4	33.8	1.7	4.47
PPS composite 2	0.7-0.3	34.04	12.0	22.1	1.5	1.42
PPS composite 3	1.56	49.00	39.0	10.0	1.7	0.52
PPS - neat	1.16	0	0	0		0.2

As a comparison, the permeability of other neat polymers in cc.mm/(m^2.day.bar) is as follows:
Nylon 66 1.36 (gold standard "barrier film")
High Density PolyEthylene: 39-79
Poly Propylene 59-102

Therefore, from a permeability point of view, PPS is a good choice as a base polymer for composite structures. The permeability of the composite materials made of PPS fall on either side of the PPS permeability with composite 2 being lower and composite 3 being slighty higher. This results is not unexpected as literature as shown that filler addition can either decrease or enhance permeability of polymer materials (Table 10).

Table 10 A sample of literature citations reporting permeance increases due to the presence of inorganic fillers.

Matrix	Filler	Permeance Increase	Reference
PTMSP	Fumed SiO_2	3.2X	Science 296 (2002)
PMP	Fumed SiO_2	2.4X	Chem. Mater. 15 (2003) 109
Polyimide	SiO_2	55%	Chem. Mater. 11 (1999) 2331
Polyimide	SiO_2	15X	J. Mem. Sci. 115 (1996) 65
Polyimide	TiO_2	3.7X - 4.3X	Desal. 146 (2002) 49

The team has estimated based on proprietary UTC information that the maximum tolerable refrigerant permeance is ~0.22 cc/ (m^2*day).

As permeability measurements were not part of the original statement of work, the team was unable to perform permeability measurements on the refrigerant in addition to oxygen. Such measurements would be essential in a future phase of the development of polymer based heat exchangers.

Based on the limited data obtained and assuming that the oxygen permeability is representative of the refrigerant permeability, it is likely that permeability may dictate the thickness of the separating layer, which would be detrimental to the heat exchange and performance. Other means of controlling refrigerant cross over include coating of the polymer.

It should also be noted that:
-applications that do not include refrigerants would not suffer from permeability constraints,
-new low GWP refrigerants operate at lower pressures which will also be an advantage from a permeability view point.

4.1.7 Material downselection

PPS and PPA were downselected as materials of choice based on the information shown in the tables below and following the material downselection methodology highlighted.
The commercially available materials (PPS, LCP. PPA and PP) were rated based on the material characterization performed at UTRC and the fabrication trials performed at UMass-Lowell. Thermal conductivity, mechanical strength, processability and cost were first assigned a color rating based on comparative performance and attribute. Since ultimately, the heat transfer performance is based on the thermal conductivity ratioed to the achievable plate or tube layer thickness, we assigned an arbitrary plate thickness corresponding to the processability criteria and assessed this parameter compared to the thermal conductivity, leading to the 'k/d' parameter rating.
Factoring in the flammability criteria, one can conclude that PPS is the preferred material for heat exchanger application even though the flammability rating of PPA could be improved by using additives.
The grade of PPS (i.e. filler loading and type)) should be downselected based on the specific application, keeping in mind the trade-offs between thermal conductivity and processability (i.e higher loadings lead to higher thermal conductivity but lower processability).

Figure 24. Downselection methodology and information.

Material	Type	Thermal Cond., k	Mechanical Strength	Processability	Cost
E5101	PPS/C/inorg				
E5103	PPS/C/inorg				
E5111	PPS/C/inorg				
E5501	LCP				
D5506	LCP				
TC-PPA	PPA				
TC-PP	PP				

Material	Type	Thermal Cond., k	Mechanical Strength	Processability	Plate thickness, d	k/d	Cost
					arbitrary		
E5101	PPS/C/inorg				3		
E5103	PPS/C/inorg				1		
E5111	PPS/C/inorg				2		
E5501	LCP				3		
D5506	LCP				3		
TC-PPA	PPA				3		
TC-PP	PP				1		

Material	Type	Mechanical Strength	Permeability	k/d	chemical compatibility/ flammability
E5101	PPS/C/inorg		TBD		
E5103	PPS/C/inorg				
TC-PPA	PPA		TBD		H-B

5 Composite Modeling

Figure 25 depicts the various modeling tools that can be brought together in the design and manufacturing of polymer-based heat exchangers, from the molecular level to the macroscale level. The Molecular dynamics and FEA models will be summarized in this section and the injection molding and HX design in section 6.

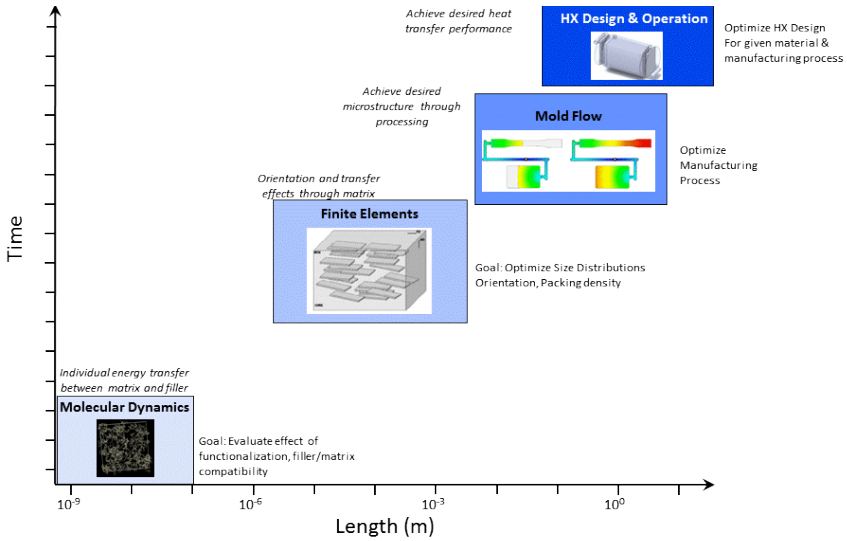

Figure 25. Time and length scale associated with polymer-based HX design

6.1 Thermal Conductivity Modeling

Heat conduction is due to propagation of a phonon that is a quantized atomic lattice wave. This phonon can be understood simply as a vessel carrying heat energy. It is well known that heat conductivity of a solid is a function of distance and velocity of the phonon [34]. Any boundary and defect in a material can disturb the mean free path of the phonon, and thus cause a decrease in thermal conductivity. This phenomenon is called phonon scattering. In the case of metals, due to the large crystal domain size and high degree of crystallinity of highly-ordered atoms, moving distance and velocity of the phonon are long and fast so that the intrinsic thermal conductivity can be very high, while for polymeric materials, their low degree of crystallinity, small crystal size and the presence of amorphous areas and chemical impurities can cause tremendous phonon scattering, leading to a dramatic decrease in thermal conductivity. Hence, the thermal conductivity of a typical metal is about one thousand times higher than that of a polymer. Understanding phonon propagation and scattering in thermally conductive polymer composites made of thermal conductive fillers in a polymer matrix is very complex for the following reasons: (1) phonon propagates through both polymer and conductive fillers; (2) phonon scatters at the boundary of polymer/filler and at the filler/filler boundary, (3) phonon scatters at grain boundary, amorphous/crystal boundary and defects or chemical impurities that are present in both polymer matrix and fillers.

In order to predict the thermal conductivity of the composite material, it is therefore necessary to understand the interactions between the matrix and the filler since efficient energy transfer between the matrix and the filler is critical to thermal performance. The interfacial thermal resistance, also known as Kapitza resistance, is a measure of the interface's resistance to thermal

flow. The resistance layer is a function of both the attraction of the filler for the matrix (enthalpy of mixing) and the ability of the matrix to geometrically surround the filler (entropy of mixing). The compatibility is determined based upon interaction energy of the two materials, where techniques such as functionalization of the filler or adding co-solvents could improve the thermal contact. The ability to geometrically surround the filler is related to the molecular structure and packing of the matrix. For a polymer, as the filler becomes smaller, there is an entropic penalty for the polymer to tightly conform around the filler, which results in either a reduction in the thermal contact or complete phase separation. The ability to wrap around a nanotube can be related to the persistence length, or the local stiffness of the polymer. Therefore, capturing the thermal resistance layer between the polymer and matrix is an important design variable to select the best material.

The first approach usually considered in the estimation of properties of composite systems is a rule of mixtures using the volume fraction or weight fraction. However, this approach fails spectacularly for determining the thermal conductivity of a composite system, with most thermal conductivities of composite systems well below what would be expected from simple weighted-averages of pure component thermal conductivity. This is the result of the interfacial resistance in heat transfer between the two components not being explicitly included, which significantly decreases the conductivity that could be achieved if no resistance layer was present.

There have been many different models developed to predict the thermal conductivity. For infinitely dilute solutions, Maxwell [35] derived the exact expression for composite thermal conductivity as

$$\frac{k_c}{k_m} = 1 + 3\left(\frac{k_f - k_m}{k_f + 2k_m}\right)\phi \tag{6-1}$$

where k_c, k_m, k_f are the thermal conductivity of the composite, matrix, and filler, respectively, and ϕ is the volume fraction of filler present. However, the lack of interaction between particles makes the Maxwell equation not useful for any finite concentration of particles. Various other dilute concentration relationships for thermal conductivity of composites have been developed [36-42]. While these models can capture the dramatic increase in thermal conductivity with increased filler volume fractions, there is typically varying degrees of success that can be applied without rigorous empirical fitting for each system of interest. Another empirical attempt was developed to account for the change in thermal conductivity that occurs over the entire concentration range, including the dramatic increases that occur from percolation [43] This method only has one parameter; however, a fair amount of knowledge of the composite system is required to use the approximations reliably in this approach as well. Ultimately, one of the main drawbacks of all these equations is the use of empirical parameters. The empirical parameters require information about the system in advance, often requiring experiments. These limitations make the empirical percolation models near impossible to use for novel composite design because even effects such as functionalization can dramatically impact the results. Even for evaluation of materials, these models can provide challenges unless all the relevant systems have been characterized and the effects such as size distribution and orientation are understood and accounted for properly.

Molecular dynamics (MD) has been used to determine the thermal conductivity in a variety of different systems. It has also been applied for understanding the thermal transport in composite materials including carbon nanotubes [44-52]. Because MD probes the individual interactions between atoms, it provides a natural method to determine the atomic level effects on the thermal

conductivity and resistance layers formed in the composite material. This technique allows for the energetic coupling between the materials to be evaluated and evaluate the impact of functionalization and dispersion on the thermal conductivity of the composite.

Non-equilibrium simulation methods are frequently used to simulate the thermal conductivity, and have also been applied to determine the resistance across composite systems [44-47]. In this approach, a heat source is created on one boundary of the system and a heat sink in created on the opposing boundary. The heat source artificially and continually adds heat to the system while the heat sink artificially and continuously removes heat from the system. Between the heat source and heat sink a thermal gradient is established. With knowledge of this thermal gradient as well as the heat flow through the system, the thermal conductivity of a normal homogeneous system can be determined by applying Fourier's Law. For composite systems, there are changes in the temperature gradient between transitioning from the matrix to the filler, which give the thermal resistance layer. The accurate representation of the phonon transport [53] limits these simulations and requires very large systems to avoid length effects [54] and quantum corrections are also necessary to capture phonon effects on the temperature during thermal transport [55]

Equilibrium MD simulations have also been used to determine the thermal resistance layer effect [48-52]. These simulations directly heat the filler particle while maintaining the matrix at a lower temperature. The two components are then allowed to thermally equilibrium through equilibrium MD. The time constant for the decay of the thermal gradient between the matrix and the filler is related to the thermal resistance, R_K:

$$R_K = \frac{\tau A_T}{c_T} \tag{6-2}$$

where A_T is the area of the nanotube and c_T is the nanotube heat capacity. This method has been validated experimentally for carbon nanotubes dispersed in a surfactant solution and found to be in excellent agreement [39]. This method depends on knowing the thermal conductivity of the filler and matrix separately. Additionally, the thermal resistance calculated only provides one piece of the overall thermal conductivity of the composite. Other methods are required to determine the overall thermal conductivity of the composite.

One method to relate the thermal resistance to the overall thermal conductivity is through analytical expressions using an effective medium (e.g. [55]) model for random orientation of nanotubes in a polymer matrix [48, 52] This method requires the thermal conductivity of the filler and matrix, the length and diameter of the nanotube, and the volume fraction along with the thermal resistance, R_K, to determine the effective thermal conductivity of the composite. This provides a direct way to evaluate the thermal conductivity. Using some transformations for the directionality of the heat transfer, a first order approximation of nanotube orientation either parallel or perpendicular can also be evaluated.

Finite element models provide another method to analyze the overall thermal conductivity of the composite [52, 56]. In this case the model can be constructed to account for various properties of the filler including dispersion, orientation, and size distribution for example. Additionally, the variation with parts that occurs during processing can be captured to determine the impacts on overall thermal conductivity. The finite element models use the solution of the larger scale system to capture the overall effects and include the heat transport through the matrix and filler as well as the thermal resistance layer.

Accuracy of theoretical predictions of thermal conductivity of composites

Non MD models with fitting parameters

Several authors investigated the accuracy of the theoretical and empirical thermal conductivity models by comparing with experimental results. Kumlutas [56] produced HDPE composites filled with tin by compression molding and compared experimental thermal conductivity of the composites with several theoretical predictions. Figure 26 shows the status of tin distribution in HDPE. The particles are almost spherical; in addition, some aggregates are observed in the images. In this study, tin particles with sizes of 20-40 μm were used, and intrinsic thermal conductivity of HDPE and tin was measured as 0.554 and 64 W/mK respectively.

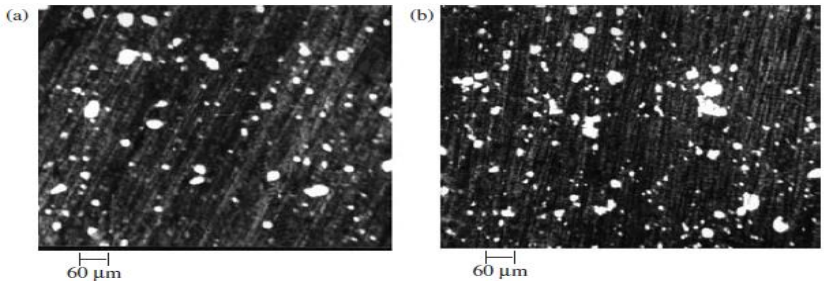

Figure 26. Microscopic photographs of HDPE filled with tin (a) 10 volume % and (b) 16 volume % [56]

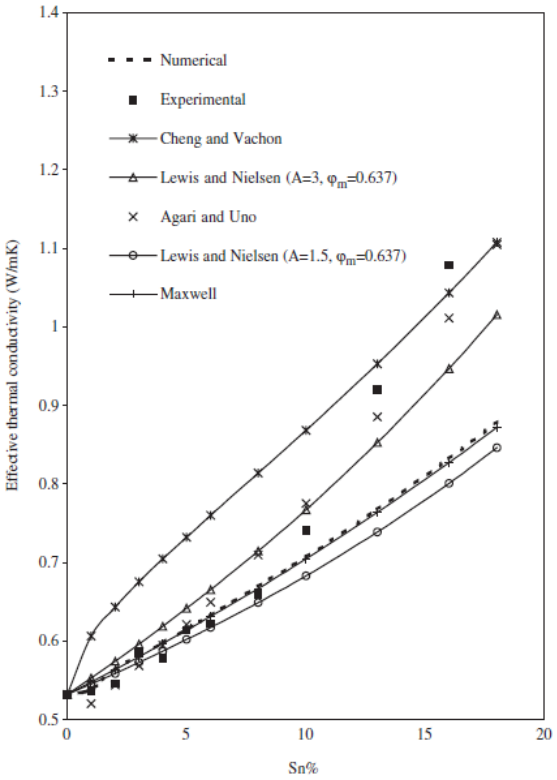

Figure 27 shows the plots of experimental results and several theoretical predictions in thermal conductivity as a function of tin volume percentage. The authors insisted that most theoretical models except that of Cheng and Vachon model [36] could predict the thermal conductivity well at low volume percentage of the filler (less than 10 volume percentage), but the predictions deviated from the experimentally determined values with the filler contents of 10 volume percentage and higher.

Figure 27. Comparison of experimental and model thermal conductivity values of tin-filled HDPE [56]

Wong and Bollampally [57] reported that the Agari and Uno model provided a good estimate for thermal conductivity of epoxy resins filled with ceramic fillers such as, alumina, and aluminum nitride. In their experiments, epoxy composites with 50 volume percentage of alumina and silica-coated aluminum nitride (SCAN) showed around 10 times higher thermal conductivity than the intrinsic thermal conductivity of the epoxy resin.

Hill and Supancic [58] investigated the thermal conductivity of platelet particles filled polymer composites and compared the experimental results with the theoretical predictions. Morphological features of the used fillers are seen in Figure 28. In their experiments, the composite with soft platelet shaped boron nitride (BN) fillers had better thermal conductivity. The soft BN is better for forming particle-to-particle connectivity in the polymer matrix than hard or stiff ceramic particles. The achieved thermal conductivity from the BN filled composite was 13 W/mK.

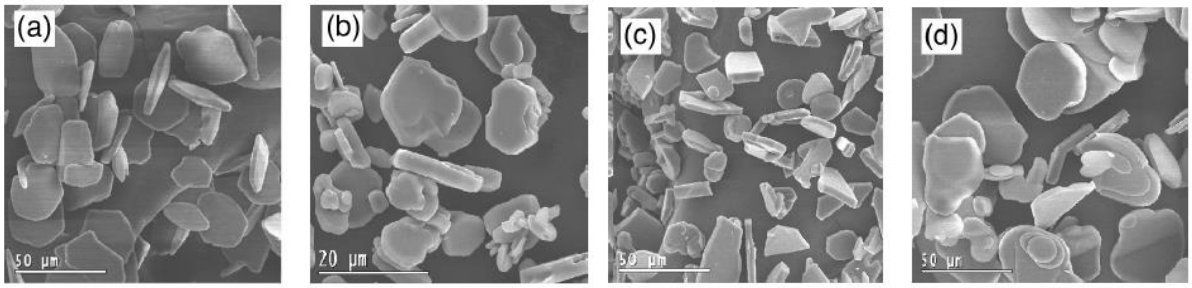

Figure 28. SEM micrographs of Platelet fillers of (a) Al2O3 (b) TiB2 (c) SiC (d) BN [58]

The authors concluded that the Maxwell model failed to predict the thermal conductivity because the model assumes no connections between the fillers. The authors added that the Cheng and Vachon model does not have the terms to take into account the shape and connectivity of fillers. Lewis and Nielsen model could estimate the thermal conductivity well as seen in Figure 29, but the authors acknowledged that the predicted results were affected by an arbitrarily chosen number of fitting parameters which is considered a disadvantage of the Lewis and Nielsen model.

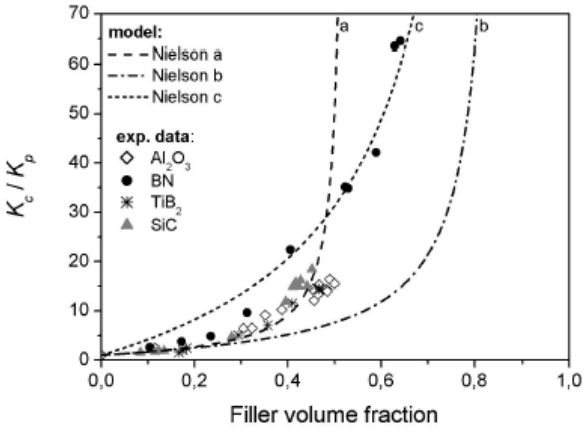

Figure 29. Lewis and Nielsen prediction for (a) A=5 and $\emptyset_m$=0.52, (b) A=5 and $\emptyset_m$=0.52 , (c) A=30, $\emptyset_m$= 0.85 [42]

MD model

In order to evaluate the composite thermal conductivity, the thermal resistance layer between the filler and the matrix needs to be determined. The thermal resistance layer provides significant resistance to thermal transport. A molecular level determination of the resistance by molecular dynamics is used, where the resistance calculated from MD is used in an effective medium approach to determine the composite thermal conductivity from the interfacial resistance and the filler and matrix thermal conductivities [59]. This method was validated using literature data for

Carbon NanoTubes (CNT) dispersed into high density polyethylene [60, 61] and polyisoprene [62]. The thermal resistance was calculated using the method in Reference [59] and the computed thermal conductivity was compared to the measured thermal conductivity. A good comparison is shown in Figure 30 between HDPE and CNT for lower volume fractions. Higher volume fractions (~20 vol%) demonstrate the model under predicts the thermal conductivity because the model assumes the fillers only interact with the matrix. The comparison between polyisoprene and CNT are also generally quite good as shown in Table 11. There is less characterization of the CNT length in this sample, so two different fiber lengths are considered. The assumption of shorter CNT length shows fairly good comparison with the experimental measurements. Overall, the method is validated and works well. The requirement is that the filler geometry is well characterized as it occurs in the composite.

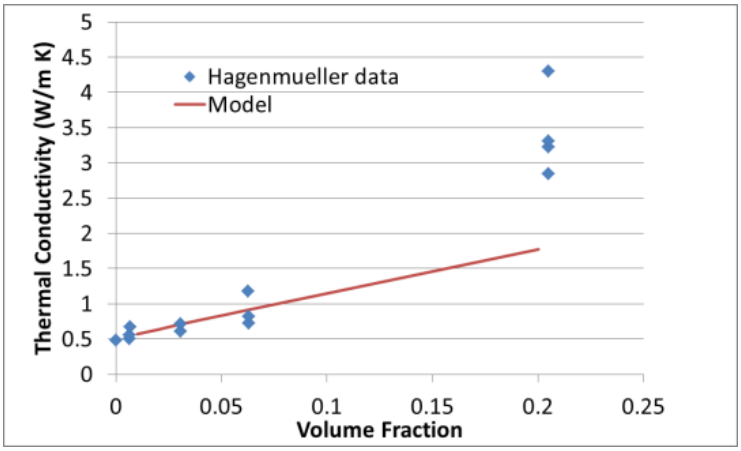

Figure 30. Comparison of the calculated and experimental thermal conductivity of HDPE and CNT from Reference [60]

Table 11. Comparison of calculated and experimental thermal conductivity of polyisoprene and CNT from Reference [61].

Measurement	1 wt%	5 wt%
Experimental	0.19	0.33
500 nm long CNT	0.22	0.49
1000 nm long CNT	0.28	0.82

Prediction of Polymer-Filler Systems

The molecular dynamics approach was used to calculate the thermal resistance between various fillers and polypropylene (PP) and polyphenylene sulfide (PPS). The fillers were selected to represent different characteristics of carbon nanotubes, bucky balls, graphene sheets, and boron-nitride nanotubes (BNNT). The calculated thermal resistance for each of these cases is shown in Table 12. There is less resistance observed for the PP composites compared to the PPS composites. Functionalization of the CNT does show some reduction in the thermal resistance. The small size of the bucky balls overall compared to the other fillers likely creates difficulty in the polymer to wrap around the structure and reduces the ability to efficiently interact and transfer energy. The lowest thermal resistance was determined for BNNT. The reduced thermal resistance of BNNT could be a coupling between the charged surface of the BNNT with polymer, especially PPS. The slight reductions in thermal resistance for the functionalization also

would correspond to this idea that the nanotube charge helps efficiently couple the two materials for thermal transport as there is slight amounts of charge on the CNT near the area of the functionalization.

Table 12. Calculated thermal resistance for various filler-matrix pairs (10^{-9} m^2 K W^{-1})

Filler	PP	PPS
SWCNT (10,0)	7.7	11.5
SWCNT (18,0)	7.3	
SWCNT (30,0)	7.3	
MWCNT [(10,0 + (18,0)]	10.8	
SWCNT (10,0) + 25% OH modification	6.8	9.0
SWCNT (10,0) + 25% COOH modification	7.5	8.8
SWCNT(10,0) in bundle of 4 tubes	10.2	
SWCNT (10,0) in bundle of 7 tubes	10.5	10.6
Bucky Ball (single)	22.8	20.0
Bucky Ball (multiple)	16.8	24.0
BN Nanotube	3.8	4.5
Graphene sheet (smaller)	5.2	7.4
Graphene sheet (larger)	6.8	8.5

UTRC-developed Finite Element Model

To allow the modeling of highly filled systems that are typical of commercially available materials, a Finite Element Analysis (FEA) model was developed for thermal conductivity prediction. The model (based on COMSOL®) solves stationary heat conduction equation with optional thermal resistance at the polymer/filler interface. The governing equation for heat conduction and the interfacial thermal resistance are listed below.

$$\rho C_p \mathbf{u} \cdot \nabla T = \nabla \cdot (k \nabla T) + Q \tag{6-3}$$

$$-\mathbf{n}_d \cdot (-k_d \nabla T_d) = -h(T_u - T_d) \tag{6-4}$$

The computational domain includes a segment of the material with several repeating filler elements. Grid independence study was conducted to ensure sufficient grid resolution. The thermal conductivity is derived based on an internal representative section, which is not affected by the surrounding boundary. Figure 31 shows a typical computational domain including 10 repeating elements with periodic boundary condition at the top-bottom pair, and temperature boundary condition at the two ends. The methodology of thermal conductivity derivation is illustrated by using two repeating elements in the domain that is >2 elements far from the boundaries no matter what kind of boundary conditions are at both ends (temperature or flux). It also shows that the thermal conductivity derived based on this method is similar to the one derived from a much large domain, therefore could be used to decide the minimum elements required in the model. The model can be used to model both in plane and through plane thermal conductivity.

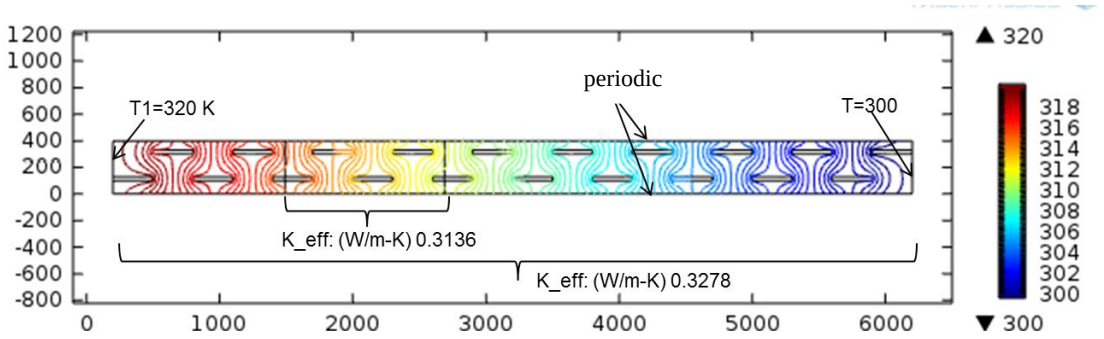

Figure 31: Typical computational domain; also the method for thermal conductivity derivation

A Sensitivity study was conducted by varying filler load, filler aspect ratio, filler alignment pattern, polymer thermal conductivity, and the effect of interfacial thermal resistance. It was found that interfacial resistance could significantly lower the thermal conductivity of the polymer composite. As an example, Figure 32 shows the degradation for filler (k_filler=1000W/K-m) loaded in polymer (k_polymer=0.15 W/K-m), with a volumetric fraction of 7.5%.

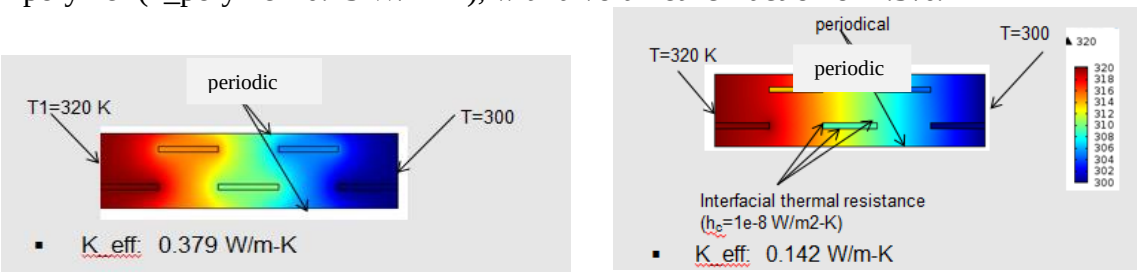

Figure 32: Degradation of polymer composite thermal conductivity due to interfacial thermal resistance

Figure 33 compares temperature contours and composite thermal conductivity as the filler aspect ratio changes. Generally, axially elongated filler with minimum gap between adjacent fillers results in higher thermal conductivity.

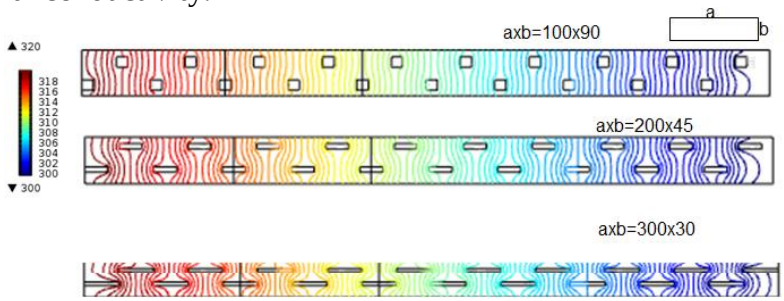

axb	K_eff
100x90	0.182
200x45	0.225
300x30	0.313
450x20	0.500

Figure 33: Comparison of temperature contours and thermal conductivity as filler aspect ratio changes.

Figure 34 shows the effect of filler loading rate, as well as filler alignment pattern and aspect ratio. As expected, it indicates that increase of filler loading rate and reduction of filler gaps would help improve the thermal conductivity of the composite.

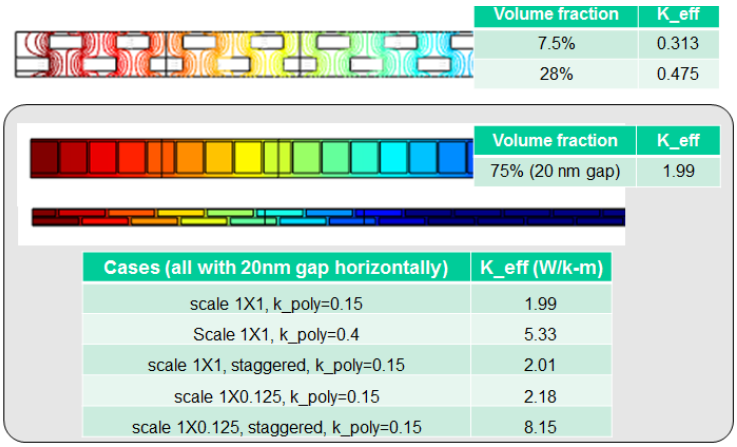

Volume fraction	K_eff
7.5%	0.313
28%	0.475

Volume fraction	K_eff
75% (20 nm gap)	1.99

Cases (all with 20nm gap horizontally)	K_eff (W/k-m)
scale 1X1, k_poly=0.15	1.99
Scale 1X1, k_poly=0.4	5.33
scale 1X1, staggered, k_poly=0.15	2.01
scale 1X0.125, k_poly=0.15	2.18
scale 1X0.125, staggered, k_poly=0.15	8.15

Figure 34: The effect of filler loading rate, as well as filler alignment pattern and aspect ratio

The model was validated based upon a commercially available material. The material was characterized using the methods outlined in Paragraph 2 of this section and, in particular, the filler gravimetric loading, aspect ratio and direction were measured and used as input for the model. As shown in Figure 35, the filler was represented as rods of equal length. It was found that the tilt angle of every other neighboring column showed a significant effect on the through plane thermal conductivity and enabled to bracket the experimentally measured thermal conductivity.

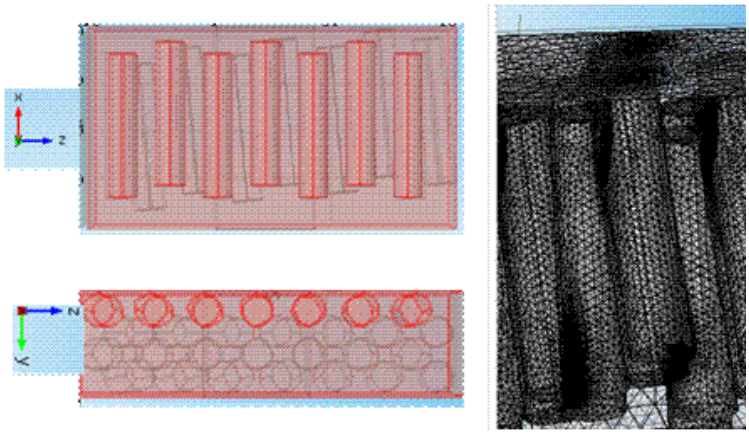

Figure 35: Filler characteristics for model validation

Therefore, the model could be used to virtually design better composite materials with improved manufacturability characteristics, for example, by reducing the filler content while maintaining the thermal conductivity.

UTRC-developed Finite Element Model – Parametric Sensitivity Study

The model was used to perform a parametric study in order to understand which parameters are most important to improving polymer thermal conductivity. The model was set up as shown in

Figure 36. The outputs from the simulation were the fill ratio (by vol.) and the in-plane and through-plane conductivities.

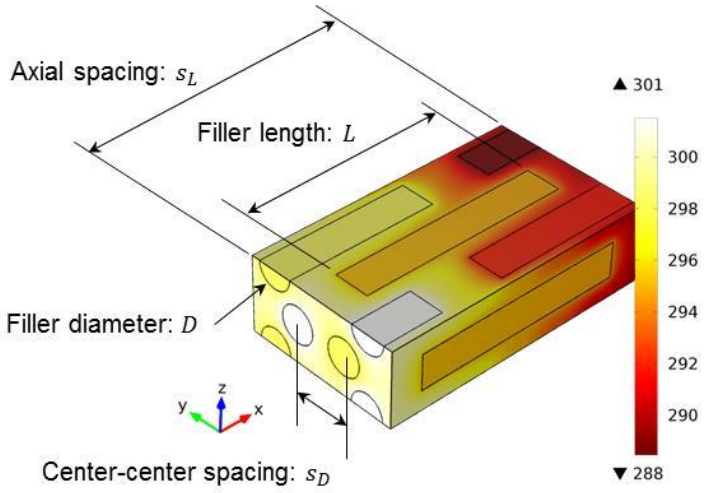

Figure 36. Representative composite volume with parameters

Table 13 shows the parameters that were investigated and their range. This resulted in 5184 parameter combinations, each requiring two simulations: one to model in-plane thermal conductivity and one to model through-plane thermal conductivity.

Table 13. Parameter range for sensitivity analysis study.

Parameter	Units	Values			
Filler diameter D_{filler}	μm	0.1	1	10	100
Filler aspect ratio L/D	—	1	6	60	—
Axial spacing ratio s_L/L	—	1.25	1.50	1.75	2.00
Ctr-ctr spacing ratio s_D/D	—	1.25	1.50	1.75	2.00
Matrix thermal conductivity k_{matrix}	W/(m·K)	0.1	0.4	1	—
Filler thermal conductivity k_{filler}	W/(m·K)	40	400	1000	—
Interfacial thermal resistance $R_{th,i}$	K·m²/W	1e-9	1e-8	1e-7	—

Table 14 gives a summary of the parametric study which shows that filler aspect ratio and matrix and filler thermal conductivity and the interfacial resistance have significant effect on the material thermal conductivity, both in plane and through plane. Such knowledge can be used to optimize the material composition and filler configuration. Figure 37 to Figure 39 show selected results from the parametric study.

Table 14. Summary of findings for parametric study.

Parameter	% Loading	In-plane	Through-plane
Axial spacing ratio s_L/L	Inversely proportional	Moderate effect; effect becomes larger when s_D/D is small	Negligible effect
Ctr-ctr spacing ratio s_D/D	Inversely proportional	Moderate effect; effect becomes larger when s_D/L is small	Moderate effect (k_z increases as s_D/D becomes small)
Filler diameter D_{filler}	No effect	Small effect (unless $R_{th,i}$ is large, then larger diameter fibers are beneficial)	Negligible effect
Filler aspect ratio L/D	No effect	Significant effect: longer-aspect fibers significantly increase k_x (especially if k_{filler} is large and/or k_{matrix} is small). Effect further increases when s_L/L and/or s_D/D is small	Negligible effect
Matrix thermal conductivity k_{matrix}	No effect	Significant effect	Significant effect
Filler thermal conductivity k_{filler}	No effect	Large effect, especially for long and/or closely-spaced fibers	Small effect, becoming more significant for closely-spaced fibers (small s_D/D)
Interfacial thermal resistance $R_{th,i}$	No effect	Becomes significant if matrix and/or filler thermal conductivity is large, fiber center-to-center spacing is small, fiber diameter is small	Becomes significant if matrix and/or filler thermal conductivity is large, fiber axial spacing is small

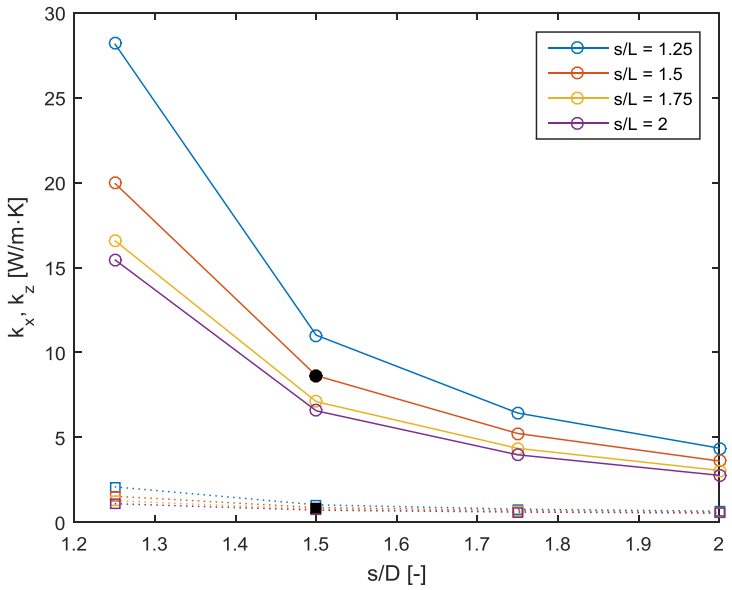

Figure 37. Effect of center-to-center spacing ratio (s/D) on in-plane thermal conductivity (k_x -solid lines) and through-plane thermal conductivity (k_z – dashed lines) at various axial spacing ratio (s/L) – As expected, both thermal conductivities increase as the composite because more highly filled.

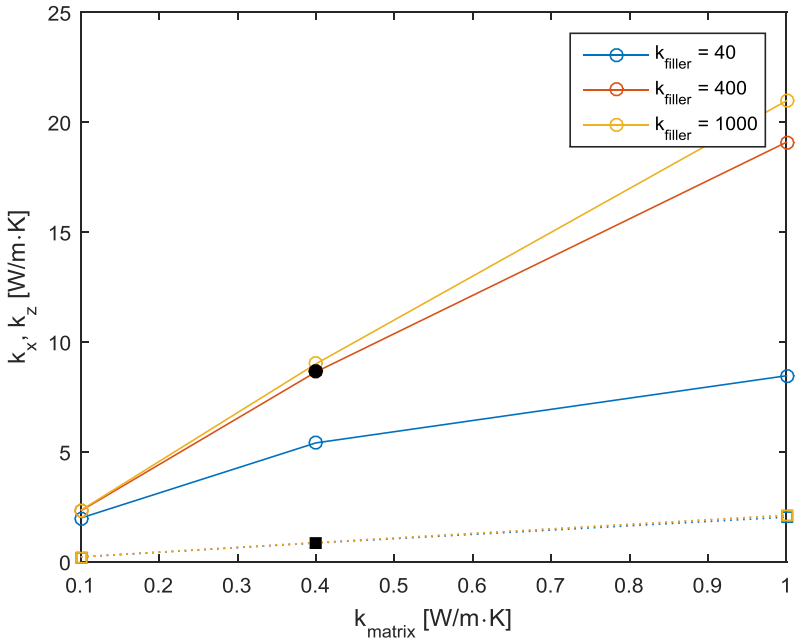

Figure 38. Effect of the polymer matrix thermal conductivity on in-plane thermal conductivity (k_x -solid lines) and through-plane thermal conductivity (k_z – dashed lines) at various filler thermal conductivities for 33% loading. The matrix thermal conductivity has a significant effect on the in plane thermal conductivity and on the through plane thermal conductivity.

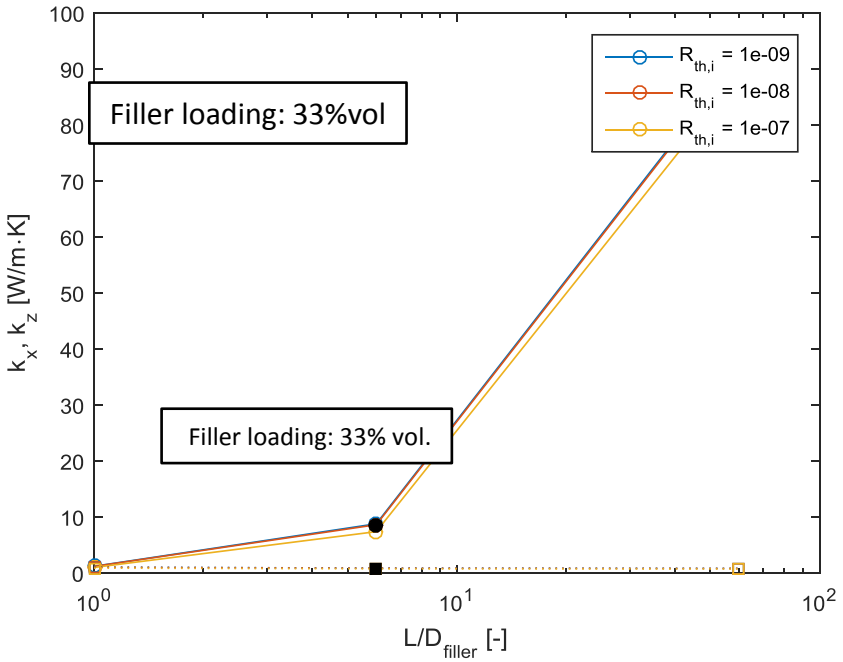

Figure 39. Effect of filler aspect ratio on in-plane thermal conductivity (k_x -solid lines) and through-plane thermal conductivity (k_z – dashed lines) at various interfacial resistances for 33% loading. Long thin fillers lead to large benefits for the in plane thermal conductivity.

6.2 Mechanical properties

There is significant interest in filled polymer composites because improvements in mechanical properties can be achieved from adding small amounts of filler. Silica and clay particles have been used in polymer composites for reinforcement for many years, while the effects of carbon nanotubes have been more recently investigated. The improvement in mechanical properties of filled composite polymers compared to the bulk materials themselves has been investigated extensively both experimentally and through modeling

Similar to thermal conductivity interactions in composite materials, an interphase region exists where the properties transition between that of the bulk material and that of the filler. The change of matrix response in the interphase region can result from conformational changes of the matrix or physical grafting between the two phases. Modeling the mechanical transfer between the two phases in this region requires an accurate description of the change in mechanical properties as these effects can influence the overall mechanical response of the material [63].

Liu and Brinson [64] used a simple comparison between different tubes and platelets dispersed in a polymer matrix to demonstrate the influence of the interphase region. The filler materials were assumed to have the same interphase properties regardless of particle shape. When comparing the same volume fraction of filler, the nanotubes were found to have significantly higher stiffness compared to the platelets because of the increased surface area to volume available for the same volume fraction of nanotubes that allows for significantly more interphase region to impact the composite properties.

Elastic property models have been developed for composites. The two main models used are the Halpin-Tsai [65,66] and Mori-Tanaka [67,68] models.

The Halpin-Tsai model is

$$\frac{E_c}{E_m} = \frac{1 + \xi\eta\phi}{1 - \eta\phi} \tag{6-12}$$

where E_c and E_m are the composite and matrix Young's modulus respectively, ϕ is the volume fraction of filler and η is given by

$$\eta = \frac{{E_c}/{E_m} - 1}{{E_f}/{E_m} + \xi} \tag{6-13}$$

where E_f is the filler Young's modulus and ξ is a directional shape parameter related to the longitudinal and transverse directions of the composite Young's modulus. The Halpin-Tsai model is for predicting stiffness for anisotropic particles and reduces to the rule of mixtures for isotropic filler particles.

The Mori-Tanaka model is

$$\frac{E_{11}}{E_m} = \frac{A_0}{A_0 + \phi(A_1 + 2\nu A_2)} \tag{6-14}$$

$$\frac{E_{22}}{E_m} = \frac{2A_0}{A_0 + \phi(-2A_3 + (1-\nu)A_4 + (1+\nu)A_5 A_0)} \tag{6-15}$$

where E_{11} and E_{22} are the longitudinal and transverse Young's modulus of the composite, ν is Poisson's ratio of the matrix and A_0, A_1, A_2, A_3, A_4, and A_5 are elements of Eshelby's matrix and properties of the filler and matrix including Young's modulus, Poisson's ratio, filler concentration and aspect ratios.

These models account for the effect of volume fraction and shape of the particles. It is assumed that a perfect-bonding interface exists between the matrix and filler and there is no interphase region with different material properties from the bulk matrix properties. These models can be effective for larger fillers with good interfacial bonding where the interphase region is very small compared to the overall effects of the matrix and filler. To further account for the interphase region, an effective interface model [69,70] was developed. Using this model, it was demonstrated that the effects of the interphase region for very small fillers can be identified, which transition to the Mori-Tanaka limit for larger filler diameters.

Molecular dynamics simulations have also been used to investigate the atomistic scale contributions to the mechanical strength of nanocomposites. Many simulations have focused on the elastic properties of the interphase region [69, 70-76]. The localized properties of the interphase region are examined, but only in the elastic region. There have been some attempts to simulate the fracture strength of polymer nanocomposites using MD [77]. In this case, polymers with a glass transition temperature above room temperature did not toughen by adding nanoplatelets. An improvement in fracture toughness was observed for polymers with a glass transition temperature below room temperature.

Finite element analysis (FEA) has been used to investigate the mechanical properties of polymer nanocomposites. The analysis was limited to the elastic properties of the materials, in many cases the evaluation of stiffness, elastic modulus, and shear modulus [78,79,80,81]. The effects of debonding were also investigated [82], revealing that while the interphase region increased the stiffness it concomitantly promotes debonding. The effects of nanotube waviness [83, 84] was also investigated and found that the waviness reduced in the effect of the interphase and resulted in less overall stiffness compared to perfectly straight nanotubes. Overall, FEA has been used to determine the effects at larger length and time scales than available through MD; however, these simulations have still been limited to elastic response and require separate description of the interphase region mechanical properties.

A coupled MD/FEA model was developed by Choi, *et al.* [63] to describe the interphase region between a silica nanoparticle and a cross-linked EPON 862 epoxy resin cross-linked with TETA hardener. An integrated approach to integrate the uniaxial tensile results from the MD simulations with those obtained from the FEA simulations to ensure continuity between the localized length scales in interphase region and the bulk polymer matrix. The Young's and shear modulus were used to ensure continuity between the atomic level and continuum level models. The results revealed that the conformation changes around particles (radii from 5.18 – 11.50 Å) did not affect the mechanical strength, but that the changes in non-bonded energetic interactions did change the mechanical properties. So far these simulations were only performed for elastic deformations.

Validation of strength models is available in the literature for example for graphite epoxy composites [85], however they invariably use a calibration parameter (for example "effective aspect ratio") that enables improvement of the fit.

The Mori-Tanaka model was developed for predicting the elastic properties of an isotropic particle in a matrix (Figure 40).

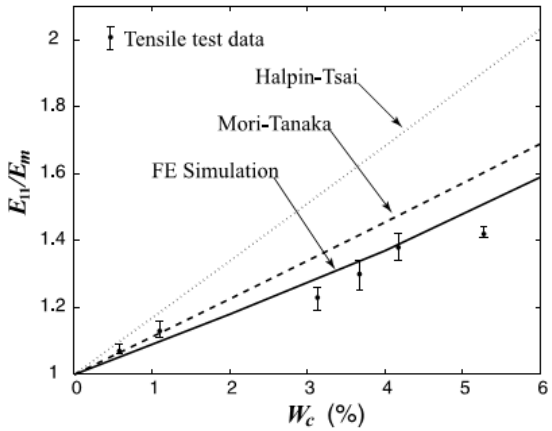

Figure 40. Experimental and calculated effective longitudinal modulus for MXD6/clay nanocomposites [86] showing the superiority of the FE model.

ABAQUS modeling

The models detailed above address material level properties. However, there is a need to evaluate strength at the component as well. To do so, an ABAQUS model was set up to evaluate the strength behavior of the down-selected of plate and frame heat exchanger. The plate configuration was based on a typical commercially available HX featuring chevron type surface enhancement to improve thermal performance (Figure 41). Note that the plates are stacked after an 180^o rotation, leading to evenly distributed contact points between the plates. The stress analysis carried out on the assembly showed that stress point will occur at the contact points (Figure 42) and, therefore, the assembly's mechanical performance will be dictated by the joining method of the plates.

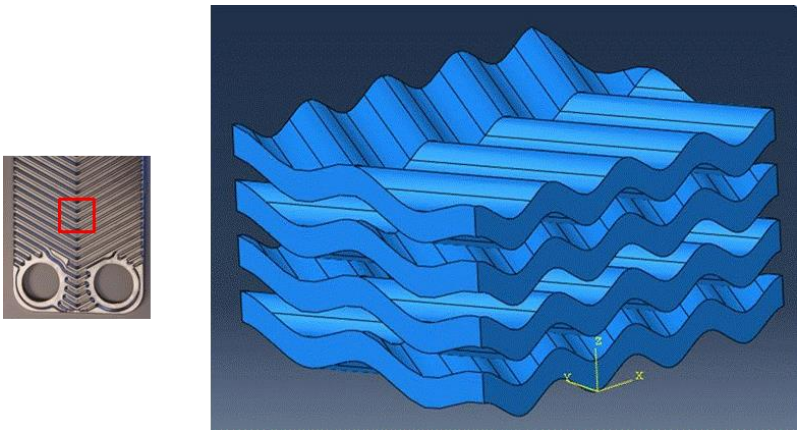

Figure 41. ABAQUS model for Plate and Frame heat exchanger.

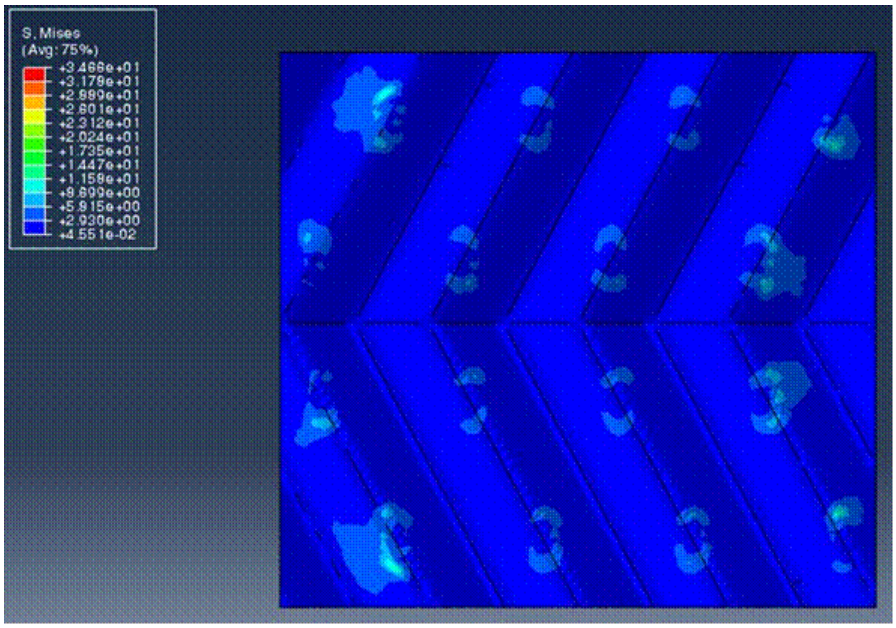

Figure 42 ABAQUS stress analysis for Plate and Frame heat exchanger.

The manufacturing techniques used and overall assembly of the HX should ensure that the strength at the contact point is adequate for the integrity of the assembly to be maintained under its operating pressure.

6.3 Gas Permeation in Composite Polymers

Gas permeation through semicrystalline polymer is generally described via Fickian model [87].

$$\boldsymbol{J = -D\frac{S\Delta p}{l}} \qquad\qquad \boldsymbol{K = -D\frac{J.l}{\Delta p}}$$

J is flux of permeating gas; *D* is diffusion coefficient; *S* is sorption coefficient or solubility; *Δp* is pressure drop across polymer interfaces; *K* is permeability ; *l* is thickness of sample. This model assumes linear-drop of pressure across polymer thickness and no interaction between polymer and permeating gas. When the above stated assumptions are not valid, it is referred to as non-Fickian behavior.

The Nielsen model is one of earliest models developed for estimating permeability of polymer composite [88,89]. As shown in Figure 43, the model assumes finite-sized rectangular platelets (ribbon-like), with gas diffusion direction normal to plane direction of the filler [89].

$$\boldsymbol{\frac{K_{composite}}{K_{matrix}} = \frac{1-\phi}{1+\frac{\alpha\phi}{2}}}$$

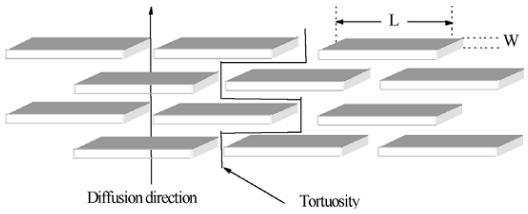

Figure 43**.** Arrangement and shape of filler as assumed by Nielsen model [88]

$K_{Composite}$ and K_{matrix} are permeabilities of polymer composite and polymer matrix respectively; φ is volume fraction of the filler; α is the layer aspect ratio ($\alpha\varphi/2$ is termed as tortuosity)
Choudalakis et al. [89] predicted relative permeability of several systems and compared it to those obtained from experiments for O_2 and H_2O vapor (Figure 44). These physical systems show good agreement with predicted values of relative permeability. Authors also mentioned that at low loading of fillers water vapor transport in montmorillonite/styrene-acrylate system is in good agreement with Nielsen model.

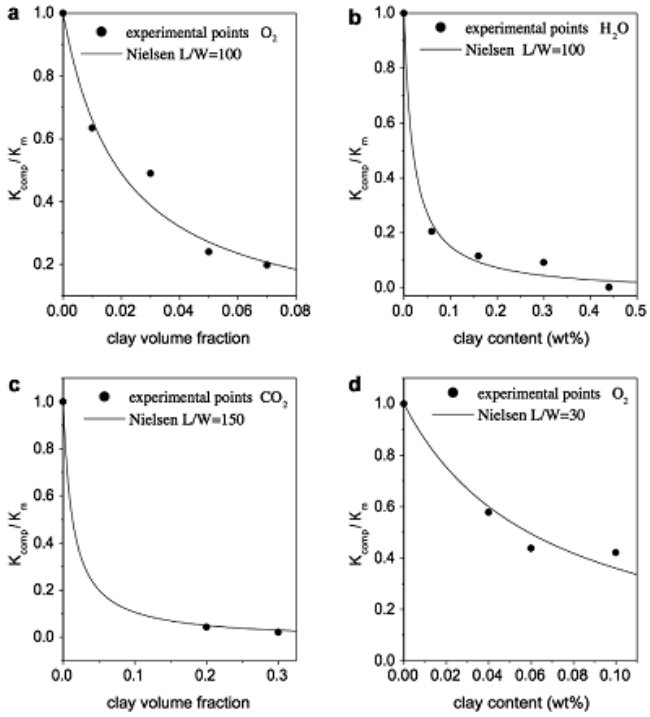

Figure 44. Comparison of experimental results to relative permeability of gases : (a) O_2 in epoxy/MMT (b) H_2O vapour in poly(e-caprolactone/MMT nanocomposite; (c) CO_2 in butyl rubber/vermiculite nanocomposite; (d) O_2 in PLA/MMT nanocomposite [89].

The Bharadwaj model [89,90,91] is similar to Nielsen model but includes the orientation factor (which modifies tortuosity term) to predict permeability. As observed by Dunkerley et al. for low loading regimes of PS/DMDT-MMT composite system, this model works well but shows large deviations from experimental data [91].

$$\frac{K_{composite}}{K_{matrix}} = \frac{1-\phi}{1+\frac{L}{2W}\phi\left(\frac{2}{3}\right)\left(S+\frac{1}{2}\right)}$$

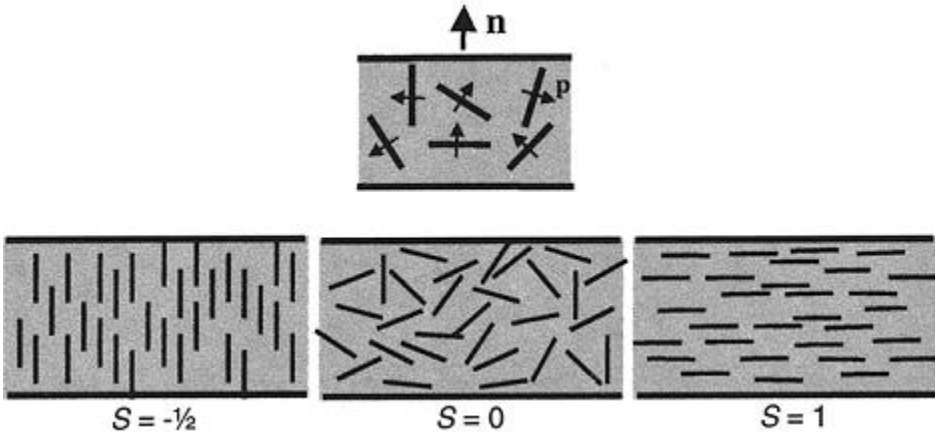

Figure 45**.** Orientation parameter of platelets [89][90]

The Cussler Model [92] is also similar to Nielsen model. However, it considers irregularity in arrangement of filler materials but not orientation. However, orientation corrected Cussler model is in good agreement with experimental data as observed by Dunkerley et al. [91]

$$\frac{K_{composite}}{K_{matrix}} = \frac{1-\phi}{1+\left(\frac{\alpha\phi}{2}\right)^2}$$

Recently, Lai et al. [93] reported that water permeability of cyclic olefin copolymer (COC)/thermally reduced graphene oxide (TRGO) composite is lower than predicted from Cussler and modified Nielsen models due to filler induced local rigidity. One of the possible reason for this deviation is exclusion of filler induced property changes/polymer-filler interactions in proposed models.

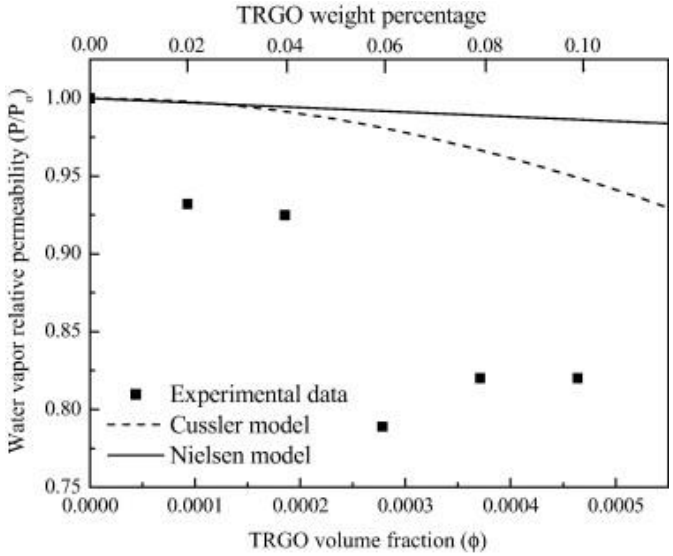

Figure 46. Experimental and modeled values of permeability of water vapor on TRGO [93]

Gusev and Lusti [94] suggested a stretched exponential function to fit experimental data with x_0 and β as fitting parameters. This model assumes disk-type filler materials. Authors claimed that this function predicts "better" estimate of permeability at higher loadings. It is observed by Schmidt et al. that incorporation of correction factor actually leads to deviation from experimental data. [91]

$$\frac{K_{composite}}{K_{matrix}} = e^{-\left(\frac{x}{x_0}\right)^{\beta}}$$

Fredrickson and Bicerano [95] model, based on scattering expansion, enabled calculation of permeability in dilute and semi-dilute regime. Similar to Gusev-Lusti model, this model also assumes disk-type filler materials. Macosko et al.[96] showed that CO_2 permeation through vermiculite-polyurethane composite agrees with model.

$$\frac{K_{composite}}{K_{matrix}} \approx F_m(\kappa\alpha\phi)$$

$$\kappa = \frac{\pi}{\ln \alpha}$$

$$F_m(\kappa\alpha\phi) = \left(\frac{1}{m}\sum_{j=1}^{m}\frac{1}{1+a_j x}\right)^2$$

2nd order approximation [95]

$$F_2(x) = \frac{1}{4}\left(\frac{1}{1+a_1 x} + \frac{1}{1+a_2 x}\right)^2$$

Table 15. Various models discussed in this report [91]

model	original formula (as published)	tortuosity factor
classic tortuosity (Nielsen[13])	$\frac{P_0}{P}(1-\phi) = 1+\frac{\alpha\phi}{2}$	$\tau = \left(\frac{\alpha\phi}{2}\right)$
reflective tortuosity (Cussler[2,15,45]) *regular array*	$\frac{P_0}{P}(1-\phi) = 1+\frac{(\alpha\phi)^2}{2}$	$\tau = \frac{(\alpha\phi)^2}{2}$
reflective tortuosity (Cussler[2,15,45]) *random array*	$\frac{P_0}{P}(1-\phi) = 1+\frac{2\alpha\phi}{3}+\frac{(\alpha\phi)^2}{9}$	$\tau = \frac{2\alpha\phi}{3}+\frac{(\alpha\phi)^2}{9}$
Gusev and Lusti[16]	$\frac{P_0}{P}(1-\phi) = e^{\left(\frac{\alpha\phi}{\sqrt{\pi}}\right)^{0.71}}$	$\tau = \left(e^{\left(\frac{\alpha\phi}{\sqrt{\pi}}\right)^{0.71}} - 1\right)$
Fredrickson and Bicerano[17,45]	$\frac{P_0}{P}(1-\phi) = 4\left[\frac{(1+x+0.1245x^2)}{(2+x)^2}\right]^2$ where $x = \frac{\pi\alpha}{2\ln\left(\frac{\alpha}{2}\right)}$	$\tau = \left(\frac{-1.01(2x+3)}{(x+2)^2+0.062x^2+0.748x+0.756}\right)$

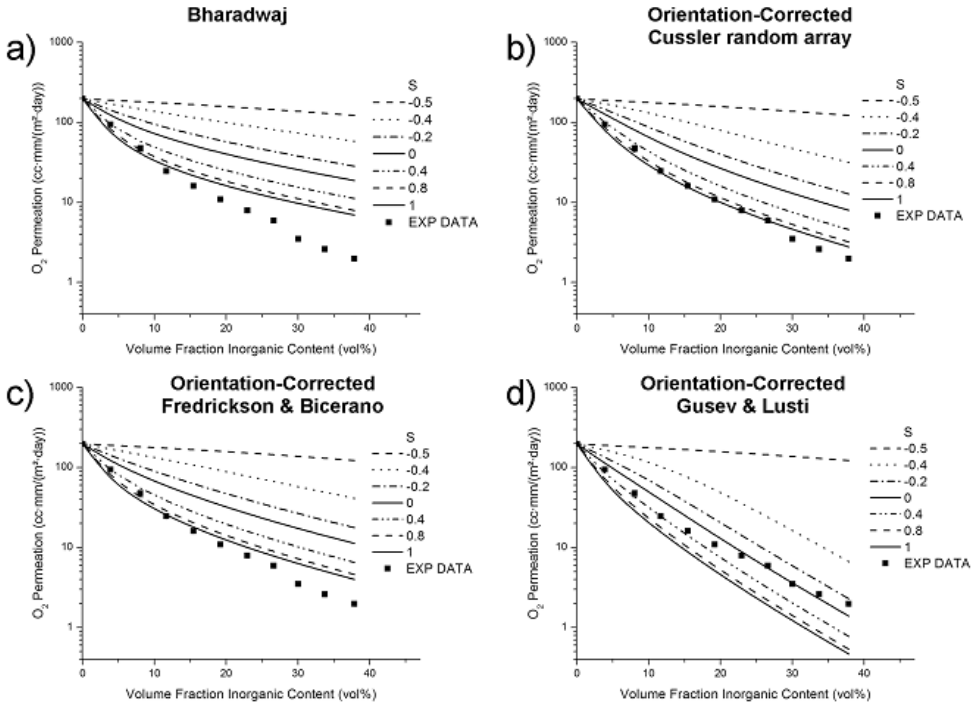

Figure 47**.** Experimental and modeled values of permeability of oxygen in polystyrene (PS)/dimethyl ditallow modified montmorillonite (DMDT-MMT) nanocomposites [91]

Orientation-corrected Gusev-Lusti and Fredrickson-Bicerano models are the best model to predict permeability of gas through polymers. Particularly for Polymer-HX with oriented particles and polymer chains, these models are useful.

6 Manufacturing options

A number of processing methods have been developed for conversion of polymers into useful products. Injection molding, compression molding, transfer molding, thermoforming, blow molding, film blowing, profile extrusion, and calendaring are some examples [97]. Among the various processing methods, choosing a proper one is critical to obtain acceptable quality at appropriate cost.

Injection molding is the one of the most popular processing method due to its utility and cost effectiveness. In this method, products even with complex shapes can be produced in mass production rates continuously. A traditional injection molding machine consists of two parts: an injection unit and a clamping unit as shown in Figure 48.

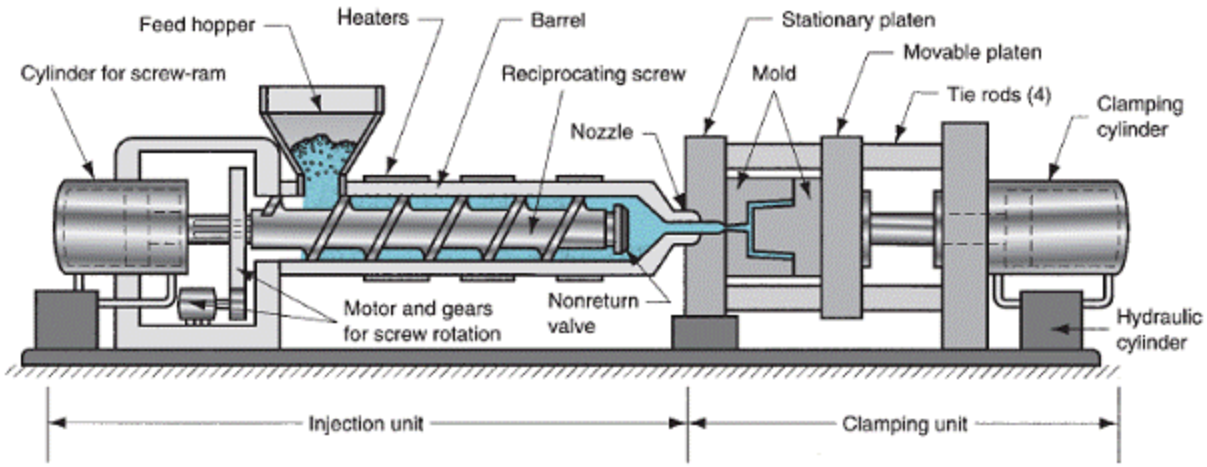

Figure 48. Two parts of a conventional hydraulic injection molding machine: injection and clamping units [98]

One cycle of injection molding has four steps in general [99]. The steps are (1) plastication: heating and melting of the plastic, (2) injection: injecting a controlled-volume shot of a melt into a closed mold under pressure. After filling, the injected material is maintained in the mold under pressure for specified time to prevent a back flow of the melt and to compensate for the decrease in volume of the melt during solidification. (3) Cooling: cooling the thermoplastic molded part in the mold, and (4) molded-part release: opening the mold, and ejecting the part. The cooling step takes most time in the cycle of injection molding, so effective cooling is important to reduce the processing time and the production cost. To shorten the time of the cooling step, a technology, such as rapid heating and cooling system has been developed [100].

Plastication is achieved by two heating mechanisms in the injection unit. One of the mechanisms is frictional heating by injection screw spinning. Another is heating from an outer heat source of heaters attached on the barrel of the injection unit. Solid resin pellets fed into the injection unit transfer to a nozzle by injection screw spinning, and the resin which is fully plasticated by the heat drifts out of the nozzle under pressure by a plunging motion of the screw. The clamping unit works on molds so that the mold does not open during the pressurized injection step.

Three motions of the clamping unit (rapid closing, slowdown of closing and clamping, and rapid open) are shown in Figure 49. The slowdown of closing before the mold faces come into contact is intended for minimizing the danger of mold damages [99]. Types of injection molding machines to be used are determined by the types of the clamping unit. A hydraulic clamp which uses a press powered by hydraulic force is a most popular type of injection molding machines. An electric clamp which is more energy efficient is use in another type of injection molding machines [99,101].

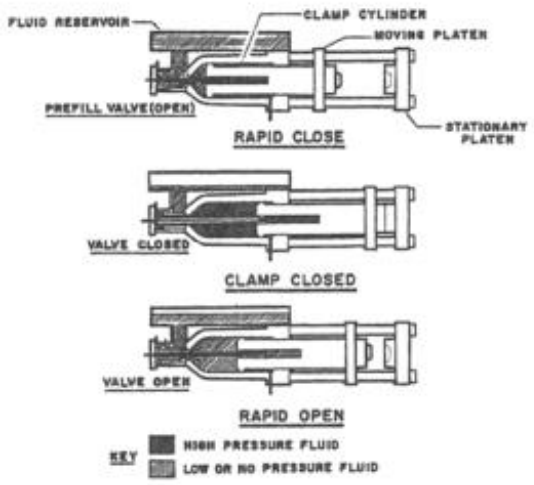

Figure 49. Hydraulic clamping actions [99]

A mold is a key part of an injection molding machine. Its design is directly related to the shape and size of the molded part. A two-plate mold which consists of two main parts – (a) a part held in the stationary platen of the clamping unit, and (b) a part held in the movable platen - is a most popular type of molds. Other types of molds, such as a three-plate mold and stack mold also exist. During injection molding, a polymer melt enters into a mold via a sprue. A sprue is placed in the stationary mold plate. The melt continuously flows through the runners and then enters the mold cavity via gates. Cavities are placed in the movable mold part. The components such as sprue, runners, gates, and cavities are shown in Figure 50.

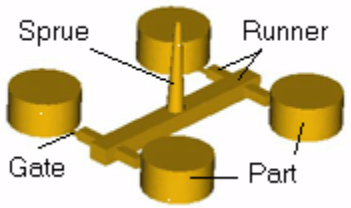

Figure 50. A schematic of an injection molded part showing sprue, runners, and gates [102]

Substantial changes of temperature and pressure occur in an injection molding process. These cause significant changes of volume of a molded part [103]. It indicates that the dimensions of a cavity should be designed taking into account the volume changes of the molded resin. The volume changes of semi-crystalline polymers are more significant and complex than those of amorphous polymers because both crystallization rate and crystallinity affect the volume changes. Approximately, it is known that the volume shrinkage of semi-crystalline polymers is around 1.5-2.0%, but that of amorphous polymers is around 0.5% [104]. For getting accurate dimensions in injection molding, understanding pressure-volume-temperature (PVT) relationships of a molded resin is important [105]. Recall that both temperature and pressure are all changed in injection molding processes.

Figure 51 shows schematics of PVT relationships of amorphous and crystalline polymers. A dramatic change of volume occurs at melting temperature (T_m) in semi-crystalline polymers. In injection molding, packing pressure is used during a cooling step to compensate for the volume

shrinkage. The principle of the packing pressure can be understood from Figure 51. For example, releasing the packing pressure to atmospheric pressure leads to an increase of the volume.

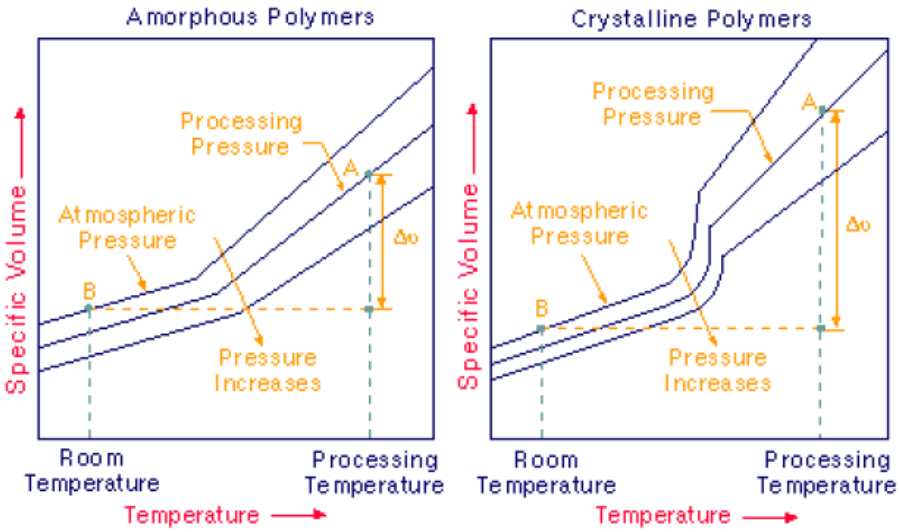

Figure 51. Schematic of volume changes of amorphous (left) and semi-crystalline polymers (right) in injection molding processes [106]

Dimensional changes of a molded part are also caused by another factor encountered in injection molding. The changes originate from releasing the residual stresses at a segment of a molded part after injection molding is done. Thus, controlling the residual stresses is also important for the quality control of the molded parts. The residual stresses are classified into two categories by their origins: flow-induced residual stresses and thermally-induced residual stresses [107,110]. Flow-induced residual stresses cause anisotropy of mechanical, thermal, and optical properties, while thermally-induced residual stresses cause warpage and stress-cracking [108] The flow-induced residual stresses are generated by high shear stresses encountered in melt flows, and the resultant molecular chain orientation near the wall of a cavity (frozen layers, Figure 52). As it can be expected, the flow-induced residual stresses are significant in a narrower cavity.

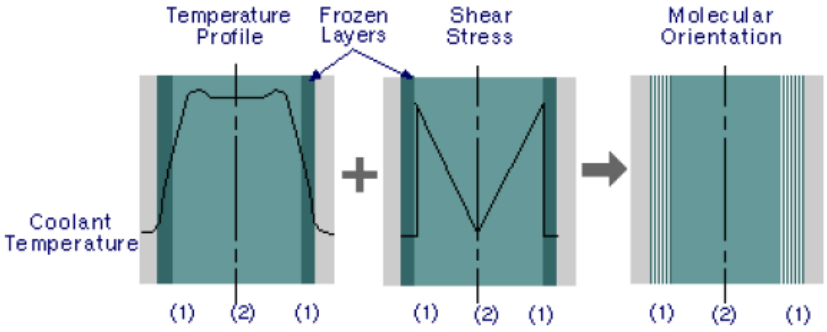

Figure 52. Schematic of flow-induced residual stresses

The thermally-induced residual stresses are generated by different cooling rates in a cavity. A melt resin of higher temperature than T_m or T_g is filled in a much cooler cavity, so the melt near the wall of the cavity solidifies faster than in the core. This different cooling rate induces compressive stresses in the surface layers and tensile stresses in the core, as earlier solidified surface layers hinder the volume shrinkage of the core part. Figure 53 shows schematics of the

thermally-induced residual stresses. If the residual stresses are anisotropic, warpage occurs after the molding process. High mold temperature and high injection speed both reduce the residual stresses because of reduced temperature gradient and shear stress in a cavity, but high mold temperature also reduces productivity. Thus, optimization of injection molding conditions is important for molded part quality and production cost. Recently, to minimize or eliminate the residual stresses, rapid thermal response (RTR) molding technique has been developed [111]. This technique prescribes mold temperature to increase rapidly over glass transition temperature before the injection of a resin, and then a rapid mold cooling after the injection step. Other problems, such as sink mark, flow mark, jetting, silver streak, weld line, or burning are well-known in injection molding [112]. To get a molded product without these problems, all factors related to injection molding, such as a mold design, processing condition, and resin property should be taken into account.

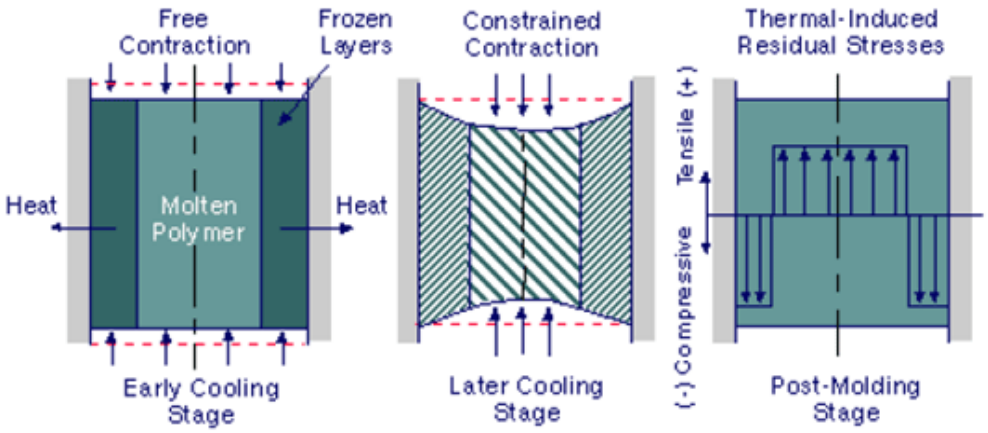

Figure 53. Schematic of thermally-induced residual stresses [111]

Injection molding conditions and properties of molded parts

Fiber reinforced polymer composites are frequently studied to investigate the effect of injection molding conditions on the properties of molded products as the property differences due to changes of processing parameters are clearly observed in such composites. Bay et al. [113] numerically studied fiber orientations in an injection molded part. The fiber orientation is directly related to the mechanical properties, such as mechanical modulus and strength. Bay et al. [113] assumed polymer melt to be a Newtonian liquid and also assumed that the velocities were independent of fiber orientation. They found that the fiber orientation was different at different depths of a molded part. The theoretical predictions were validated by companion experiments. However, the prediction of fiber orientations at the flow front (Fountain region) was invalid due to the complication of recirculating flows in the region. Figure 54 shows schematic of melt flow regions in a cavity. Frozen layers are formed near the wall of a cavity due to a higher cooling rate at the wall. At the gate region, the flow changes to converging flow due to formation of the frozen material layers, while at the flow front diverging flows (Fountain flow) occur.

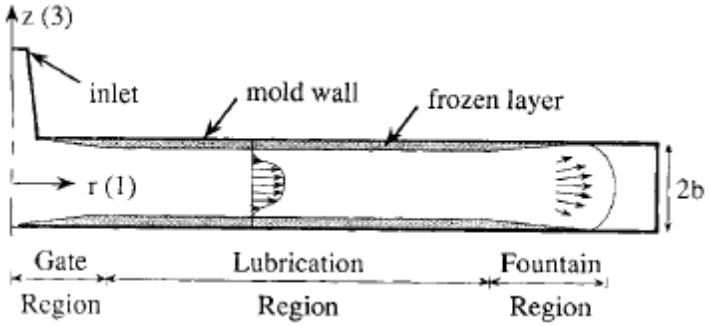

Figure 54. Flow regions during injection mold filling [113]

Gupta et al. [114] also studied fiber orientation in a molded part of a short fiber reinforced polymer composite while the injection speed was used as a parameter. Converging flows due to the formation of solidified layers on the wall of a cavity caused fibers to align to the melt flow direction. However, the diverging flows at the melt front aligned the fibers transverse to the melt flow direction. The effect of the converging flows was dominant, especially for lower injection speed and smaller thickness of the cavity. This indicates that the fibers should align more to the melt flow direction if a cavity is narrow or the injection speed is low. Figure 55 shows the extent of fiber alignment in different positions of a molded part. At or near the gate, most fibers are aligned to the melt flow direction regardless of the depth of a cavity. This is due to the converging flow effect. The fiber alignment in the core's (mid-plane) gradually changes due to the increasing effect of diverging flow as one travels away from the gate. However, most fibers in the frozen layers show alignment to the melt flow direction regardless of the positions. Fiber alignment in the flow direction is not favorable for a heat exchanger application where through plane thermal conductivity controls the rate of heat transfer.

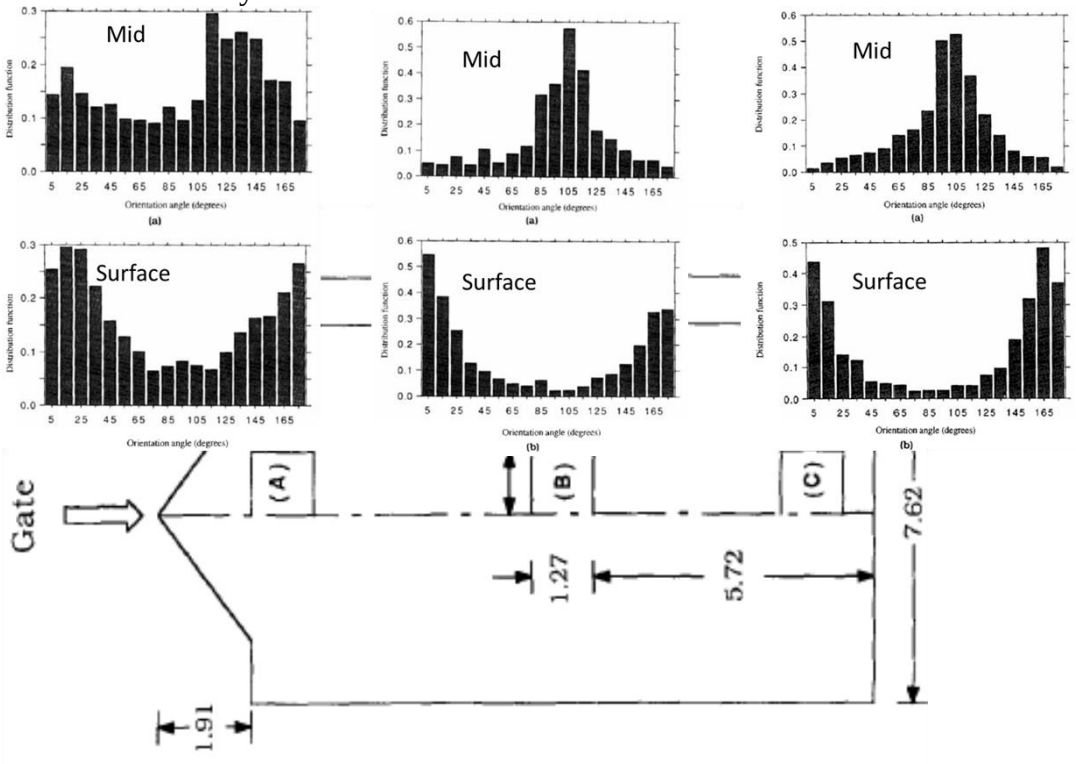

Figure 55. Fiber alignment in different positions of a molded part [114]

Bijsterbosch et al.[115] studied injection molding of long glass fiber reinforced polymer composites. Chopped glass strands of 9 mm length and 20 μm diameter were compounded with polyamide 6. Fiber lengths and orientations after molding a dumbbell shaped tensile bar were investigated. Mild injection molding conditions were used to minimize the degradation of the fibers in the study. For example, injection conditions of 0 bar for back pressure and 50 rpm for screw speed were studied. Also, low injection speed was used to obtain the highest possible fiber orientation. From this study, it was found that injection molding significantly shortens the length of the fibers, the extent of which depends primarily on the fiber concentration. The fiber length was found to be shortened to 1.6 mm from its 9 mm original value in the composite with fiber concentration of 2 vol%. The fiber length reduced further to 0.6 mm in when the fiber concentration was raised to 25 vol%.

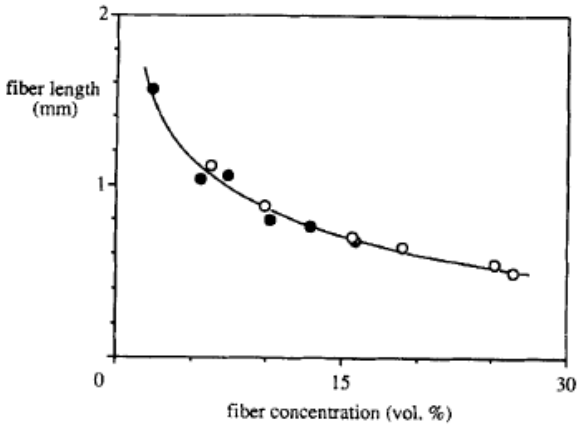

Figure 56. Fiber length vs. fiber concentration [115]

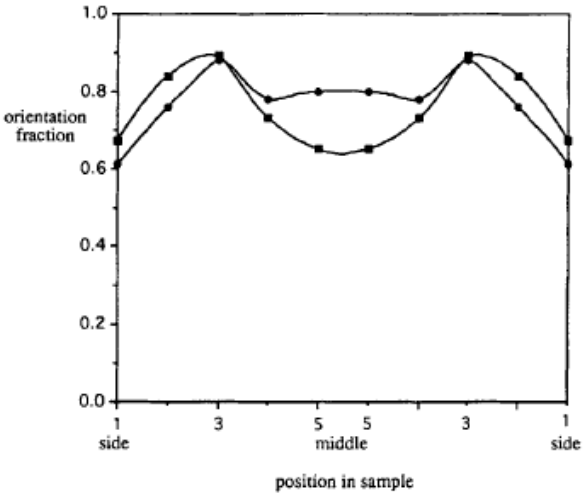

Figure 57. Fiber orientation over cross-section ■ a high degree of impregnation pellets, ● low degree of impregnation pellets [115]

Figure 56 shows the result of fiber length vs. fiber concentrations in injection molded articles. This study showed that the highest degree of fiber orientation was achieved at a location near the surface and not at the surface as seen in Figure 57. Fibers located at the surfaces and in the cores showed similar extent of fiber orientations, but the fibers located in between the surface and the

core aligned the most to the melt flow direction. Modeling has shown that the final fiber length can greatly affect the thermal conductivity.

Mahmoodi et al.[116] provided very useful information from a study of the effect of injection molding conditions of PS/CNT composites on electrical and EMI shielding properties. The authors diluted a 20 wt% master-batch of PS/CNT to 5 wt% using a twin-screw extruder and obtained pellets. Pellets containing 5 wt% CNT in PS matrix were used for injection molding. Four processing parameters, such as mold temperature, melt temperature, injection/holding pressure, and injection speed were used for the investigation as seen in Table 16 and Table 17. This study also investigated the effect of mold design on the electrical and EMI shielding properties. Three different cavities with different runners and gates were prepared for the investigation as seen in Figure 58.

Table 16. Experimental design showing the two-level, four factor factorial design. C1-mold temperature, C2-melt temperature, C3- injection/holding pressure, and C4-injection speed

Exp. #	Factors			
	c_1 (°C)	c_2 (°C)	c_3 (bar)	c_4 (mm/s)
1	–	–	–	–
2	–	–	–	+
3	–	–	+	+
4	–	–	+	–
5	–	+	–	–
6	–	+	–	+
7	–	+	+	+
8	–	+	+	–
9	+	+	–	–
10	+	+	–	+
11	+	+	+	+
12	+	+	+	–
13	+	–	+	–
14	+	–	+	+
15	+	–	–	+
16	+	–	–	–

Table 17. Levels (set points) of the experiments

Level	Factors			
	c_1 (°C)	c_2 (°C)	c_3 (bar)	c_4 (mm/s)
+	60	240	100	240
–	25	215	60	24

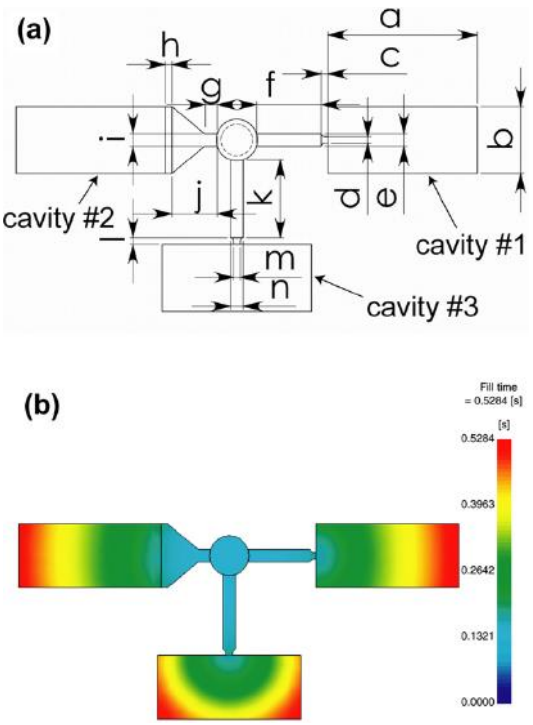

Figure 58. A schematic of the designed mold (a) and filling simulation of the cavities using Moldflow software (b)[116]

Approximately seven orders of magnitude difference of volumetric resistance in thickness direction were found depending on the injection molding conditions. All specimens injection molded with minimal melt temperature (215℃) showed the highest resistance. Low melt temperature which corresponds to high melt viscosity led to a high degree of CNT alignment (a low degree of CNT connectivity). It is well-known in literature that shear stresses are useful in the alignment of fibers, thus high shear stresses resulting from high viscosity led to greater CNT alignment in the melt flow direction. This study showed that the specimen formed with high injection speed (240 mm/s) had high volumetric resistance than the specimen formed with low injection speed (24 mm/s). Recall that fibers should align more to the melt flow direction in the case of low injection speed and a narrow cavity [114]. Therefore, the difference may have originated from the effect of shear heating. In previous study, it was seen that an increase of melt temperature due to shear heating from high injection speed should also reduce the viscosity, therefore, the value of shear stress. However, shear heating in the case of PS/CNT composite may not be significant to affect the viscosity as CNT is a good thermal conductor and can help dissipate any local heat originating from local shear heating effects. The relationship between shear stresses and CNT alignments were also found. The specimen formed in cavity #1 showed higher volumetric resistance than those formed in cavity #2, and #3. Overall, the results of the effect of injection molding conditions on volumetric resistance in the thickness direction are summarized in Figure 59.

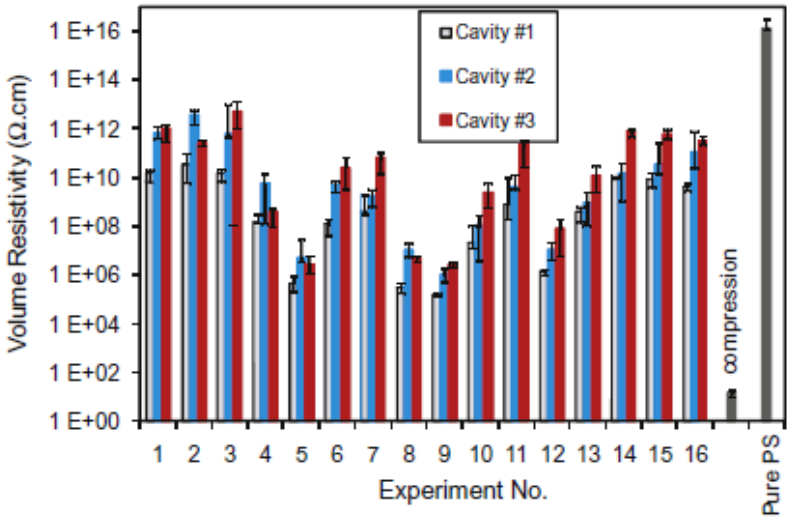

Figure 59. Volume resistivity of the molded parts in the thickness direction [116]

Volumetric resistance in the flow direction was also similar to that in the thickness direction. Seven orders of magnitude difference were observed depending on the injection molding conditions. As it can be expected, the highest volumetric resistance was measured with the specimen formed in cavity #1 in which highest shear stresses are applied. The lowest resistance was observed with the specimen formed in cavity #2 which has a fan gate. Low shear stresses are applied in a fan gate than in a regular gate. This study rests on the fact that melt temperature and injection speed were two key parameters determining the volumetric resistance. EMI shielding efficiency was proportional to the electrical conductivity as seen in Figure 60. The authors insisted that absorption mechanism of the EMI shielding is dominant in the specimen formed by compression molding, but reflection mechanism is dominant in the specimen formed by injection molding. The absorption increases with a decrease of the CNT alignment.

This work highlights the importance of manufacturing parameters and mold design on the final product performance. Additional ideas and methods that could be investigated for manufacturing of composite parts are detailed in the next section.

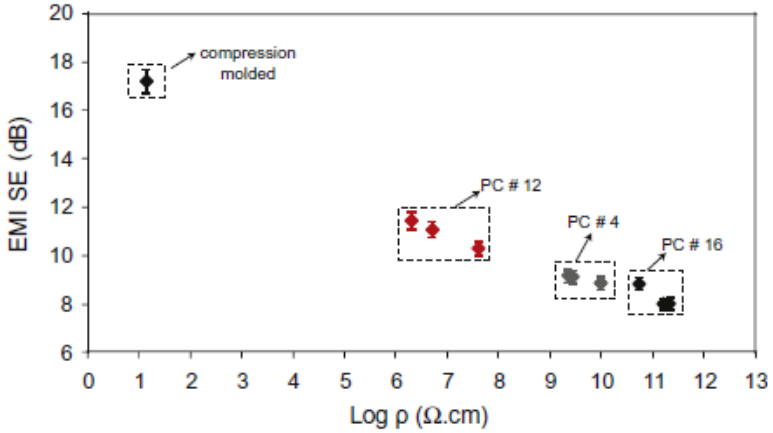

Figure 60. EMI SE (dB) of the injection and compression molded composites vs. volumetric resistance [116]

Other manufacturing methods

Reaction injection molding is an appropriate process for molding thermoset resins into a molded product [117]. A thermoset resin, such as epoxy, is mixed with an amine hardener in a mixing head, and the mixture is injected into a mold as described in Figure 61. Because of low viscosity of thermoset resins, low injection pressure is available in this processing method. In general, mold temperature is set to be much higher than that of the traditional injection molding for the curing reactions to occur.

If a molded part is very thick, some problems, such as sink mark or shrinkage cannot be avoided. In this case, the gas injection molding (or gas assisted injection molding, GIM) method can be used [118]. This processing method uses a gas and fills the gas inside a core via a nozzle or runner right after the resin injection as seen in Figure 62. Reduction of materials cost is an advantage of this processing method. However, non-uniform wall thicknesses (fingering) and rough inner surfaces are problems frequently associated with GIM.

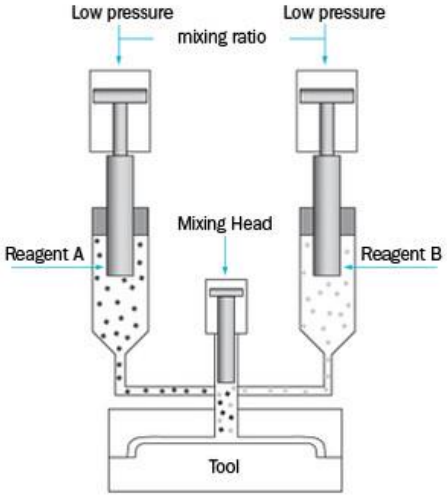

Figure 61. A schematic of reaction injection molding [119]

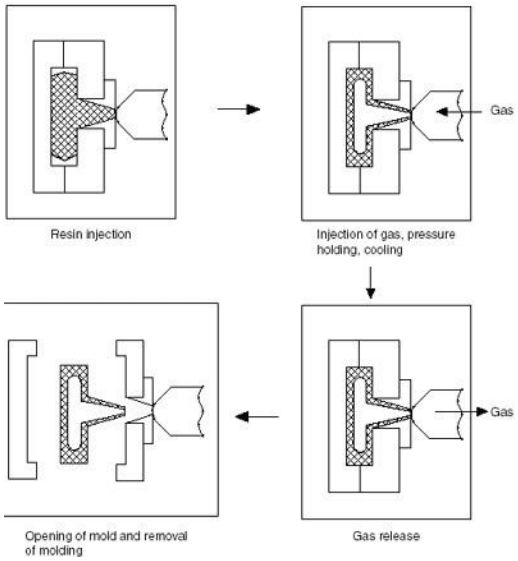

Figure 62. Gas assisted injection molding process [120]

A similar method that uses injection molding with water as the filling fluid (Water assisted injection molding) has also been used [121]. This method can overcome the problems of the fingering and the rough inner surface associated with GIM. Reduced cycle time by effective cooling of a melt in a core by the water is an additional advantage for this processing method. However, setting proper process conditions for producing products with acceptable quality is an issue of the water assisted injection molding.

In general injection molding, a melt resin flows through a runner and is filled in a cavity via a gate in a mold. After injection molding, the runner parts are disposed of or recycled. Beyond this traditional mold design, there is a runner-less mold which is mostly called a hot-runner mold [122]. The hot-runner keeps the temperature high to contain a resin melt in it, and the resin is injected directly to a cavity from the hot-runner as seen in Figure 63. With this hot-runner system, molded parts are runnerless, and therefore, it saves the materials. The hot-runner system can carry out injection molding with high injection speed and low injection pressure because a resin is kept in a melt state. Because a resin is exposed to heat for a long time in the hot-runner system, thermal degradation or burning can occur. Thus, a thermally stable resin, such as polycarbonate is favored when hot-runner systems are used.

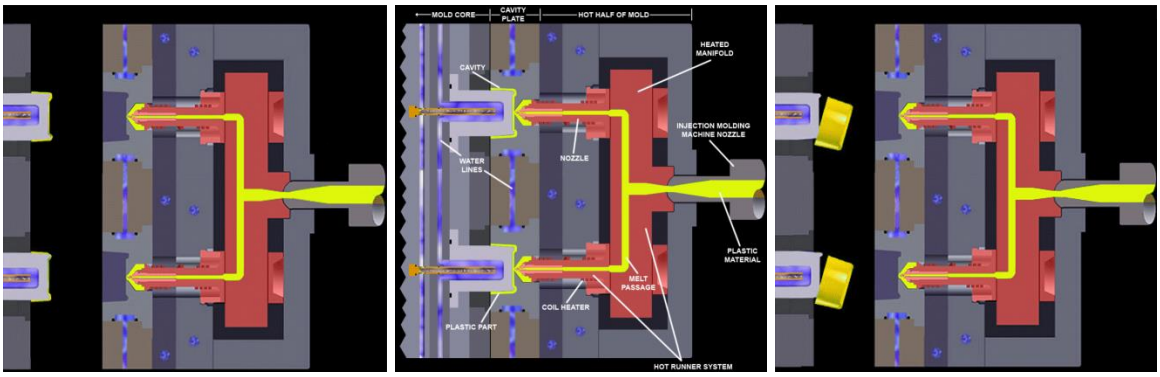

Figure 63. Mold open (left), injection (middle) and part ejection (right) cycles in hot-runner system [123]

Another technique in modifying the traditional mold system is using a valve gate. A valve gate is originally intended for use of the hot-runner to control the injections of a melt resin. The valve gate can be usefully applied to overcome the problem of forming weld lines. This is by sequential valve gating, as is illustrated in Figure 64.

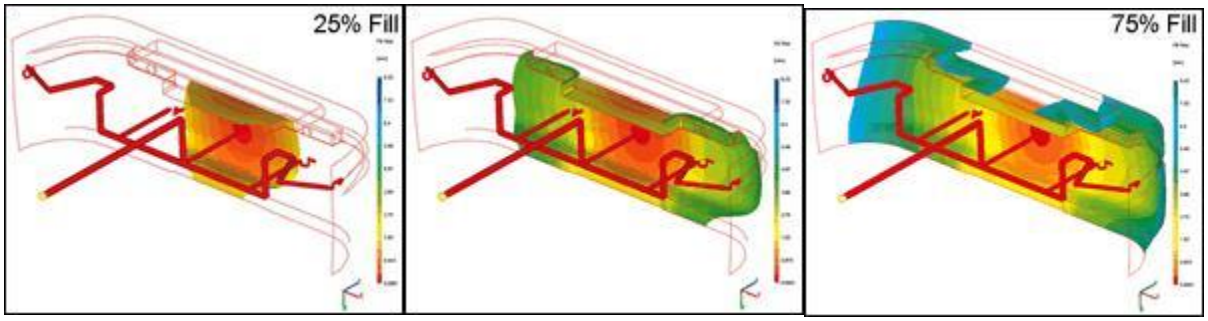

Figure 64. Sequential valve gating to remove weld lines [124]

As seen in Figure 64, the center gate is open first to fill a melt resin in a middle part of a cavity, and right after the melt passing the adjacent two side gates, the center gate valve is closed, but

the valves of the two side gates still open to fill the lateral parts of the cavity. Opening and closing successive gates are controlled by the same manner. Formation of weld lines can be avoided by controlling the time of the sequential valve gating.

Injection-compression molding is a method invented by a combination of the two processing methods: injection and compression molding [125]. The melt resin is injected at an injection stage as in the traditional injection molding process, but a cavity (or a mold) is kept slightly open at the injection step as seen in Figure 65. After the injection, the cavity (or the mold) is closed, thus compressing the resin inside as in a typical compression molding. Two different methods are used to compress the resin; one is to use an ejecting unit by which only the cavity undergo the motion of opening and closing. Another is to use a clamping unit by which an entire mold is in motion.

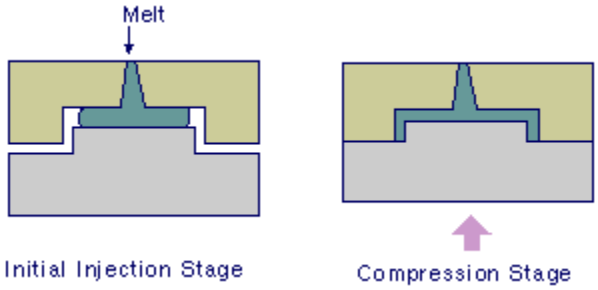

Figure 65. Injection-compression molding [126]

Injection-compression molding is well-known process in the plastic-optics industry because this method can manufacture products with minimal level of residual stresses [127-129]. The residual stresses in an optical product, such as an optical lens lead to different refractions of light. The injection-compression is also favored in manufacturing products with precision dimensions because the compression step allows a molded body in a cavity to have uniform pressure. Injection-compression molding is also considered a powerful tool to mold products from highly viscous polymers that are hardly produced by the traditional injection molding process, such as a polymer composite filled with high concentration of fillers. Much lower injection pressure can be carried by the injection-compression molding because a melt resin is injected with the cavity open.

Several studies investigated the relationships between processing parameters and product properties in the injection-compression molding [127-130]. Young [127] studied distributions of residual stresses and shrinkages in a pick-up lens. This study revealed that the mold temperature and compression time are two key parameters affecting the properties. High mold temperature and short compression time were recommended to minimize distributions of the residual stresses and shrinkages (**Error! Reference source not found.** and **Error! Reference source not found.**). The compression pressure was a minor factor for the properties. The results indicate that controls of the thermally-induced residual stresses are critical for the properties.

As a similar result, Chen et al. [128] studied volume shrinkages of a molded part formed by the injection-compression molding. They found that faster switch time from injection to compression, and faster compression time reduced the part shrinkages. Both studies are in an agreement that a low cooling rate which reduces the thermally-induced residual stresses improved dimensional stability.

In contrast, a study showed that the flow-induced residual stresses are the major factors affecting the properties. Chen et al.[130] studied birefringence and showed that higher compression speed, larger compression stroke, and shorter switch time (higher injection speed) exhibited greater effects on an increase of part birefringence. The result indicates that the major factor is the flow-induced residual stresses. However, birefringence could also be controlled by the mold temperature as in another study [129] which is in turn controls the thermally-induced residual stresses. In any case, the injection-compression molding has been actively studied for minimizing the residual stresses.

There are no published studies investigating the injection-compression molding of thermally conductive polymer composites to the best of our knowledge as most of the practical processing knowledge is kept proprietary.

The following part of this report suggests several ideas for production of the HX plates and the HX assembly.

Figure 66. The geometry of a brazed plate for HX (left) and bipolar plate (right)[131]

Figure 66 shows the geometry of a HX plate which includes many flow channels. The geometry of the plate is remarkably similar to that of bipolar plates which are used in fuel cells (Figure 66). Polymer bipolar plates are produced from thermally conductive polymer composites, and are mostly manufactured by the traditional injection molding method.in which the high viscosity of the thermally conductive polymer composites limits the plate size [132].

In production of the bipolar plates, molding the plate without distribution of thicknesses is important because a number of the plates are stacked in the fuel cell system as seen in Figure 67. Small thickness differences in one piece of the bipolar plate causes plate distortion and fuel leakage in the stacks. Molding the HX plate precisely in dimensions without distribution of the thicknesses should also be taken into account because the plates are designed to be assembled to form channels through which a refrigerant flows. The injection-compression molding provides a benefit for producing molded parts with minimized distribution of thicknesses because the entire body of a resin in a cavity experiences uniform pressure at the compression stage.

Figure 67. Stacks of bipolar plates (black parts) in a fuel cell [133]

The effect of injection speed and mold temperature should be considered in an experimental manufacturing study.

Very high speed injections by which the entire volume of a cavity is filled without sufficient time of cooling and solidification of the melt resin is attractive when processing thermally conductive material. Injection molding machines with injection speed up to 1,000 mm/sec are available nowadays. Drawback of high injection speed include problems due to flow-induced residual stress, burning marks and filler damages from shear heating and shear stress respectively.

Mold temperature is a key parameter to control the quality of molded products. Mold temperature also affects material property itself, and the effect is more significant in the case of semi-crystalline polymers, such as polyphenylene sulfide (PPS) which is the leading candidate material. It is well known that a mold temperature around 130 ℃ (which is slightly higher than the cold-crystallization temperature (around 120℃) of PPS) is required to obtain high level of crystallinity in PPS and PPS composites. Recall that thermal conductivity and permeation are all related to the crystallinity of the matrix polymers; the higher crystallinity leads to the higher thermal conductivity and lower permeation. The properties of crystallinity, post mold shrinkages, heat deflection temperatures (HDT), and mechanical properties depend on the mold temperature [134]. Figure 68 and Figure 69 respectively show the crystallinity and the tensile strength of PPS against mold temperatures.

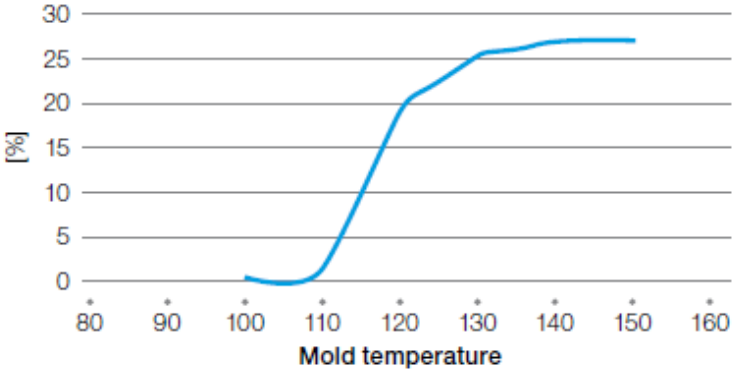

Figure 68. Crystallinity at various mold temperatures measured by XRD [133]

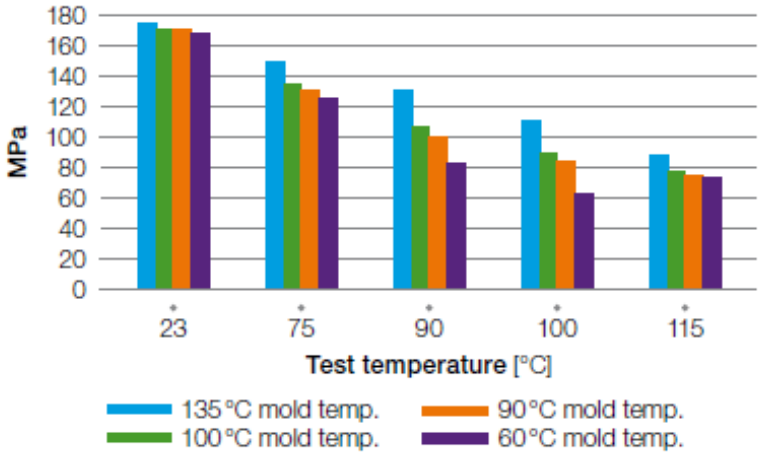

Figure 69. Tensile strength tested at elevated temperatures [133]

In the injection-compression molding of the plates from the PPS composites, the high mold temperature of 130℃ will also have the effect of reducing the thermally-induced residual stresses, and therefore the molded part will have better dimensional stability. Other processing parameters, such as compression time, compression stroke should also be determined experimentally.

The plates are designed to be used in an assembled system and should withstand pressure around 300-600 psi. In fuel cell applications, each bipolar plate has bolting holes for the assembly as seen in Figure 70.

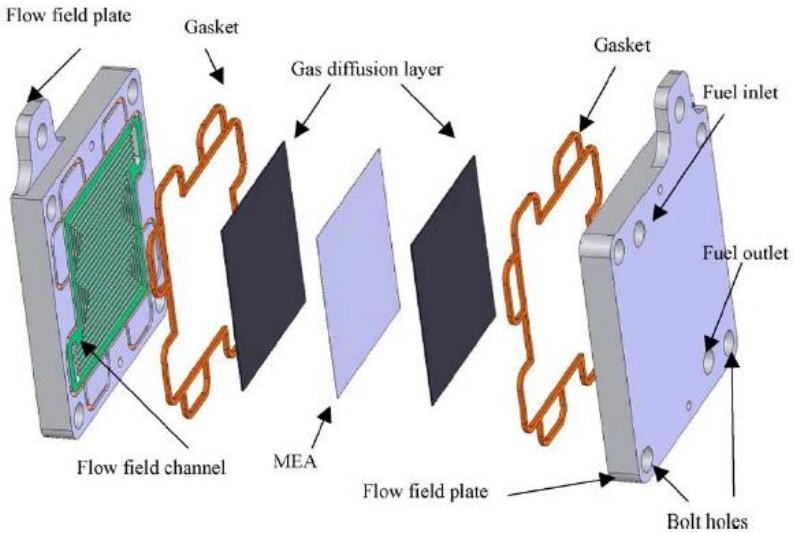

Figure 70. Components of the single cell, bipolar plates have bolting holes for assembly [135]

In fuel cells, the assembly pressure applied by bolts is important. Not enough assembly pressure may lead to leakage of fuels, high contact resistance, and malfunctioning of the cells, but too much pressure results in damage to the plates and membranes [135]. The insert injection is the method where an insert (metal, ceramics, or multiple combinations of materials) is inserted into a mold in advance of a melt injection, and then, the melt encapsulates the insert by the injection, and forms the molded product into a single unit [136]. An example part molded by the insert injection molding is seen in Figure 71. This processing method is frequently used in aerospace,

medical, and automobile industries. In the HX plate, metallic bolting holes could be inserted by the insert injection molding.

Figure 71. A molded part by an insert injection molding [137]

Potential manufacturing techniques have been suggested in this section for the HX plates and some fabrication trials performed by the UMass –Lowell team are described in the next section.

A next natural step in the development of polymer composite-based heat exchangers would be to demonstrate the manufacturability at cost and durability of a full size heat exchanger. The methods suggested here are at high technology readiness level (TRL) for neat polymers and some are used commercially for composite materials, but cost assessment for the cost sensitive market such as HVAC is unclear.

Other lower TRL manufacturing techniques such as 3D printing should also be assessed as they may open up even more design options that cannot be realized by traditional techniques such as molding.

A recent review [138] highlights the current limitations of 3D printing in three categories:

-Material: Currently, limited to thermoplastic polymer with low glass transition temperature and suitable melting viscosity that may not be compatible to the application (for example refrigerant compatibility). Synthesis of matrix materials with special properties is needed with focus on material cost reduction and environmental impact.

-Performance: Most of the printed composites have low mechanical strength (due in part to the presence of voids) and require additional post-treatment steps (such as involving infiltration or consolidation) to meet requirements, increasing cost and processing time.

-Machine: Industry adoption is limited by part size, printing resolution and speed. There is a need for better process control and automated response to process change.

7. Plate and Frame Heat Exchanger Application

7.1 Plate and Frame Heat Exchanger Optimization

The optimization of a Plate and Frame HX seeks to provide the most cost effective configuration that still meets thermal capacity and liquid-side pressure drop under the given set of refrigerant and liquid conditions. As a first order, this can be assessed by minimizing the HX weight and volume.

Four materials were considered for the optimization: two commercially available composite materials (PPS1 and PPS2), a fictitious thermally enhanced material superior to PPS1 (denoted PPS1+) and the virgin material PPS. Material properties for these four materials are given in Table 18. The optimization was carried out on the plate thickness. The optimization was constrained by the rules given in Table 19.

The optimization results (Figure 72) showed that plate thickness is a bigger driver of HX size than material thermal conductivity. Thinning the plate reduces thermal resistance and material volume and weight; increasing conductivity only reduces thermal resistance. As summarized in the next section, fabrication trials have shown that materials with higher thermal conductivity were harder to process due to their highly filled nature and due to the rapid heat loss they encounter, leading to thicker components. These results confirm that increasing the thermal conductivity of the material unilaterally will not lead to an optimized component.

Table 18. Material properties considered for optimization

	Material Properties		Optimization Runs			
	Thermal Conductivity (Thru-Plane) [W/m·K]	Density [kg/m³]	3.0 mm Plate	1.5 mm Plate	0.75 mm Plate	0.3 mm Plate
PPS1	10	1700	X	X		
PPS2	4	1540	X	X	X	
Fictitious Material: PPS1 with Enhanced k (PPS1+)	20	1700	X	X	X	
Unfilled PPS	0.3	1360				X

Table 19. Constraints for optimization

Parameter	Constraint
Capacity	= Baseline
Liquid ΔP	≤ Baseline
Plate width	≥ 4 inch Required for manifolding
Plate aspect ratio	≥ 3 (Required for flow distribution)
Refrigerant Outlet State	= Baseline
Liquid Inlet State	= Baseline
Refrigerant ΔP	Unconstrained (but any negative capacity impact caused by ΔP is captured)

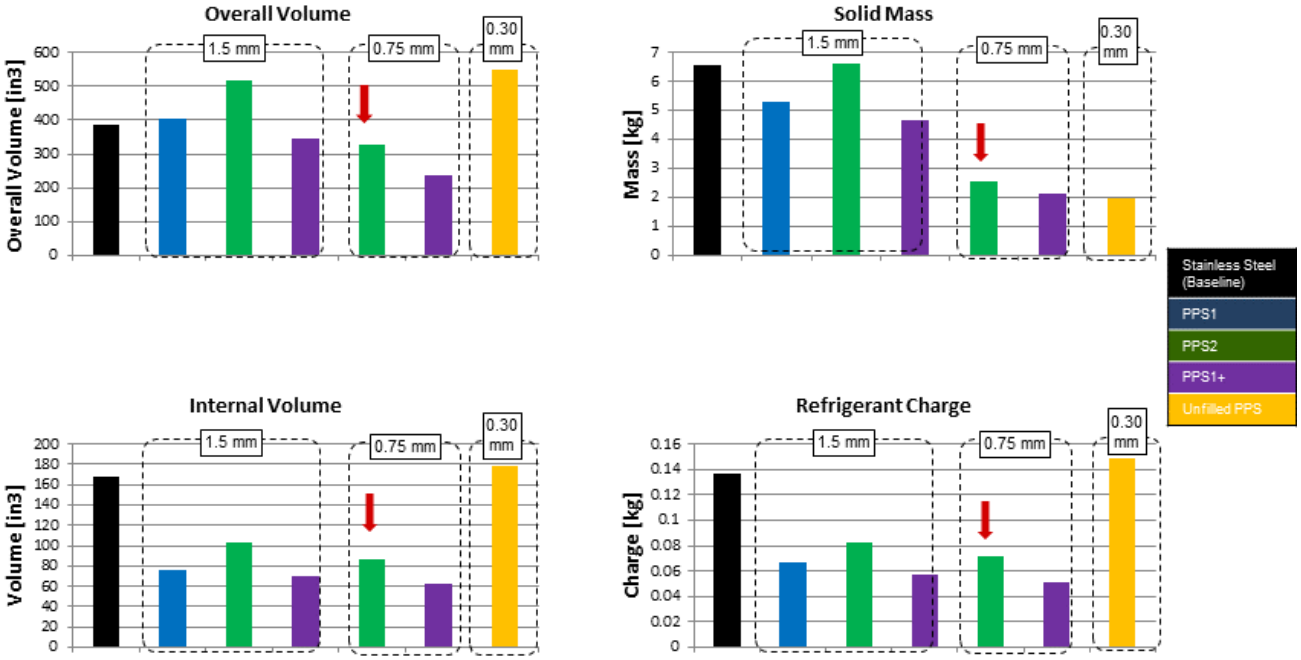

Figure 72. Optimization results for Plate and Frame HX showing that the ability to manufacture a thin plate is as important as the thermal conductivity of the material. In this case, a 0.75 mm plate thickness with a material thermal conductivity of 4 W/mK offers a better performance than a 1.5 mm thick plate with a material thermal conductivity of 10 W/mK

7.2 Manufacturing and Fabrication trials

During the processing trials conducted by UMass Lowell, it became apparent that there would be significant challenges in processing large aspect ratio parts with such highly filled, thermally conductive resins. One such challenge is the melt freeze-off or freezing of the material before the entire injection mold cavity is filled. This was accentuated when processing 1mm thick by 150mm diameter disks (Figure 73). If melt freeze-off occurs, the material flow becomes unpredictable, full filling of the mold can't be achieved, and the edges of the part are poorly consolidated. Another challenge discovered during processing is that weld/knit lines which occur when melt fronts meet exhibit very low mechanical properties. Weld/knit lines are a common source of part failure if the impinging melt fronts can't consolidate sufficiently to provide a virtually defect free weld. With highly filled materials, melt viscosities are inherently very high thus substantially inhibiting the ability to consolidate at the impinging melt fronts. Additionally, these highly thermally conductive polymer composites exhibit melt freeze off which results in freezing of the melt fronts before they impinge and can lead to very weak weld lines.

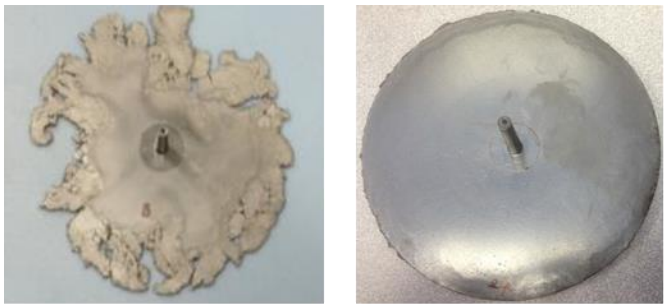

Figure 73. Images of a short shot 150mm disk demonstrating significant melt freeze-off (left) and a good 150mm injection molded disk with refined injection molding parameters (right) made by the University of Massachusetts at Lowell.

Figure 74. Short shot dual gated dog bone specimen depicting accentuated melt freeze-off and weld line

The University of Massachusetts team used the MoldFlow simulation software to evaluate the effect of various process parameters on the injection molding process.

Effect of Mold Cavity Depth
The mold cavity depth will dictate the plate thickness. As shown in Figure 75, the material melt front travels further as the cavity depth increases. Therefore, the plate thickness of the HX plate will be limited by the fabrication process.

Effect of Gate Number/Location
As expected, dual gated parts filled more completely than center gated or single edge gated parts. However, creation of weld lines will affect strength properties of the final part as shown in the experimental section.

Effect of Fill Velocity
A higher flow velocity leads to a faster and more complete fill. This cannot be compensated by increasing the mold temperature. This indicates that processing of materials with enhanced thermal conductivity is likely driven by thermal effects and may require optimization of the mold and the associated heating and cooling process parameters.

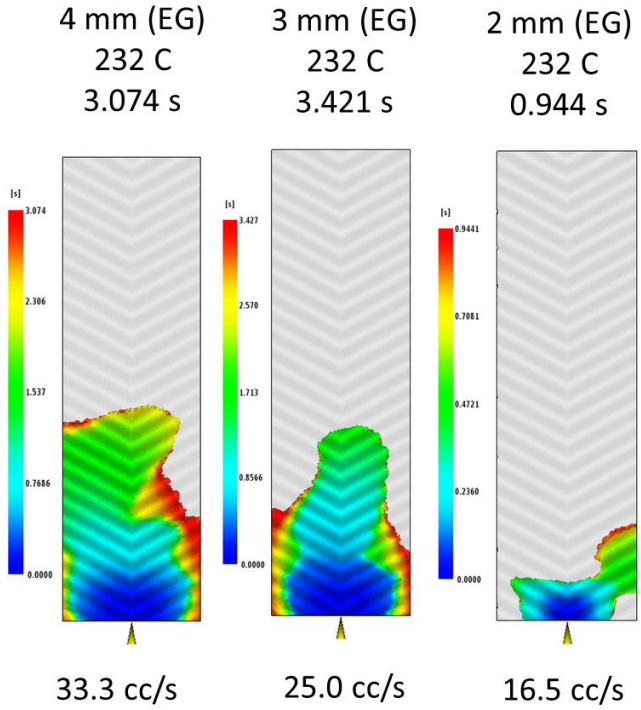

Figure 75. Fill pattern versus mold depth shown at top of figure (in mm). Although none of these simulations led to completely filled plates, the fill ratio was higher for deeper molds. Gate location is indicated by the yellow arrow.

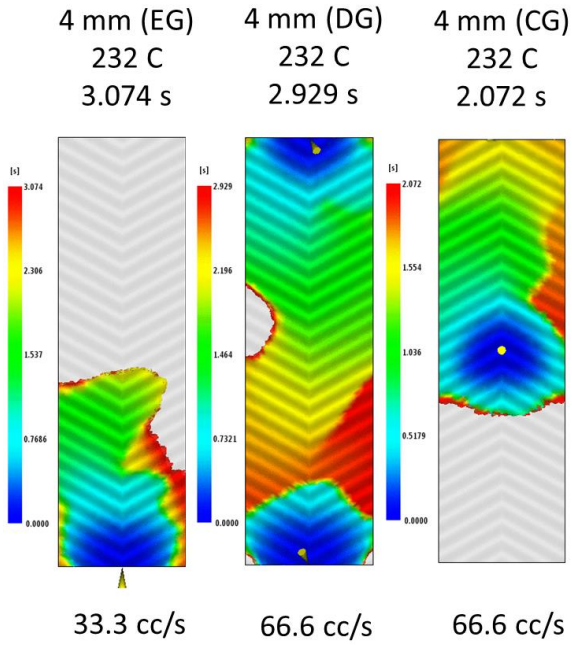

Figure 76. Fill pattern versus gating. From left to right: one bottom gate (middle), two gates (middle top, middle bottom) and one center gate. The two gated process leads to a better fill since the material front travels a shorter distance.

.

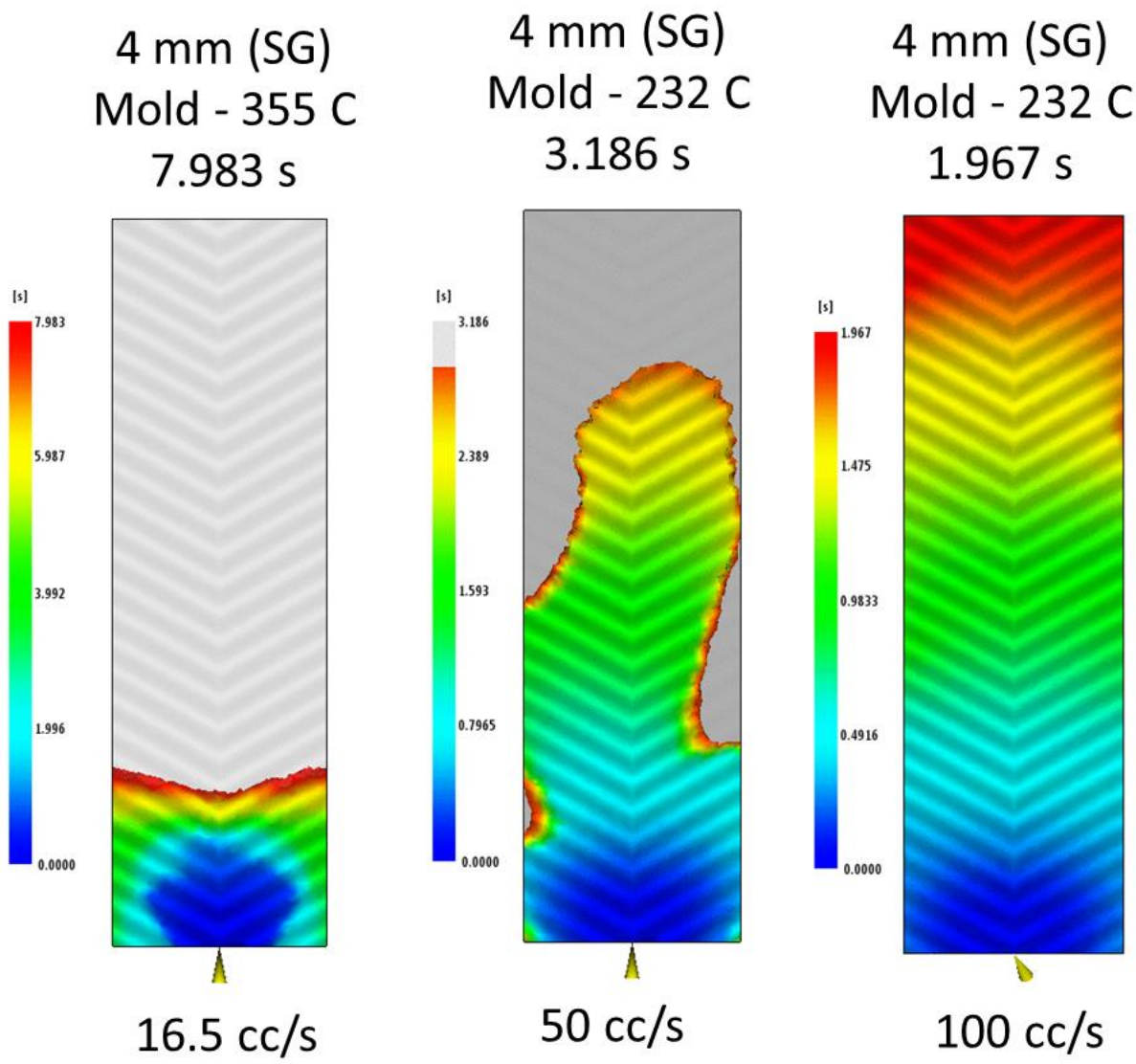

Figure 77 . Fill pattern versus fill velocity. Higher flow velocity leads to faster and more complete fill. The fill velocity cannot be compensated by mold temperature

7.3 Cost assessment of polymer-based brazed plate heat exchanger

A cost assessment of a typical brazed plate heat exchanger such as the one shown in Figure 78 was carried out using BOOTHROYD DEWHURST, Inc. DFM tool. DFM Concurrent Costing software provides an understanding of the primary cost drivers associated with manufacturing of a product.

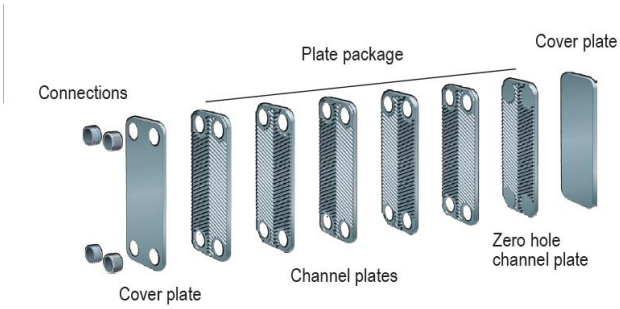

Figure 78. Typical arrangement for a brazed plate heat exchanger (from http://www.swep.net/globalassets/products/f80/f80-en.pdf)

A manufacturing plan was established for the injection molding of a polypropylene-based heat exchanger and for the forming and brazing of a stainless steel 304 heat exchanger of same capacity. Assumptions were made regarding the labor rate, reject rate, material cost.

The cost for a SS 304 heat exchanger manufactured in the US was estimated at around $600 and around $200 if manufactured in China. These numbers were consistent with the selling price of a F80 heat exchanger.

The cost of a propylene based brazed plate heat exchanger made in the US via injection molding depended greatly on the material cost and varied between $100 to $150 for a material cost between $1.7 $ per kg (for example polypropylene) and $25 per kg (composite PPS).

These costs show that large savings are possible even with a US manufacturing base.

Figure 79 and Figure 80 show the breakdown of cost for the metal and plastic heat exchangers.

The cost of the metal based heat exchanger is driven by the processing of the plates whereas the cost of the plastic heat exchanger is driven by the assembly at low material cost and both by the material cost and assembly cost for a more expensive material.

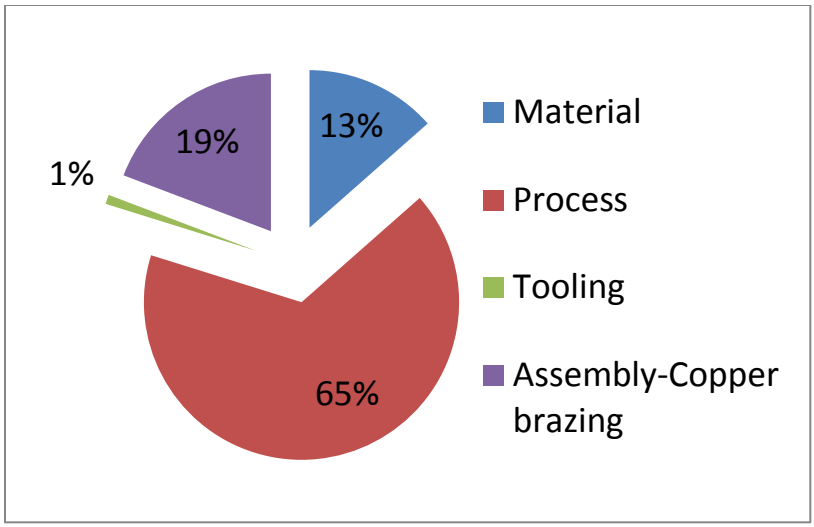

Figure 79. Cost breakdown for a SS304 brazed plate heat exchanger manufactured in the US.

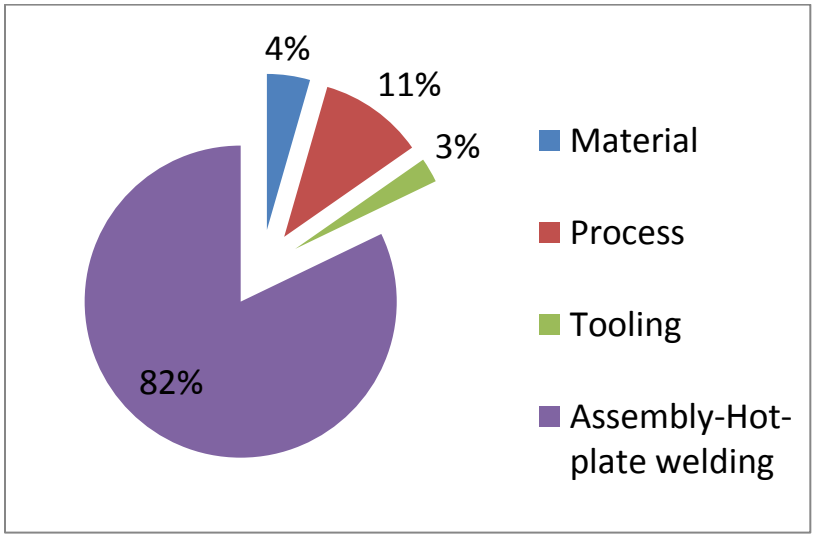

Figure 80. Cost breakdown for Polypropylene brazed plate heat exchanger manufactured in the US.

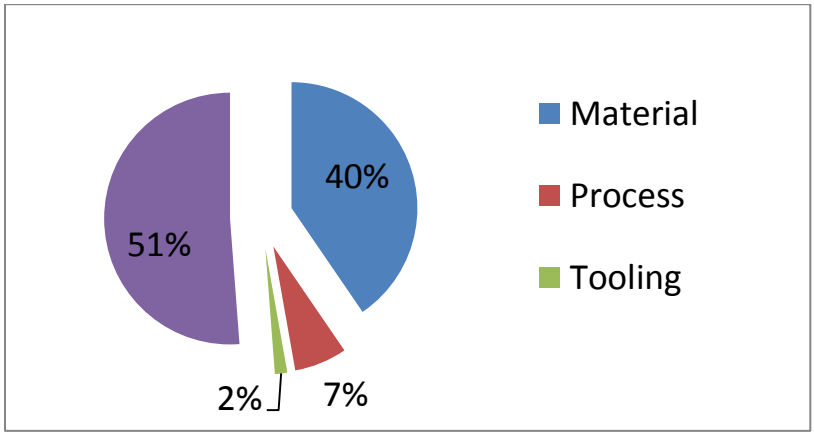

Figure 81. Cost breakdown for composite brazed plate heat exchanger manufactured in the US.(material cost $25/kg)

8. Products:

a) **Publications, Conference Papers, and Presentations:**

Some of the work performed under the project was summarized in a thesis and a publication as shown below:

- MS thesis from University of Massachusetts (Lowell) titled "A study of the effects of Filler Content in Processing and Properties of Thermally Conductive Plastics" by Afrin Roja Jahir Hussain. (2016)
- Hussain. A. et al., "Review of polymers for heat exchanger applications: Factors concerning thermal conductivity", Applied Thermal Engineering, in print, 2017

b) **Inventions, Patent applications, and/or licenses:**

Two invention disclosures were made:

1- Polymer Heat Transfer Devices with Refrigerant Barrier Layers
2- Hybrid Metal-Polymer Heat Exchanger

c) **Website(s) or other Internet site(s):**

Nothing to report

REFERENCES

[1] Daedal Research "Global Heat Exchanger Market: Trends and Opportunity 2014-2019" (2014)

[2] Jacobi M. et al., ARTI Report No. 06030-01 - NOVEL MATERIALS FOR HEAT EXCHANGERS Phase I Final Report -March 2008.

[3] Hussain, A. et al. "Review of polymers for heat exchanger applications: Factors concerning thermal conductivity", *Applied Thermal Engineering*, approved for publication, 2017

[4] Y.P. Mamunya, V.V. Davydenko, P. Pissis, E.V. Lebedev, Electrical and thermal conductivity of polymers filled with metal powders, Eur. Polym. J. 38 (2002) 1887–1897, http://dx.doi.org/10.1016/S0014-3057(02)00064-2.

[5] A. Boudenne, L. Ibos, M. Fois, J.C. Majeste, E. Gehin, Electrical and thermal behavior of polypropylene filled with copper particles, Compos. Part Appl. Sci. Manuf. 36 (2005) 1545–1554, http://dx.doi.org/10.1016/j.compositesa.2005.02.005.

[6] S. Chin, Recent progress in the development and properties of novel metal matrix nanocomposites reinforced with carbon nanotubes and graphene nanosheets, Mater. Sci. Eng. R. 74 (2013) 281–350, http://dx.doi.org/10.1016/j.mser.2013.08.001.

[7] B.L.M. Veca, M.J. Meziani, W. Wang, X. Wang, F. Lu, P. Zhang, Y. Lin, R. Fee, J.W. Connell, Y. Sun, Carbon nanosheets for polymeric nanocomposites with high thermal conductivity, Adv. Mater. (2009) 2088–2092, http://dx.doi.org/10.1002/adma.200802317.

[8] A.A. Balandin, S. Ghosh, W. Bao, I. Calizo, D. Teweldebrhan, F. Miao, C.N. Lau, Superior thermal conductivity of single-layer graphene, Nano Lett. (2008).

[9] K. Pielichowska, K. Pielichowski, Phase change materials for thermal energy storage, Prog. Mater. Sci. 65 (2014) 67–123, http://dx.doi.org/10.1016/j.pmatsci.2014.03.005.

[10] Chen, Y.; J. Ting, Ultra high thermal conductivity polymer composites, Carbon 40 (2002) 359–362.

[11] Ha, S. M.; H.L. Lee, S.-G. Lee, B.G. Kim, Y.S. Kim, J.C. Won, W.J. Choi, D.C. Lee, J. Kim, Y. Yoo, Thermal conductivity of graphite filled liquid crystal polymer composites and theoretical predictions, Compos. Sci. Technol. 88 (2013) 113–119, http://dx.doi.org/10.1016/j.compscitech.2013.08.022.

[12] Chung, D.D. Materials for thermal conduction, Appl. Therm. Eng. 21 (2001) 1593–1605, http://dx.doi.org/10.1016/S1359-4311(01)00042-4.

[13] Leung, S. N.; M.O. Khan, E. Chan, H. Naguib, F. Dawson, V. Adinkrah, L. Lakatos-Hayward, Analytical modeling and characterization of heat transfer in thermally conductive polymer composites filled with spherical particulates, Compos. Part B Eng. 45 (2013) 43–49, http://dx.doi.org/10.1016/j.compositesb. 2012.10.001.

[14] Ishida, H.; S. Rimdusit, Very high thermal conductivity obtained by boron nitride- filled polybenzoxazine, Thermochim. Acta 320 (1998) 177–186, http://dx. doi.org/10.1016/S0040-6031(98)00463-8.

[15] Yeol, S,; H. Min, S.Y. Kim, J.R. Youn, Synergistic improvement of thermal conductivity of thermoplastic composites with mixed boron nitride and multi-walled carbon nanotube fillers, Carbon 50 (2012) 4830–4838, http://dx. doi.org/10.1016/j.carbon.2012.06.009.

[16] Wang, X.; V. Ho, R.A. Segalman, D.G. Cahill, Thermal conductivity of high-modulus polymer fibers : supplemental materials, Macromolecules 46 (2013) 4937–4943.
[17] Kim, H.-S.; Y.S. Chae, B.H. Park, J.-S. Yoon, M. Kang, H.-J. Jin, Thermal and electrical conductivity of poly(l-lactide)/multiwalled carbon nanotube nanocomposites, Curr. Appl. Phys. 8 (2008) 803–806, http://dx.doi.org/10.1016/j.cap. 2007.04.032.
[18] Ahn, K.; K. Kim, M. Kim, J. Kim, Fabrication of silicon carbonitride-covered boron nitride/Nylon 6,6 composite for enhanced thermal conductivity by melt process, Ceram. Int. 41 (2015) 2187–2195, http://dx.doi.org/10.1016/j.ceramint. 2014.10.018.
[19] Muratov, D. S.; D.V. Kuznetsov, I.A. Il'inykh, I.N. Burmistrov, I.N. Mazov, Thermal conductivity of polypropylene composites filled with silane-modified hexagonal BN, Compos. Sci. Technol. 111 (2015) 40–43, http://dx.doi.org/10. 1016/j.compscitech.2015.03.003.
[20] Lee, G.W.; M. Park, J. Kim, J.I. Lee, H.G. Yoon, Enhanced thermal conductivity of polymer composites filled with hybrid filler, Compos. Part Appl. Sci. Manuf. 37 (2006) 727–734, http://dx.doi.org/10.1016/j.compositesa.2005.07. 006.
[21] Chiu, H. T.; T. Sukachonmakul, M.T. Kuo, Y.H. Wang, K. Wattanakul, Surface modification of aluminum nitride by polysilazane and its polymer-derived amorphous silicon oxycarbide ceramic for the enhancement of thermal conductivity in silicone rubber composite, Appl. Surf. Sci. 292 (2014) 928–936, http://dx.doi.org/10.1016/j.apsusc.2013.12.081.
[22] Han, Z.; A. Fina, Thermal conductivity of carbon nanotubes and their polymer nanocomposites: a review, Prog. Polym. Sci. Oxf. 36 (2011) 914–944, http://dx. doi.org/10.1016/j.progpolymsci.2010.11.004.
[23] Tsekmes, I.A.; R. Kochetov, P.H.F. Morshuis, J.J. Smit, Thermal conductivity of polymeric composites: a review, in: 2013 IEEE Int. Conf. Solid Dielectr. ICSD (2013) 678–681, http://dx.doi.org/10.1109/ICSD.2013.6619698.
[24] Sanada, K.; Y. Tada, Y. Shindo, Thermal conductivity of polymer composites with close-packed structure of nano and micro fillers, Compos. Part Appl. Sci. Manuf. 40 (2009) 724–730, http://dx.doi.org/10.1016/j.compositesa.2009.02.024.
[25] M.J. Sobkowicz, E.A. White, J.R. Dorgan, Supramolecular bionanocomposites 3: effects of surface functionality on electrical and mechanical percolation, J.Appl. Polym. Sci. 122 (2011) 2563–2572.
[26] G. Droval, J. Feller, P. Salagnac, P. Glouannec, Thermal conductivity enhancement of electrically insulating syndiotactic poly (styrene) matrix for diphasic conductive polymer composites, Polym. Adv. Technol. (2006) 732–745, http:// dx.doi.org/10.1002/pat.
[27] C. T'Joen, Y. Park, Q. Wang, A. Sommers, X. Han, A. Jacobi, A review on polymer heat exchangers for HVAC&R applications, Int. J. Refrig. 32 (2009) 763–779, http://dx.doi.org/10.1016/j.ijrefrig.2008.11.008.
[28] J.P. Hong, S.W. Yoon, T. Hwang, J.S. Oh, S.C. Hong, Y. Lee, J. Do Nam, High thermal conductivity epoxy composites with bimodal distribution of aluminum nitride and boron nitride fillers, Thermochim. Acta 537 (2012) 70–75, http://dx.doi.org/10.1016/j.tca.2012.03.002.
[29] D.M. Bigg, Thermally conductive polymer compositions, Polym. Compos. 7 (1986) 125–140, http://dx.doi.org/10.1002/pc.750070302.
[30] E. Kandare, A.A. Khatibi, S. Yoo, R. Wang, J. Ma, P. Olivier, N. Gleizes, C.H. Wang, Composites: Part A improving the through-thickness thermal and electrical conductivity of carbon fibre/epoxy laminates by exploiting synergy between graphene and silver nano-inclusions, Compos. Part A 69 (2015) 72–82, http:// dx.doi.org/10.1016/j.compositesa.2014.10.024.

[31] H.S. Tekce, D. Kumlutas, I.H. Tavman, Effect of particle shape on thermal conductivity of copper reinforced polymer composites, J. Reinf. Plast. Compos. 26 (2007) 113–121, http://dx.doi.org/10.1177/0731684407072522.
[32] S. Agarwal, R. Gupta, Thermal conductivity of polymer nanocomposites, in: Polym. Nanocomposites Handb., CRC Press, 2009. http://dx.doi.org/10.1201/9781420009804-c17.
[33] K. Sanada, Y. Tada, Y. Shindo, Thermal conductivity of polymer composites with close-packed structure of nano and micro fillers, Compos. Part Appl. Sci.Manuf. 40 (2009) 724–730, http://dx.doi.org/10.1016/j.compositesa.2009.02.024.
[34] Kittel, C., *Introduction to Solid State Physics*. Wiley: 2005.
[35] Maxwell, Electricity and Magnetism, Oxford: Clarendon, 1873

[36] Bruggeman, D.A.G. "Berechnung verschiedener physikalischer Konstanten von heterogenen Substanzen. I. Dielektrizitätskonstanten und Leitfähigkeiten der Mischkörper aus isotropen Substanzen," *Annalen der Physik,* vol. 416, no. 7, pp. 636-664, 1935.

[37] Cheng S. and R. I. Vachon, "The Prediction of Thermal Conductivity of Two and Three Phase Solid Heterogeneous Mixtures," *International Journal of Heat and Mass Transfer,* vol. 12, pp. 249-264, 1969.

[38] Lewis T. and L. Nielsen, "Dynamic Mechanical Properties of Particulate-filled Polymers," *Journal of Applied Polymer Science,* vol. 14, no. 6, pp. 1449-1450, 1970.

[39] Agari, Y. and T. Uno, "Estimation on Thermal Conductivities of Filled Polymers," *Journal of Applied Polymer Science,* vol. 14, pp. 1449-1471, 1986.

[40] Agari, Y.; A. Ueda and S. Nagai, "Thermal Conductivity of Composites in Several Types of Dispersion Systems," *Journal of Applied Polymer Science,* vol. 42, no. 6, pp. 1665-1669, 1991.

[41] Agari, Y.; A. Ueda and S. Nagai, "Thermal Conductivity of Polyethylene Filled with Disoriented Short-cut Carbon Fibers," *Journal of Applied Polymer Science,* vol. 43, no. 6, pp. 1117-1124, 1991.
[42] Agari, Y.; A. Ueda and S. Nagai, "Thermal Conductivity of a Polymer Composite," *Journal of Applied Polymer Science,* vol. 49, no. 9, pp. 1625-1634, 1993.
[43] Zhang, G.; Y. Xia, H. Wang, Y. Tao, G. Tao, S. Tu and H. Wu, "A Percolation Model of Thermal Conductivity for Filler Polymer Composites," *Journal of Composite Materials,* vol. 44, no. 8, pp. 963-970, 2010.

[44] Luo T. and J. R. Lloyd, "Enhancement of Thermal Energy Transport Across Graphene/Graphite and Polymer Interfaces: A Molecular Dynamics Study," *Advanced Functional Materials,* vol. 22, pp. 2495-2502, 2012.

[45] S.-K. Chien, Y.-T. Yang and C.-K. Chen, "Influence of hydrogen functionalization on thermal conductivity of graphene: Nonequilibrium molecular dynamics simulations," *Applied Physics Letters,* vol. 98, no. 3, p. 033107, 2011.

[46] Y. Y. Zhang, Q. X. Pei, X. Q. He and Y.-W. Mai, "A molecular dynamics simulation study on thermal conductivity of functionalized bilayer graphene sheet," *Chemical Physics Letters,* vol. 622, pp. 104-108, 2015.

[47] M. Alaghemandi, F. Muller-Plathe and M. C. Bohm, "Thermal conductivity of carbon nanotube-polyamide-6,6 nanocomposites: Reverse non-equilibrium molecular dynamics simulations," *Journal of Chemical Physics,* vol. 135, no. 18, p. 184905, 2011.

[48] T. C. Clancy and T. S. Gates, "Modeling of interfacial modification effects on thermal conductivity of carbon nanotube composites," *Polymer,* vol. 47, pp. 5990-5996, 2006.

[49] V. U. Unnikrishnan, D. Banerjee and J. N. Reddy, "Atomistic-mesoscale interfacial resistance based thermal analysis of carbon nanotube systems," *International Journal of Thermal*

Sciences, vol. 47, pp. 1602-1609, 2008.

[50] S. T. Huxtable, D. G. Cahill, S. Shenogin, L. Xue, R. Ozisik, P. Barone, M. Usrey, M. S. Strano, G. Siddons, M. Shim and P. Keblinski, "Interfacial heat flow in carbon nanotube suspensions," *Nature Materials,* vol. 2, pp. 731-734, 2003.

[51] S. Shenogin, A. Bodapati, L. Xue, R. Ozisik and P. Keblinski, "Effect of chemical functionalization on thermal trasnport of carbon nanotube composites," *Applied Physics Letters,* vol. 12, no. 2229-2231, p. 85, 2004.

[52] Y. Kuang and B. Huang, "Effects of covalent functionalization on the thermal transport in carbon nanotube/polymer composites: A multi-scale investigation," *Polymer,* vol. 56, pp. 563-571, 2015.

[53] . Che, T. Cagin and W. A. Goddard III, "Thermal conductivity of carbon nanotubes," *Nanotechnology,* vol. 11, no. 2, pp. 65-69, 2000

[54] P. K. Schelling, S. R. Phillpot and P. Keblinski, "Comparison of atomic-level simulation methods for computing thermal conductivity," *Physical Review B,* vol. 65, p. 144306, 2002.

[55] C.-W. Nan, G. Liu, Y. Lin and M. Li, "Interface effect on thermal conductivity of carbon nanotube composites," *Applied Physics Letters,* vol. 16, no. 3549-3551, p. 85, 2004.

[56] Dilek Kumlutas, I. H. T. *Journal of Thermoplastic Composite Materials* **2006,** 19, 441-455.

[57] Wong, C. P.; Bollampally, R. S. *Journal of Applied Polymer Science* **1999,** 74, (14), 3396-3403.

[58] Hill, R. F.; Supancic, P. H. *Journal of the American Ceramic Society* **2002,** 85, (4), 851-857.

[59] T Clancy and T S Gates, *Polymer* 47 5990 (2006)

[60] R Heggenmueller, *et al.*, *Macromolecules* 40 2417 (2007)

[61] R Heggenmueller, *et al.*, *Macromolecules* 39 2964 (2006)

[62] Tonpheng, *et al. Macromolecules* 42 9295 (2009)

[63] . Choi, H. Shin, S. Yang and M. Cho, "THe influence of nanoparticle size on the mechanical properties of polymer nanocomposites and the associated interphase region: A multiscale approach," *Composite Structures,* vol. 119, pp. 365-376, 2015

[64] Liu H. and L. C. Brinson, "Reinforcing efficiency of nanoparticles: A simple comparison for polymer nanocomposites," *Composites Science and Technology,* vol. 68, pp. 1502-1512, 2008

[65] Halpin, J.C. "Effects of Environmental Factors on Composite Materials," 1969

[66] Halpin J.C.and J. L. Kardos, "The Halpin-Tsai Equations: A Review," *Polymer Engineering and Science,* vol. 16, no. 5, pp. 344-352, 1976.

[67] Mori T. and K. Tanaka, "Average stress in matrix and average elastic energy of materials with misfitting inclusions," *Acta Metallurgica,* vol. 21, no. 5, pp. 571-574, 1973.

[68] Benveniste, Y. "A new approach to the application of Mori-Tanaka's theroy in composite materials," *Mechanics of Materials,* vol. 6, no. 2, pp. 147-157, 1987

[69] Odegard, G.M.; T. C. Clancy and T. S. Gates, "Modeling of the mechanical properties of nanoparticle/polymer composites," *Polymer,* vol. 46, pp. 553-562, 2005.

[70] Thostenson E. T. and T.-W. Chou, "On the elastic properties of carbon nanotube-based composites: modeling and characterization," *Journal of Physics D: Applied Physics,* vol. 36, p. 573, 2003

[71] Zhu L. and K. A. Narh, "Numerical simulation of the tensile modulus of nanoclay-filled polymer composites," *Journal of Polymer Science B: Polymer Physics,* vol. 42, no. 12, pp. 2391-2406, 2004

[72] Sheng, N.; M. C. Boyce, D. M. Parks, G. C. Rutledge, J. I. Abes and R. E. Cohen, "Multiscale micromechanical modeling of polymer/clay nanocomposites and the effective clay particle," *Polymer,* vol. 45, no. 2, pp. 487-506, 2004.
[73] Frankland, J.V.; A. Caglar, D. W. Brenner and M. Griebel, "Molecular Simulation of the Influence of Chemical Cross-Links on the Shear Strength of Carbon Nanotube-Polymer Interfaces," *Journal of Physical Chemistry B,* vol. 106, no. 12, pp. 3046-3048, 2002.
[74] Gou, J.; B. Minaie, B. Wang, Z. Lian and C. Zhang, "Computational and experimental study of interfacial bonding of single-walled nanotube reinforced composites," *Computational Materials Science,* vol. 31, no. 3-4, pp. 225-236, 2004.
[75] Frankland, J.V.; V. M. Harik, G. M. Odegard, D. W. Brenner and T. S. Gates, "THe stress-strain behavior of polymer-nanotube composites from molecular dynamics simulation," *Composites Science and Technology,* vol. 63, no. 11, pp. 1655-1661, 2003
[76] Song M. and L. Chen, "Molecular Dynamics Simulation of the Fracture in Polymer-Exfoliated Layered Silicate Nanocomposites," *Macromolecular Theory and Simulation,* vol. 15, pp. 238-245, 2006.
[77] Fertig III, R.S. and M. R. Garnich, "Influence of constituent properties and microstructural parameters on the tensile modulus of a polymer/clay nanocomposite," *Composites Science and Technology,* vol. 64, no. 16, pp. 2577-2588, 2004.
[78] Hbaieb, K.; Q. X. Wang, Y. H. J. Chia and B. Cotterell, "Modelling stiffness of polymer/clay nanocomposites," *Polymer,* vol. 48, no. 3, pp. 901-909, 2007.
[79] Mesbah, A.; F. Zairi, S. Boutaleb, J. M. Gloaguen, M. Nait-Abdelaziz, S. Xie, T. Boukharouba and J. M. Lefebvre, "Experimental characterization and modeling stiffness of polymer/clay nanocomposites within a hierarchical multiscale framework," *Journal of Applied Polymer Science,* vol. 114, no. 5, pp. 3274-3291, 2009.
[80] Cricri, G.; E. Garofalo, F. Naddeo and L. Incarnato, "Stiffness Constants Predictions of Nanocomposites Using a Periodic 3D-FEM Model," *Journal of Polymer Science B: Polymer Physics,* vol. 50, pp. 207-220, 2011.
[81] Needleman, A.; T. L. Borders, L. C. Brinson, V. M. Flores and L. S. Schadler, "Effect of an interphase region on debonding of a CNT reinforced polymer composite," *Composites Science and Technology,* vol. 70, pp. 2207-2215, 2010.
[82] Fisher, F.T.; R. D. Bradshaw and L. C. Brinson, "Fiber waviness in nanotube-reinforced polymer composites--I: Modulus predictions using effective nanotube properties," *Composites Science and Technology,* vol. 63, no. 11, pp. 1689-1703, 2003.
[83] Bradshaw, R.D.; F. T. Fisher and L. C. Brinson, "Fiber waviness in nanotube-reinforced polymer composites--II: modeling via numerical approximation of the dilute strain concentration tensor," *Composites Science and Technology,* vol. 63, no. 11, pp. 1705-1722, 2003.
[85] Davison, S. P. Enviro-Mechanica; Durability of garphite/EpoxyComposite Materials, , Virginia Tech Thesis, 2003 https://theses.lib.vt.edu/theses/available/etd-11192003-134415/unrestricted/Dissertation2etdb.pdf
[86] Sheng, N.; Boyce, M.; Parks, D.; Rutledge, G.; Abes, J.; Cohen, R. Multiscale Micromechanical Modeling Of Polymer/Clay Nanocomposites And The Effective Clay Particle. Polymer 2004, 45,
[87] Siracusa, V. Food Packaging Permeability Behaviour: A Report. Int. J. of Polymer Science 2012, 2012, 1-11.
[88] Nielsen, L. Models For The Permeability Of Filled Polymer Systems. *Journal of Macromolecular Science: Part A - Chemistry* 1967, *1*, 929-942.
[89] Choudalakis, G.; Gotsis, A. Permeability Of Polymer/Clay Nanocomposites: A Review. *European Polymer Journal* 2009, *45*, 967-984.

[90] Bharadwaj, R. Modeling The Barrier Properties Of Polymer-Layered Silicate Nanocomposites. *Macromolecules* 2001, *34*, 9189-9192.
[91] Dunkerley, E.; Schmidt, D. Effects Of Composition, Orientation And Temperature On The O_2 Permeability Of Model Polymer/Clay Nanocomposites. *Macromolecules* 2010, *43*, 10536-10544.
[92] Cussler, E.; Hughes, S.; Ward, W.; Aris, R. Barrier Membranes. *Journal of Membrane Science* 1988, *38*, 161-174.
[93] Lai, C.; Fu, Y.; Chen, J.; Wang, D.; Sun, Y.; Huang, S.; Hung, W.; Hu, C.; Lee, K. Composite Of Cyclic Olefin Copolymer With Low Graphene Content For Transparent Water-Vapor-Barrier Films. *Carbon* 2015, *90*, 85-93.
[94] Gusev, A.; Lusti, H. Rational Design Of Nanocomposites For Barrier Applications. *Adv. Mater.* 2001, *13*, 1641-1643.
[95] Fredrickson, G.; Bicerano, J. Barrier Properties Of Oriented Disk Composites. *The Journal of Chemical Physics* 1999, *110*, 2181
[96] Qian, Y.; Lindsay, C.; Macosko, C.; Stein, A. Synthesis And Properties Of Vermiculite-Reinforced Polyurethane Nanocomposites. *ACS Appl. Mater. Interfaces* 2011, *3*, 3709-3717.
Section 7
[97] . J.F. Agissant, P. A., J. PH. Sergent, P. J. Carreau: Polymer Processing: Principles and modeling; Oxford University Press 1991.
[98] http://www.mechscience.com/wp-content/uploads/2015/03/clip_image00222.gif. 11.2015.
[99] Rosato, D. V. R., M.G. Rosato: *Injection molding handbook*; Spriner Science+Business Media: New York, 2000.
[100] Yao, D.; Kim, B.: Development of rapid heating and cooling systems for injection molding applications. *Polymer Engineering & Science* **2002**, *42*, 2471-2481.
[101] Emoto, A.: Injection apparatus for an electric injection molding machine. Sumitomo Heavy Industries, L., Ed.: USA, 1996; Vol. US5679384 A
Emoto, A.: Injection apparatus for an electric injection molding machine. Sumitomo Heavy Industries, L., Ed.: USA, 1996; Vol. US5679384 A.
[102] http://www.nttd-es.co.jp/products/e-learning/etrainer/trial/en/mold/kiso/sample/step3/runner.htm. 11.2015.
[103] K.M.B. Jansen, D. J. v. D., E.V. Burgers: Experimental Validation of Shrinkage Predictions for Injection Molded Products. *International Polymer Processing* **1998**, *13*, 99-104.
[104] John P. Beaumont, R. L. N., R. Sherman: *Successful injection molding : process, design, and simulation*; Hanser Publishers Munich, 2002.
[105] J. Greener, R. W.-F.: *Precision Injection Molding*; Hanser Publications: Munich, 2006.
[106] http://www.cnf-moldmaking.com/News%20Center/Shrinkage%20and%20warpage,%20china%20injection%20mold%20%20China%20Mould%20maker%20%20china%20injection%20mold%20factory,%20mold%20china.htm. 11.2015.
[107] Isayev, A. I.; Crouthamel, D. L.: Residual-Stress Development in the Injection-Molding of Polymers. *Polymer-Plastics Technology and Engineering* **1984**, *22*, 177-232.
[108] Zoetelief, W. F.; Douven, L. F. A.; Housz, A. J. I.: Residual thermal stresses in injection molded products. *Polym Eng Sci* **1996**, *36*, 1886-1896.
[109] Isayev, A. I.: Orientation development in the injection molding of amorphous polymers. *Polymer Engineering & Science* **1983**, *23*, 271-284.

[110] Chen, M.; Yao, D. G.; Kim, B.: Eliminating flow induced birefringence and minimizing thermally induced residual stresses in injection molded parts. *Polymer-Plastics Technology and Engineering* **2001**, *40*, 491-503.
[111] http://www.cnf-moldmaking.com/News%20Center/Residual%20stress,%20china%20mold%20supplier%20%20China%20Mould%20maker%20%20china%20injection%20mold%20factory,%20mold%20china.htm. 11.2015.
[112] Kameoka, S.; Haramoto, N.; Sakai, T.: Development of an expert system for injection molding operations. *Advances in Polymer Technology* **1993**, *12*, 403-418.
[113] Bay, R. S.; Tucker, C. L.: Fiber orientation in simple injection moldings. Part I: Theory and numerical methods. *Polymer Composites* **1992**, *13*, 317-331.
[114] Gupta, M.; Wang, K. K.: Fiber orientation and mechanical properties of short-fiber-reinforced injection-molded composites: Simulated and experimental results. *Polymer Composites* **1993**, *14*, 367-382.
[115] Bijsterbosch, H.; Gaymans, R. J.: Polyamide 6—long glass fiber injection moldings. *Polymer Composites* **1995**, *16*, 363-369.
[116] Mahmoodi, M.; Arjmand, M.; Sundararaj, U.; Park, S.: The electrical conductivity and electromagnetic interference shielding of injection molded multi-walled carbon nanotube/polystyrene composites. *Carbon* **2012**, *50*, 1455-1464.
[117] Prepelka, D. J.; Wharton, J. L.: Reaction Injection Molding in the Automotive Industry *Journal of Cellular Plastics* **1975**, *11*, 87-98.
[118] Potente, H.; Hansen, M.: The Gas-Assisted Injection-Molding Process - Comparison between Experiment and Simulation. *International Polymer Processing* **1993**, *8*, 345-351.
[119] http://rapid-prototype.de/index.php?id=76. **11.2015**.
[120] http://www.argomold.com/html/INJECTION-MOLD-P5-6-Gas-Assisted-Injection-Molding.asp. 11.2015.
[121] Liu, S.-j.; Chen, Y.-s.: Water-assisted injection molding of thermoplastic materials: Effects of processing parameters. *Polymer Engineering & Science* **2003**, *43*, 1806-1817.
[122] Unger, P.: *Hot Runner Technology*; Hanser Publishers: Munich, 2006.
[123] https://en.wikipedia.org/wiki/Hot_runner. 11.2015.
[124] http://www.ptonline.com/articles/sequential-valve-gating. 11.2015.
[125] Watanabe, S.: Injection-compression mold Fuji Photo Film Co., Ltd., 1989; Vol. US5044925 A.
[126] http://kdmold.myweb.hinet.net/MOLDABILITY/b2400001.htm. 12.2015.
[127] Young, W.-B.: Effect of process parameters on injection compression molding of pickup lens. *Applied Mathematical Modelling* **2005**, *29*, 955-971.
[128] Chen, S. C.; Chen, Y. C.; Peng, H. S.: Simulation of injection–compression-molding process. II. Influence of process characteristics on part shrinkage. *Journal of Applied Polymer Science* **2000**, *75*, 1640-1654.
[129] Kang, S.; Kim, J. S.; Kim, H.: Birefringence distribution in magneto-optical disk substrate fabricated by injection compression molding. *OPTICE* **2000**, *39*, 689-694.
[130] Chen, S.-C.; Chen, Y.-C.; Peng, H.-S.; Huang, L.-T.: Simulation of injection-compression molding process, Part 3: Effect of process conditions on part birefringence. *Advances in Polymer Technology* **2002**, *21*, 177-187.
[131] http://www.globalsources.com/si/AS/General-Optics/6008800041116/pdtl/Bipolar-Plate/1005536773.htm. 12.2015.
[132] http://www.directindustry.com/prod/serenergy/product-119739-1293605.html. 12.2015.

[133] Greer, M. R.; Reaume, A.; Kowalski, G.: The Importance of Mold Temperature on the Properties of PPS Parts. http://www.solvay.com/en/binaries/Ryton-PPS-Mold-Temperature-205305.pdf.
[134] Lee, S.-J.; Hsu, C.-D.; Huang, C.-H.: Analyses of the fuel cell stack assembly pressure. *Journal of Power Sources* **2005**, *145*, 353-361
[135] Suzuki, T.; Yasuda, T.; Miyauchi, O.; Yotsuyanagi, J.: Method of insert injection molding Showa Denko Kabushiki Kaisha, 1983; Vol. US4865793 A.
[136] Heinzel, A.; Mahlendorf, F.; Niemzig, O.; Kreuz, C.: Injection moulded low cost bipolar plates for PEM fuel cells. *Journal of Power Sources* **2004**, *131*, 35-40.
[137] http://www.xcentricmold.com/about-injection-molding.php. 12.2015.
[138] Wang, X., Wang, K.; Zhou, Z.; Gou, J.; Hui, D. : 3D printing of Polymer Matrix Composites: A Review and Prospective *Composites Part B: Engineering*, **2017**, *10*, 442-458.